Spring 1999

Finite element simulation of creep buckling of CIPP liners under external pressure

Qiang Zhao
Louisiana Tech University

INFORMATION TO USERS

This manuscript has been reproduced from the microfilm master. UMI films the text directly from the original or copy submitted. Thus, some thesis and dissertation copies are in typewriter face, while others may be from any type of computer printer.

The quality of this reproduction is dependent upon the quality of the copy submitted. Broken or indistinct print, colored or poor quality illustrations and photographs, print bleedthrough, substandard margins, and improper alignment can adversely affect reproduction.

In the unlikely event that the author did not send UMI a complete manuscript and there are missing pages, these will be noted. Also, if unauthorized copyright material had to be removed, a note will indicate the deletion.

Oversize materials (e.g., maps, drawings, charts) are reproduced by sectioning the original, beginning at the upper left-hand corner and continuing from left to right in equal sections with small overlaps. Each original is also photographed in one exposure and is included in reduced form at the back of the book.

Photographs included in the original manuscript have been reproduced xerographically in this copy. Higher quality 6" x 9" black and white photographic prints are available for any photographs or illustrations appearing in this copy for an additional charge. Contact UMI directly to order.

UMI

A Bell & Howell Information Company
300 North Zeeb Road, Ann Arbor MI 48106-1346 USA
313/761-4700 800/521-0600

FINITE ELEMENT SIMULATION OF CREEP BUCKLING OF *CIPP* LINERS UNDER EXTERNAL PRESSURE

by

Qiang Zhao, M.S.

A Dissertation Presented in Partial Fulfillment
of the Requirements for the Degree
Doctor of Philosophy

COLLEGE OF ENGINEERING AND SCIENCE
LOUISIANA TECH UNIVERSITY

May 1999

LOUISIANA TECH UNIVERSITY

THE GRADUATE SCHOOL

April 8, 1999
Date

We hereby recommend that the thesis prepared under our supervision by Qiang Zhao

entitled Finite Element Simulation of Creep Buckling of CIPP Liners under External Pressure

be accepted in partial fulfillment of the requirements for the Degree of Doctor of Philosophy

Raja Nassar Dud E NG
Supervisor of Thesis Research

Richard L. Greechie
Head of Department

Applied & Computational Analysis & Modeling
Department

Recommendation concurred in:

Advisory Committee

Approved:
Richard L. Greechie
Director of Graduate Studies

Approved:
Jerry M. McDonough
Director of the Graduate School

Leslie K. Guice
Dean of the College

GS Form 13
2/97

ABSTRACT

The problem of long-term structural behavior of CIPP liners under external hydrostatic pressure has been characterized as a structural instability problem which is induced by time-dependent material deformation or creep. It is also a contact problem since the liner deflection is externally constrained by the host pipe. The intrinsically nonlinear problem is investigated by means of finite element simulation, with emphases on (a) the essential structural behaviors and mechanisms of buckling, and (b) the influences of inelastic material properties (i.e. yield strengths and creep rates) and geometrical parameters on liner's buckling resistance. Results from a series of numerical simulations, verified by experimental observations of short- and long-term buckling test data, are used to derive an appropriate CIPP liner design strategy.

The problem is treated as a ring encased in a rigid wall, which is circular or slightly oval. The liner is considered subject only to hydrostatic pressure, built up by infiltration through cracks in the deteriorated host pipe, which is assumed constant during the liner's service life. Material properties of a specific CIPP material are used to represent a family of liner products made of polyester. The mechanical behavior of the material can be characterized as linear elastic-perfect plastic, and its creep behavior can be modeled by the Bailey-Norton law. The dependency of the inelastic properties on stress state is incorporated into the finite element model by using a "composite" beam element which combines two normal beam elements, one of which resists tension and the

other resists compression. Experimentally observed properties such as yield limits and creep strain rates for both uniaxial tensile and compressive tests can thus be incorporated in the analysis.

The essential structural behavior of constrained liners is investigated by simulating the deflection evolution of a liner under instantaneous conditions. The two conventionally accepted buckling modes, one- and two-lobe modes, are found to give lower and upper bounds for all possible critical pressures, which are significantly higher than those of corresponding free liners. A liner first deforms as a free pipe into a two-lobe pattern because of the existence of an initial gap. It will transition to a one-lobe mode when one of the two competing lobes becomes dominant. The finite element results show excellent agreement with experimental observations. Because mode transition and hence the critical pressure depend greatly on geometric factors which are usually not controllable in pipe rehabilitation, predictions based on the conservative one-lobe model should be used in liner design.

The relationship between critical time and external pressure derived from finite element simulation results show that critical time can be expressed as a monotonic function of the ratio of applied pressure to the critical (short-term) pressure. This relationship shows as expected that critical time at the two extreme pressure levels (zero and critical pressure) is infinity and zero, respectively. The model gives excellent agreement with the finite element results, and is better than other models used in the literature to correlate experimentally observed buckling times with pressure levels.

The buckling resistance of CIPP liners depends greatly on several geometric parameters of the liner-host-pipe system. Finite element simulations are carried out to

investigate the effects of three essential geometric parameters (i.e. the dimension ratio of the liner, the gap between the liner and its host pipe, and the ovality of the host pipe) and two geometric imperfections (i.e., variation in liner thickness and initial local imperfection in liner shape).

Several issues which are important in design, including the discussion on failure states, and an appropriate way to choose a safety factor, are discussed. A methodology is presented by which finite element simulation results can be used to CIPP liner design. Design curves are given for designing CIPP liners made of a specific CIPP resin. An empirical design equation is presented which can determine a safe and cost-effective thickness for a given design pressure and given host-pipe configuration.

DEDICATION

This work is dedicated to my grandfather, Dr. Shuxuan Zhao (Chao Shu-Hsuan, M.D.), who passed away during my study at Louisiana Tech University, and to my grandmother, Tianrong Zhu. I will always be grateful for their influence on me regarding my attitude toward life and career.

TABLE OF CONTENTS

LIST OF TABLES

LIST OF FIGURES

ACKNOWLEDGEMENTS

I wish to express my sincere appreciation and gratitude to my advisors Drs. Raja F. Nassar and David E. Hall for their time and effort in guiding me throughout the studies, especially the dissertation research. Without their involvement and the confidence they placed in me, without the emotional and financial supports they granted, this endeavor would have been difficult. I would like to thank Dr. Leslie K. Guice for his technical comments on my research topics and the abundant references he provided. I also thank Dr. Barry L. Kurtz for the time he invested in reading and suggesting improvements to this dissertation. Thanks is also due to Drs. Richard Greechie and Norm Pumphrey, Jr. for their generous financial support.

I would like to thank Drs. Jessie C. Boot and John E. Gumbel for the inspirations I got from their pioneering work and discussions with them. Thanks also goes to the Trenchless Technology Center and Dr. Raymond L. Sterling for the experimental data they made available to me. I also appreciate the College of Engineering and Science for providing office space for me with both hardware and software necessary for the computational investigation through the joint effort of Drs. Nassar and Guice.

I appreciate the help and friendship from my colleague students who were also involved in the investigation of CIPP liner buckling, especially Jian Zhao, Xiaosheng Lu, Mark Stolkeld, and Shanyun Wang. I like to thank all my friends in Ruston, on and off campus, for their affections throughout my days at Louisiana Tech University.

I would also like to thank my wife, Ruiyuan Yang, for her continual support and tolerance of my lengthy devotion to the research. The last but not the least thanks go to my parents and parents-in-law, for their taking the utmost care of my son, Guanyun, to whom I owe a lot. Without their help, my study at Louisiana Tech University wouldn't have been possible.

CHAPTER 1

INTRODUCTION

Damaged sewer pipelines should be repaired to maintain the system efficiency and keep the groundwater clean. Traditional rehabilitation techniques require a huge amount of trench work and a long operation period, and often lead to inconvenience in traffic and the community.

In recent years, the development of trenchless techniques have made it possible to avoid the tedious and time consuming open-trench operations. Because most of the damaged sewer pipes are structurally sound, what needs to be done in rehabilitation is to resume water-tightness, i.e. stopping the sewer effluent leaking and avoiding the inflow of groundwater. This need can be met by the installation of a thin plastic liner inside the damaged sewer pipe segment to provide a separation between the sewer refuse and the surrounding environment.

1.1 The CIPP Technique

The Cured-In-Place Pipe (CIPP) technique can be employed to install plastic liners in damaged sewer pipes. The current practice is to invert a resin impregnated pipe relining into the damaged sewer segment and then heat it to let the liner cure in-place and take the shape of the pipe.

The actual loading condition applied to the installed liner may be quite complicated due to interactions and load transfers within the soil-pipe-liner system. Previous research and field applications suggested that the cracked pipe-soil system is usually strong enough to carry ground and traffic loads.

Therefore, the loads from the surrounding soil are mainly carried by the original pipes. The only significant loading on the liners is the external pressure resulting from the groundwater table. The liners should be designed to resist the sustained external pressure without a large deflection or even collapse (buckling) during the whole service period, which is usually set to 50 years.

1.2 Background and Research Need

It is known that slender or thin-walled structural elements are susceptible to buckling when the loads acting upon them give rise to compressive stresses. The reason is that when the cross-section is subjected to compressive dominant stresses, any deflection, whether due to initial imperfection or load eccentricity, will cause an increase in the bending moment which in turn will induce additional deflection. In the classical or instantaneous case, buckling occurs when a certain pressure (referred to as the critical pressure) is approached.

The buckling behavior of thin-walled cylindrical shells subject to external pressure was first studied in the late nineteenth century. The shell can often be treated as a ring due to the symmetry along the longitudinal direction. The buckling mode of a free ring is flattening of the ring, as shown in Fig. 1.1. A typical load-deflection curve is shown in Fig. 1.2, in which the critical pressure, based on an ideal initial geometrical

configuration, is demonstrated by a dashed line. It is shown in the figure that, when the critical pressure is approached, a small increase in load causes a disproportionately large deflection in the load-deflection curve. The critical load is found to be very sensitive to initial geometric imperfections.

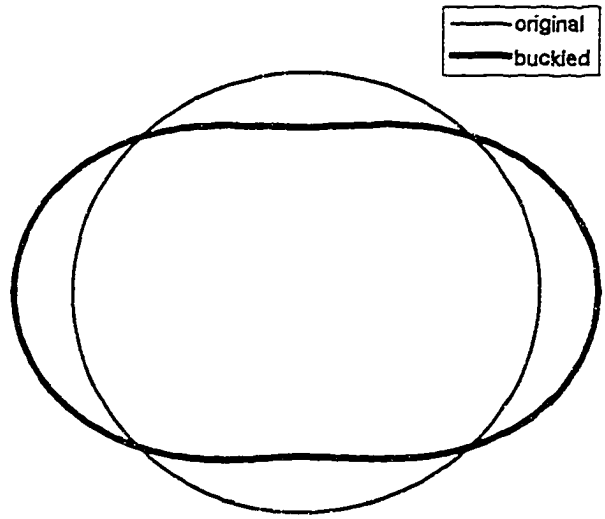

Fig. 1.1 Typical buckling mode for a free-standing pipe

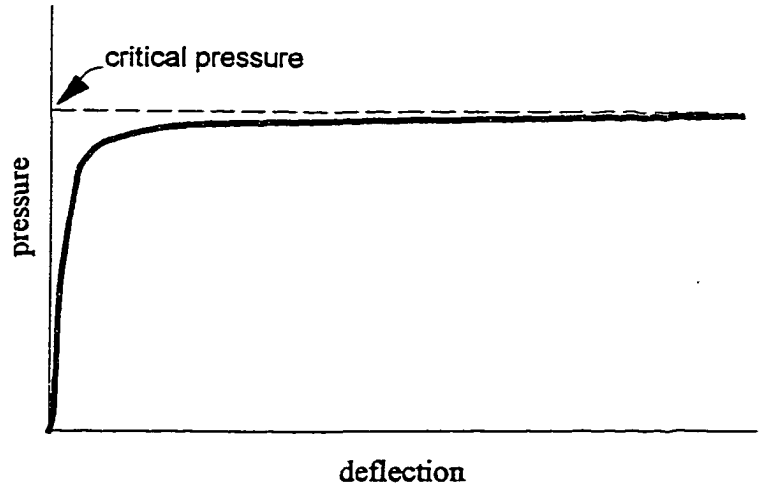

Fig. 1.2 Typical pressure-deflection curve for free pipe buckling

When a thin-walled cylindrical shell is confined within a rigid cavity, the shell's resistance to buckling may be enhanced drastically. This is because the flattening process prior to the final collapse is constrained, and thus provides a strong support to the shell. The enhancement effect is dependent upon the liner geometry characterized by the ratio of liner diameter to liner thickness. The critical pressure of a constrained liner with certain D/t ratios can be tens of times higher than that of a similar free liner.

Because of the deteriorated condition of the host pipe and of the limitations of the manufacturing and installation techniques, the actual fitting condition for CIPP will not be ideal. As such a gap will exist between the liner and the pipe. Considering that the support from the host pipe is important, any gap between the liner and the pipe may considerably reduce the contact area and thus the enhancement from the pipe. Therefore, in the case of constrained buckling, the magnitude and distribution of the gap is one of the most important factors. Similarly, the ovality of the damaged host pipe may also have a significant influence.

Since the global flattening of the liner is now constrained by the pipe, the characteristic buckling mode is also changed. A small portion of the liner cross-section will deflect inward, while the rest will sustain tight contact with the pipe (Fig. 1.3). This phenomenon will lead to high stress on the severely deformed portion and will cause plastic strain if the material yield limit is not high enough. Therefore, material failure (plastic yield) is more frequently involved in the buckling analysis of constrained liner than in free pipe.

The nature of buckling is mainly a structural phenomenon which is associated with a slim cross-section and compressive loading, but material properties may also be

highly involved. Conventionally, the total strain can be separated into an elastic and inelastic part. The inelastic part can be further decomposed into a time-independent (plastic) and time-dependent (creep) components. Creep refers to the phenomenon of a solid changing its shape over time even when the loads remain constant.

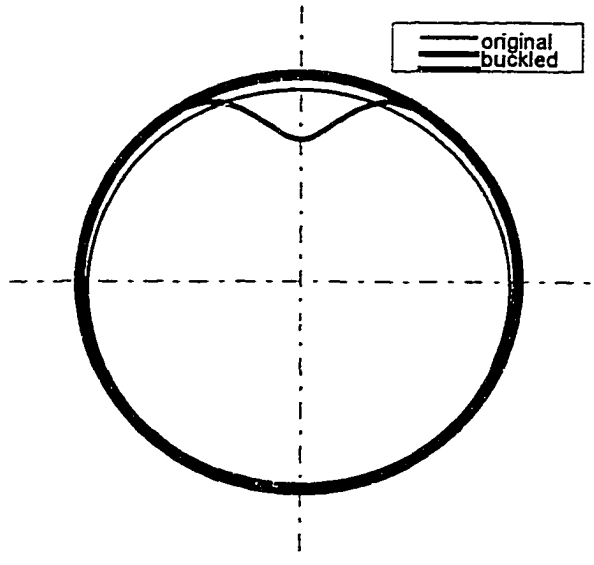

Fig. 1.3 Typical buckling mode for an encased pipe

If the structural material exhibits time-dependent (creep) behavior, the phenomenon of structural instability is quite different. Buckling can occur under any compressive load, however small, provided the load is sustained for a sufficiently long time. The mechanism is that any deflection will increase with time, thus increasing the bending moment which in turn increases deflection until eventually it leads to collapse. Therefore, in the context of creep-induced buckling, the time until buckling (usually referred to as critical time) is the most important feature to investigate.

Creep induced buckling has been observed to share numerous similarities with instantaneous buckling, including identical buckling modes. Therefore, it is not

uncommon to trace creep buckling analysis to knowledge obtained from the elastic or elastoplastic buckling.

As previously discussed, the problem of long-term behavior of constrained CIPP liners undergoing external hydrostatic pressure can be characterized as *time-dependent material deformation* (creep) induced *structural instability*, which is complicated by *contact* between the liner and the host pipe. These three major resources of nonlinearity determine that the problem should be solved with *finite displacement* formulas. Interactions among these nonlinear phenomena reflect the unique nature of the problem.

To provide answers to these questions, the following problems will be studied:

- Mechanical properties of CIPP materials.
- Short-term buckling of liners constrained in rigid host pipes, with emphasis on how initial imperfections influence the critical pressure.
- Creep induced buckling of constrained CIPP liners.

Each of these problems listed above has been studied individually by various investigators. The new challenge is to give a whole picture of the problem which clearly demonstrates the role of each factor and its interaction with other factors. Recent research has considered the effects of initial geometric configurations of liners and the enhancement resulting from the external constraints. However, the scope was actually limited to the prediction of the instantaneous buckling phenomenon.

1.3 Objectives and Scope

The primary objective of this research is to explore the theoretical background to the creep-induced buckling of encased cylindrical shells subject to external pressure by

means of finite element simulation. After the fundamental structural behaviors of encased cylinders are studied, a numerical investigation towards the durability prediction of CIPP liners under typical rehabilitation conditions will be carried out. Emphasis is focused on the effect of the creep phenomenon of CIPP materials on the long-term buckling behavior of the encased liner. Effects of other factors, including non-ideal fitting between the liner and host pipe and initial imperfections of the liner, will also be determined and quantitatively characterized.

A suitable model which can reflect all the important mechanical properties of CIPP materials should be established to fulfill the objectives of the research. The model will be formulated from the constitutive relationship observed from currently available material characterization tests. A representative CIPP material manufactured by Insituform Technologies, Inc. is used to generate input data for the numerical investigation, because the mechanical properties of that material have been extensively studied. The complete database includes information from both material and physical tests, under instantaneous and up to 12,000-hour long-term testing conditions. Although a specific material is used, the methodology can be used also for other materials. It is assumed that the trends discovered here can be generalized to other CIPP liners.

The finite element technique is chosen to provide the necessary solution procedures. With the aid of a sophisticated finite element package, ABAQUS, the intrinsically nonlinear problem can be handled with ease, so as to focus on the simulation of long-term behavior of the encased liners, in which we are most interested. The constitutive relationship mentioned above is incorporated into the finite element model by using an original combination of capabilities available in ABAQUS.

The scope of the study is limited to the assumptions that the host pipe can resist the traffic and top soil loads and that the shape of the host pipe has remained circular or slightly oval. The only load acting on the liner is the hydrostatic pressure due to the underground water table. A ring model is considered adequate to represent thin-walled liners under the conditions being considered.

The buckling behaviors of encased CIPP liners are investigated in order to reveal the characteristic buckling modes and the effects of geometric and material parameters on the critical pressure and critical time, under short- and long-term loading conditions, respectively. Results are compared to experimental observations to verify the validity of the models.

A parametric study is then carried out to investigate the effect of each of the selected factors on the buckling time of the liner. This step is significant to the thorough understanding of long-term behavior of CIPP liners. As will be discussed in detail in the following chapters, critical pressure (in short-term buckling) and critical time (in long-term buckling) are related to the selected factors via nonlinear relations. In physical tests, these parameters cannot be accurately measured and hence exact predictions of critical pressure and critical time are not possible. Precisely controlled tests can only be conducted numerically to isolate one factor from another so as to understand the role each factor plays. Inadequate knowledge in this aspect can be regarded as the main reason for poor understanding of duration prediction of CIPP liners.

CHAPTER 2

BUCKLING OF THIN-WALLED PIPE LINERS

CIPP liners installed in deteriorated sewer pipes are susceptible to buckling under external hydrostatic pressure. The primary concerns of the present study are focused on the long-term buckling behavior of encased liners subject to sustained pressure in which the time-dependent deformation of the polymeric material is the driving force for the final collapse. This chapter is intended to give a brief review of previous research efforts upon which the present study has been based. The scope is focused on fundamental buckling theories for thin-walled cylinders encased in rigid cavities and on the factors influencing accurate prediction of the buckling resistance.

2.1 Overview

In light of the present interest, the buckling problems concerning cylinders subject to external pressure can be classified into four categories as shown in Table 2.1, with pioneering research work in each of the categories listed.

A thin-walled cylinder is a standard structural element widely used in various applications. In designing such a structure, the instability criterion should be emphasized in addition to stress verifications, because it may fail by losing its desired configuration under

loads inducing compressive hoop stresses before (or soon after) the allowable stress is reached.

Table 2.1 Classification of buckling of thin-walled cylinders

	Instantaneous Buckling	Creep-Induced Buckling
Free-Standing	Fairbairn (1858) Bresse (1866) Bryan (1888)	Sundstrom (1958) Hoff (1959) Ellington (1960)
Constrained	Amstutz (1950, 1953) Glock (1977)	Welch (1989)

Fairbairn (1858) was recognized as the first investigator of the buckling of steel pipes subject to external pressure. His experimental results revealed that the buckling pressure was influenced by two characteristic geometrical parameters: pipe length and the ratio of diameter to wall thickness. Since then, buckling has been regarded more of a *stiffness issue* than a *strength issue*.

Bresse (1866) was probably the first to give an analytical solution to the buckling pressure which is still used in current design practices. In his solution, derived by using a small deflection theory, the buckling pressure was expressed in terms of the elastic modulus E, and two parameters representing the geometry of the cross-section of the pipe, the mean radius R, and the moment of inertia I.

$$P_{cr} = \frac{3EI}{R^3} \tag{2.1}$$

The length effect does not appear explicitly in Eqn. (2.1), yet the equation reflects the extreme of a very short pipe, for which the assumption of plane stress is appropriate. On the other hand, a similar solution for a very long pipe was given by Bryan (1888) by employing the minimum potential energy criterion, as

$$P_{cr}^{CL} = \frac{2E}{(1-\nu^2)}\left(\frac{t}{D}\right)^3 \qquad (2.2)$$

where the effective modulus $E/(1-\nu^2)$ was used to assume the plane strain condition of an infinitely long pipe.

Many factors can deviate buckling pressures observed in real structures away from theoretical predictions. Among those factors, imperfect geometric configuration represented by the out-of-roundness (or ovality) of the cylinder is of most concern, because the characteristic deflection pattern (or the first-order buckling mode) of a free-standing pipe is oval in shape (Fig. 1.1).

Material failure is usually of little importance when the pipe is free from external constraints, since buckling will occur before the yield strength is approached for typical dimensional ratios common to engineering structures.

2.2 Buckling of Pipe Liners

Buried pipes and linings to waterway tunnels or sewer pipelines are typical examples of cylinders whose outward deflections are constrained. The corresponding static and buckling analyses are intrinsically nonlinear contact problems.

The support from the surrounding soil to buried pipes works like an elastic foundation. The wall will move backward with the outward deflection of a buried pipe but has no effect on the inward movement, as was assumed by Cheney (1971). On the other hand, the constraint (from rocks or concrete sewer pipes) to a liner could be considered as a rigid wall, which allows for no outward deflection.

The buckling resistance of steel linings subject to hydrostatic pressure induced by

infiltration through cracks in rocks and concrete grouts or overpressure during grouting was studied by a number of investigators throughout the world for over three decades since Amstutz published his pioneering work in 1950 and 1953. Results from these studies, which relate to the prediction of instantaneous buckling of CIPP liners, are reviewed in this section.

It was not a surprise to see that quite a few distinct characteristics had been revealed in these studies that distinguish the buckling behavior of a constrained liner from that of a free-standing pipe. Liners' resistance to buckling is enhanced drastically due to the support from the rigid wall. The ratio of the critical pressure of a constrained elastic ring to the classical critical pressure of a free ring

$$K = P_{cr} / P_{cr}^{CL} \tag{2.3}$$

is usually referred to as the enhancement factor. The enhancement is influenced by three major factors which are addressed in the following sections.

2.2.1 Buckling Modes

When a pipe is constrained externally by a rigid wall, the well-known two-lobe buckling mode as shown in Fig. 1.1 becomes impossible. Furthermore, the eigen-analysis approach to the solution of critical pressure and buckling mode is not applicable because of the nature of the contact problem.

Early attempts to the solution of this problem did not have "a sound theoretical basis" (Yamamoto and Matsubara, 1982). Vaughan (1957) and Borot (1957) assumed that the liner will buckle into a uniform sinusoidal wave around the circumference (Fig. 2.1). It was pointed out by McCaig and Folberth (1962) and by Yamamoto and Matsubara (1981)

that this assumption may lead to overestimation of a liner's critical pressure. According to the Canadian engineers (McCaig and Folberth, 1962), Amstutz (1953) "assumed more correctly" that "a single lobe would form in one particular spot," and the shape of the buckled portion was again a sinusoid wave around a mean line with a new mean radius (Fig. 2.2). Amstutz's model gave considerably lower critical pressure predictions than those of Vaughan and Borot. The validity of his model was checked against field data from 14 successful and failed installations by McCaig and Folberth (1962), and against a specially designed laboratory test by a Swiss engineer (Ullmann, 1964). Just as Amstutz assumed, a single lobe mode was observed in Ullmann's test, which formed "near the welding seam where a 4mm deep depression was observed before the test."

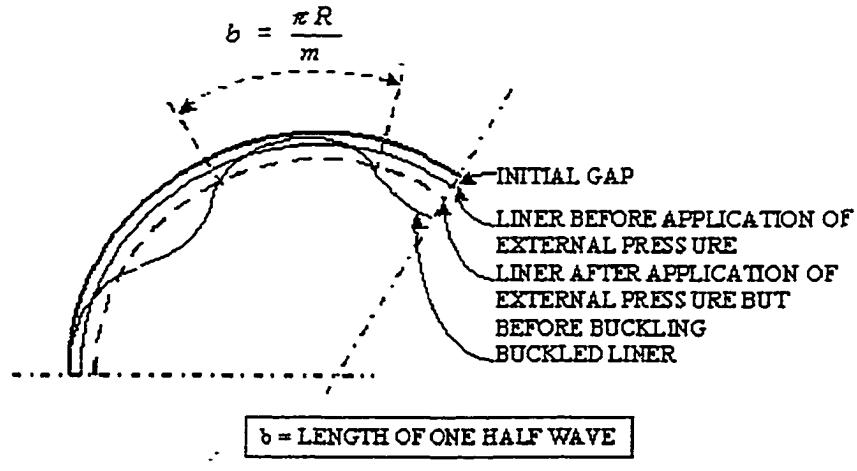

Fig. 2.1 Schematic of model used by Vaughan (1957) and Borot (1957)

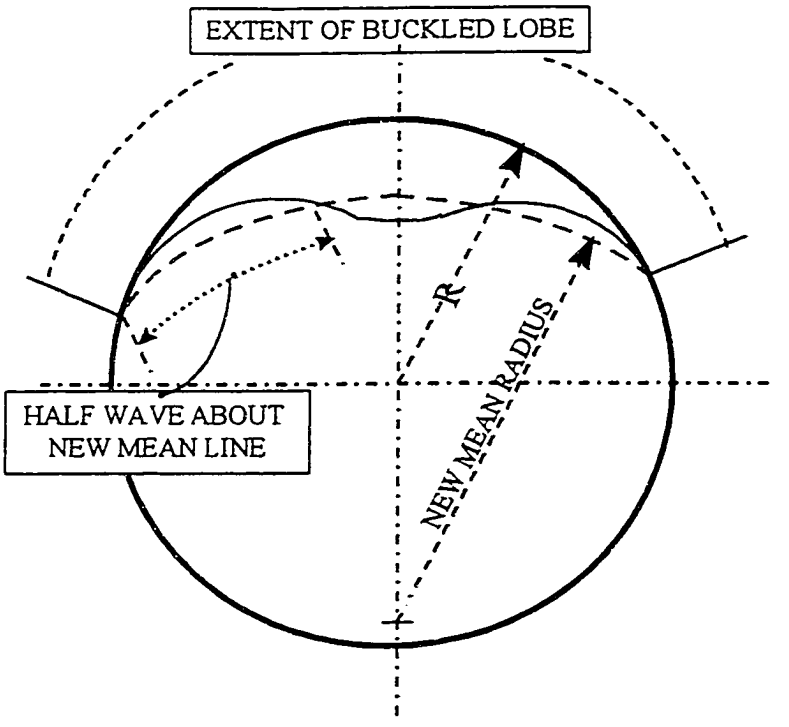

Fig. 2.2 Schematic of model used by Amstutz (1950, 1953)

Glock's Model. The first theoretically sound model for the buckling of a steel liner was derived by Glock (1977), who also adopted the one-lobe mode which was widely accepted at his time by researchers of liners and of buried pipes (Cheney, 1971). In Glock's analysis, the radial deflection in the buckled portion was assumed to have the functional form

$$u = u_0 \cos^2\left(\frac{\pi\theta}{2\phi}\right) \tag{2.4}$$

in which 2ϕ denoted the deflected region (Fig. 2.3). The steep shape of the deformed liner may reflect the post-buckling deflection pattern of a constrained liner better than a sinusoid does. By employing the principle of minimum potential energy and assuming a linear elastic stress-strain relation throughout the buckling process, Glock gave a concise

solution in a similar form to Timoshenko's equation

$$P_{cr}^{G} = \frac{E}{(1-\nu^2)}\left(\frac{t}{D}\right)^{2.2} \tag{2.5}$$

According to Omara et al. (1997), the exponent 2.2 has been repeatedly derived under different constrained buckling problems by several authors (shrink buckling of rings by Chicurel (1968); buried pipe buckling by Cheney (1971); and rings encased in a rigid wall by Glock (1977)), even though quite different assumptions of deflected ring profiles were used.

Based on Glock's solution, the enhancement factor can be determined from Eqns. (2.5) and (2.1), as

$$K^{G} = \frac{1}{2}\left(\frac{D}{t}\right)^{0.8} \tag{2.6}$$

This factor is much higher than 1 for the dimension ratios (D/t) commonly used in engineering applications. Since a pipe liner is subjected to higher pressure than a free standing pipe can resist, the yield strength may be reached before the onset of buckling. Therefore, Glock's model, which is based on a purely elastic relationship, may overestimate the buckling resistance of liners. Another reason for overestimation is that the model does not take into consideration any imperfections in the initial ring-wall configuration.

2.2.2 Material Failure

The effect of material failure was first addressed by Amstutz (1969), who stated that the yield limit might be reached first in an outer fiber (in the compressive side) at the

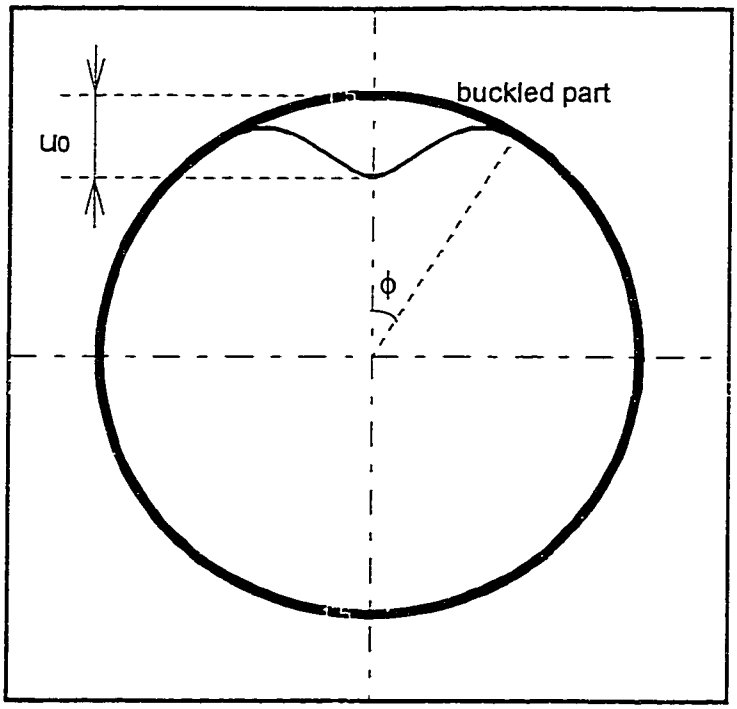

a. predefined deflection pattern

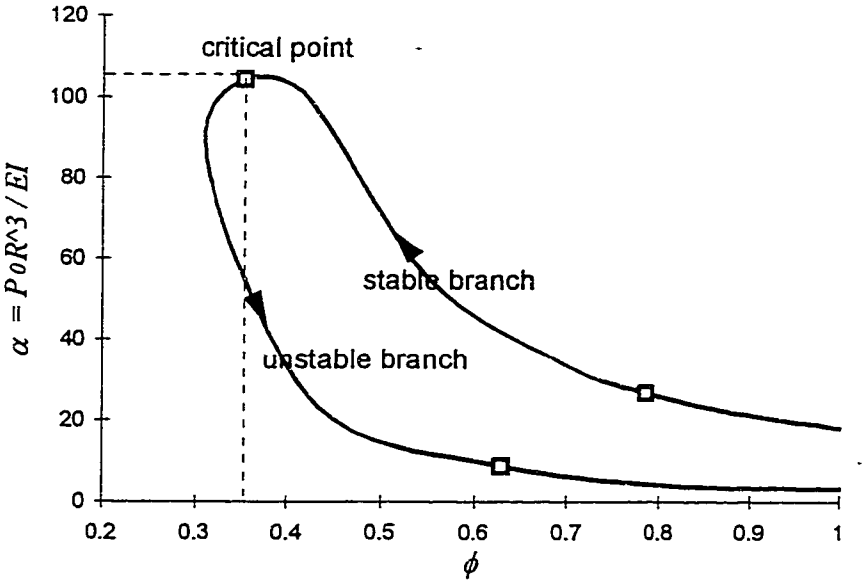

b. pressure-deflection curve

Fig. 2.3 Schematic of model used by Glock (1977)

spot where the maximum deflection occurs. This argument was supported by Ullmann's (1964) test, although not explicitly stated in his paper. From the pressure-stress data measured on the internal surface of the sample liner (Fig. 2.4), one can trace that the liner collapsed soon after the compressive stress exceeded the yield limit of 400 MPa at node 11. (From a simple calculation, the compressive stress at node 10, that is, on the outer surface of the liner where strain gauges could not be applied in an external pressure test, should have exceeded the tensile yield limit.) This consideration was later supported by a numerical investigation conducted by Yamamoto and Matsubara (1981).

2.2.3 Effects of Annular Spacing or Gap

The effect of annular spacing or gap between the steel liner and the waterway tunnel were included in models proposed by Amstutz, Vaughan, and Borot. It was common knowledge to the tunnel engineers that "The smaller the gap, the greater the critical external pressure on buckling" (McCaig and Folberth, 1962). Although grouting was normally performed to minimize the undesirable effect, the existence of gap was actually unavoidable even under laboratory condition (Ullmann, 1964).

The effect of gap on a liner's critical pressure is difficult to quantify by the classical approaches discussed earlier, especially when elastoplastic behavior is taken into account. This problem was not satisfactorily resolved until Yamamoto and Matsubara conducted their series of numerical studies in early 1980's.

Yamamoto and Matsubara's Study. A finite element analysis was reported by Yamamoto and Matsubara (1981) in which both gap (distribution as well as size) and material nonlinearity were taken into account, and there was no need for a pre-defined

liner deflection pattern. The pressure under which a liner buckles was referred to as the *ultimate pressure* (instead of the conventional term, the *critical pressure*) to emphasize the elastoplastic solution obtained from a nonlinear load-deflection analysis.

By taking advantage of convenient geometrical modeling capabilities provided by the finite element approach, Yamamoto and Matsubara considered three typical gap distribution patterns: initial deflection (or more precisely, imperfection), even, and uneven gaps (Fig. 2.5). For a given yield strength of 235 MPa, the ultimate pressure predictions were given in a dimensionless format $P_{cr}R/Et$ over a representative range of liner-tunnel configurations characterized by the radius thickness ratio (R/t) and the dimensionless gap (maximum gap/radius). In this paper they concluded that

1) The liner buckles into a one-lobe mode in the *uneven gap* and *initial deflection* cases, whereas it buckles into a two-lobe in the *even gap* case.
2) For a given R/t value, the enhancement factor K (as defined in Eqn. 2.5) decreases with an increase in gap.

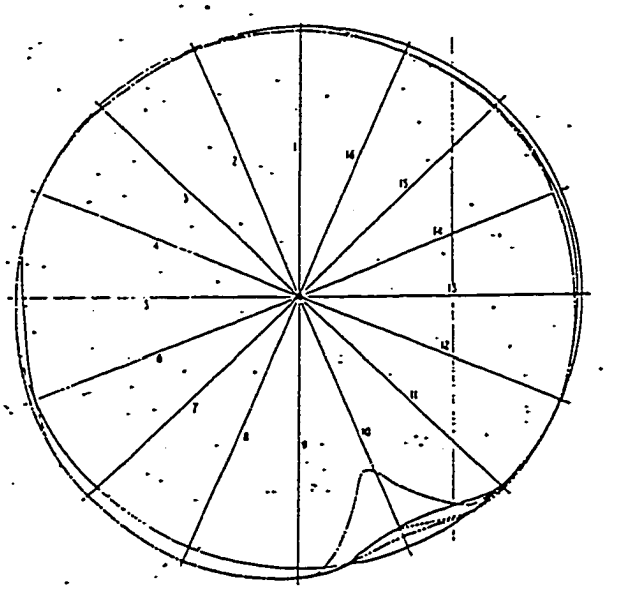

Fig. 2.4 Ullmann's (1964) test results

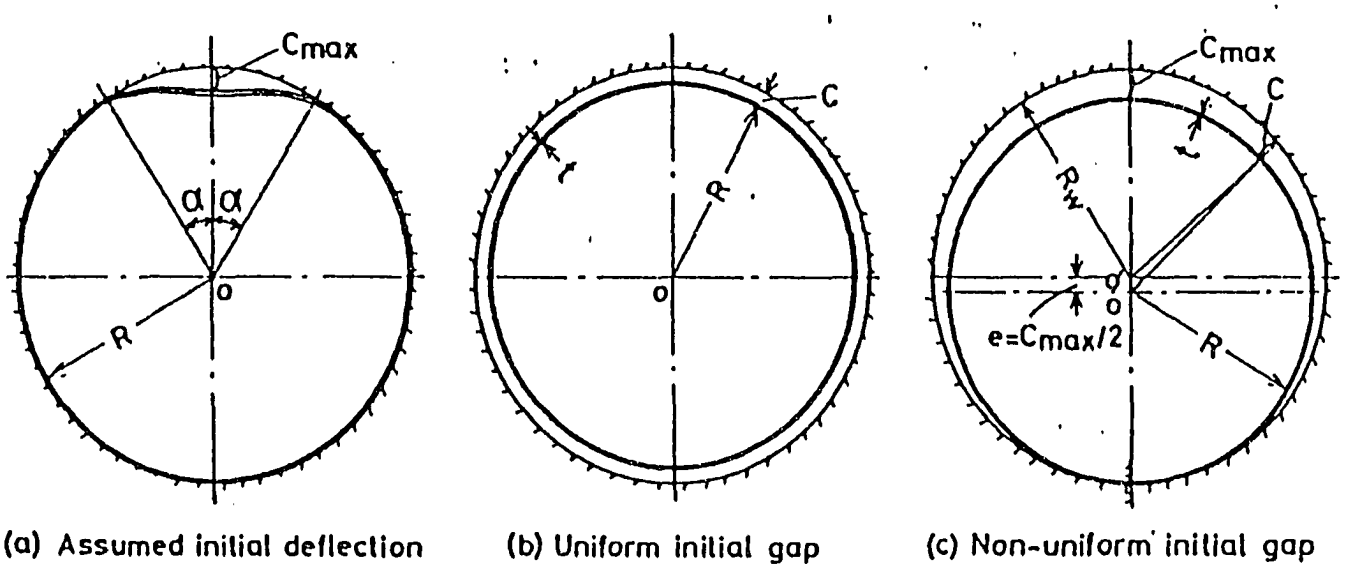

Fig. 2.5 Schematic of models used by Yamamoto and Mastubara (1981)

3) For a given gap/radius ratio, K increases with an increase in R/t ratio.

4) The critical pressure associated with one-lobe mode deflection (under uneven gap) was lower than that associated with two-lobe buckling mode (under even gap), provided the total gap is the same. Therefore, predictions by using the one-lobe mode were proposed to be used for practical purposes.

5) The effect of plastic yield is significant in the cases of even (when gap is small) and uneven (when gap is large) gaps, and not significant for the case of initial deflection.

2.3 Creep-Induced Buckling

As is pointed out in Chapter 1, the fundamental difference between classical and creep-induced buckling is that, in the classical case, instability occurs when the increasing load reaches a certain value (critical load), whereas in creep-induced buckling, time is the driving force. A structural element whose material creeps will buckle under a sustained load (usually lower than the classical critical value) when a finite critical time is reached.

Early studies (as reviewed by Hoff, 1958, and Gerdeen and Sazawal, 1961) emphasized that a finite critical time exists only when the creep strain rate is a nonlinear function of stress. Otherwise, critical time becomes infinitely large. This restriction may not hold when the effects of stress redistribution and maximum allowable displacement are taken into account. Fortunately, the empirical creep laws for commonly used engineering materials such as metals and polymers are usually nonlinear, as will be discussed in Chapter 3. Therefore, this fact makes it possible to accept the following intuitive assumptions (adapted from Hoff, 1958):

1) A structural element will not buckle when no compressive load is applied.

2) A structural element will buckle instantaneously when the *critical load* is applied.

3) When a compressive load smaller than the critical value is applied, an element whose material creeps will buckle when a finite critical time is reached (provided the loading is continuous).

4) A greater load will correspond to a shorter critical time, and vice versa.

Despite of the difference mentioned above, creep-induced buckling has been observed sharing numerous similarities with its classical counterpart, among which the most important aspect is the identity between the creep and instantaneous buckling modes (Sammari and Jullien, 1995). Therefore, it is not uncommon to trace creep buckling analysis to the knowledge obtained from the elastic or elastoplastic analysis.

Just like instantaneous buckling, creep buckling is also highly sensitive to initial imperfections in structure geometry, because any initial deflection in a structural element will increase with time, which directly increases the bending moment (or internal stresses). The increase in stress in turn increases creep rate and hence deflection, until the structural element eventually collapses. Because of the nonlinear stress-creep strain rate relation, the effect of initial imperfection in a creep buckling problem may be much more serious than that in a similar instantaneous buckling problem.

Another analogy between creep and instantaneous buckling includes the concept of critical deformations, e.g. critical strain and critical deflection. Gerard (1956) conjectured that an initially perfect column could first buckle under the creep process when the total strain is the same as the (critical) *strain* at which it would buckle under the classical critical load with the absence of creep. This conjecture was proved not to be generally valid by Hoff (1958). Hoff then suggested in the same paper that the most realistic

approach should be based on the critical *deflection* of a column under instantaneous loading, which can be calculated by using the realistic (non-linear) stress-strain relation of the material. Critical time could then be determined by the time needed to reach the *critical deflection*, based on realistic creep data of the material. However the two concepts may not seem much different from a practical standpoint. Some simplified methods based on the critical strain concept were claimed to give good predictions (Chern, 1978), while others were not as satisfactory (Menges and Gaube, 1969).

Pipes Subject to External Pressure. The creep buckling of (free-standing) cylindrical shells under uniform external pressure was first investigated by Sundstrom (1957), but a later study by Hoff's et al. (1959) based on a sandwich model had more influence on later studies. In the sandwich model, an outer and an inner sheet is used to resist the hoop stress and an undeformable core annulus is used to support the shear stress. The effect of elastic deformation was neglected, except for the calculation of the initial deformation as the result of loading. Bargmann (1972) modified the method by including elasticity throughout the analysis. Ellington (1960) employed the principle of potential energy, which allowed him to take into account the elasticity and a linear stress distribution through the pipe wall. These methods gave explicit solutions, yet were restricted to the use of the Norton-Bailey type creep law

$$\dot{\varepsilon}^{CR} = A\sigma^n t^m \tag{2.9}$$

Nishiguchi et al. (1990) made a further improvement by allowing the incorporation of general formed creep laws into the calculation. The only assumptions employed were the linear strain distribution in the pipe wall and a quasi-elliptical cross section

characterized by a single shape factor adopted from Hoff et al. (1959). Nonlinear stress distribution through the wall of the tube was allowed, and the growth of the displacement field was represented by the change of the shape factor with time governed by an ordinary differential equation. A numerical procedure, such as the Euler's method, was necessary to solve the problem incrementally.

Finite element approaches were frequently used in more recent investigations (Heller and Anderson, 1984; Nishiguchi et al. 1990; Sammari and Jullien, 1995; Kaji et al., 1996; Koundy et al., 1996; Eslami and Shariya, 1997), mainly because of the powerful nonlinear solution capabilities provided by the finite element models. These capabilities have been found essential in incorporating specific creep laws and factors like geometric imperfections, so as to accurately predict critical time.

2.4 Buckling of CIPP Liners

The instantaneous buckling of CIPP liners was first tested by Aggarwal and Cooper (1984). From 49 specimens with *D/t* ratios ranging from 30 to 90, they found that the enhancement factors varied from 6.5 to 25.8. These observations were used as the foundation to the practically used ASTM (1993) design guideline in which an enhancement factor of 7 is recommended for any liner where a "tight fitting" is available.

A number of experimental and analytical studies on the structural behavior of constrained CIPP liners has been carried out since the late 1980's (Boot and Welch, 1989; Welch, 1989). The following methodology used by Boot and Welch (1989) and by Shotton and Boot (1995) represents a state-of-the-art approach for the study of CIPP liners during the past decade.

1) Determination of the long-term constitutive behavior of CIPP material over a fifty year period.
2) A series of short- and long-term buckling tests to (a) assess the imperfection sensitivity, and (b) calibrate the mathematical model.
3) Development of a mathematical model suitable for predicting liner behavior subject to long term creep under external pressure in order to achieve a rational design criterion.

2.4.1 Material Characterization

Various polymeric materials have been used in commercial CIPP products and related experiments, including polyester, polyvinyl chloride (PVC), vinyl ester, epoxy, and polyurethane. Polyester seems the most widely used. Five out of the seven products studied in the long-term tests by Guice et al. (1994) were made of polyester.

An InsituForm product, *Insituform Enhanced*, using an unsaturated polyester (UP) resin has been studied by several research groups. The standard quasi-static tests on this product were first reported in Guice et al. (1994). The classical linear elastic-perfectly plastic behavior was observed, and the material failure was characterized by stable fracture accompanied with a "creaking" sound. The elastic modulus determined from bending test was considerably lower than that by tension test whereas the ultimate strength in bending was more than twice the tension strength. By employing a four-point bending apparatus and larger specimen depth than recommended in ASTM D 2990-77, Boot and Javadi (1998) minimized the difference between axial and "flexural" moduli observed by Guice et al. (1994) and verified other observations.

Welch (1989) was the first to study the time-dependent behavior of polymeric

materials for liner life prediction by using a polyurethane (PUR) resin. Similar tests for the Insituform UP resin were conducted by Lin (1995) under tension, compression, and bending conditions for 3,000 hours, and continued by Mahalingam (1996) to 6,000 hours under bending. Torsion tests were also included in a more comprehensive characterization program by Boot and Javadi (1998). It was observed in the tests that the materials crept at different rates under different stress states. As for the Insituform resin, the creep rates descended in the following order: tension, flexural, and compression.

To adopt creep data obtained in the first several thousands of hours to the design life span of 50 years, various extrapolation techniques have been discussed by these investigators. High temperature tests were proposed by Hall et al. (1997) to accelerate creeping so as to reduce the test period.

2.4.2 Buckling Tests

A series of 10,000-hour buckling tests were conducted at the Trenchless Technology Center (TTC) at Louisiana Tech University (Guice et al, 1994.; TTC, 1998b). Short-term tests were conducted at TTC (1998a) and elsewhere (Welch, 1989; Lo et al., 1994, Javadi and Boot, 1998) for better knowledge of constrained buckling.

Various commercially available CIPP products were evaluated by Guice et al. (1994). The diameter-thickness ratio was in a range of 30 to 70, and the load ratio, which is the ratio of the sustained pressure to the critical pressure observed in the instantaneous test, was in the range of 40% to 80%. Results of linear regression analyses, which correlated the external pressure to the buckling time, suggested that the ratio of long-term to instantaneous critical pressure would be in the range of 34% to 46%. Wide variations

were observed in times to buckling, to which thorough theoretical explanations are needed.

The failure mechanisms of the *Insituform Enhanced* liners under short- and long-term conditions were very similar: "a sudden 'dimpling' of the liner" (at a certain spot near the mid-span) initiated with "some 'creaking' sound, indicating large deformations of the material" (Guice et al., 1994). Leaking might be noticed during or after snap-through (TTC, 1998c). By using a different test setup, in which liners were not clamped at the ends, Welch (1989) observed that the failure would start at both ends of the specimen and propagate to the center. For liners installed in the field, both failure mechanisms may occur, depending upon specific deterioration modes of their host pipes (as classified in WRC, 1993). For the cases of a *hole* (H) or a *circumferencial crack* (CC) near the mid-span, the liner may buckle in the middle whereas for the case of a *longitudinal crack* (CL), buckling may be initiated near the ends.

The deflected profiles of liners were also measured in tests by using LVTD's (Welch, 1989; TTC, 1998a). Typically, a liner deflected in a two-lobe mode which was roughly symmetric along a certain unpredictable direction. In most cases, a liner would collapse into a one-lobe mode (as also observed in Ullmann's (1964) steel liner test), with one dominant lobe snapping through while the opposite lobe was being released partially or completely (TTC, 1998a). Occasionally, there would be one liner which buckled into the one-lobe mode right away (Boot and Welch, 1996; TTC, 1998a).

Deteriorated sewer pipes may lose their original circular shape. The effect of host pipe ovality on liner resistance were also tested by Welch (1989), and Hall (1998a). Results showed that the effect was significant. The gap between a liner and its host pipe was also

measured by using feeler (Guice et al, 1994), or, more preferably, by measuring the volume of the annular spacing (TTC, 1998a).

However, geometrical factors are usually hard to control in manufacturing and are even difficult to detect accurately. As an example, the variation in the thickness of a liner (according to test records, e.g., Omara, (1996)) could be as high as $\pm 15\%$ of the mean thickness value.

2.4.3 Analytical and Numerical Studies

Welch (1989) is the only reference, known to the author, who conducted a creep buckling analysis of constrained cylindrical shells. A finite element approach was employed, which could handle the rigid wall constraint and large displacement. The liner was modeled with two-node beam elements. Because different mechanical properties were found in CIPP materials under different loading conditions, the flexural and axial deformations were treated separately, with incorporation of specific creep properties characterized from tests. The critical time was predicted for a given nominal liner diameter and thickness and external pressure. Design curves were then plotted for the design pressure corresponding to a design life of 50 years.

The two-lobe buckling mode was assumed to reflect the typical deflected shape of the liner observed in the accompanying short-term tests. Although the plane stress assumption which gave the lower bound predictions was employed, the numerical estimations to the buckling pressure were slightly, yet consistently, higher than the test results (Boot and Welch, 1996).

An analytical modeling of collapse resistance of CIPP liners was conducted by Lo

and Zhang (1993) focusing on the effect of radial gap between the encased liner and its host pipe. The elastic solution to a clamped shallow arch under uniform pressure (Timoshenko and Gere, 1961) was adopted and the critical pressures (in terms of the enhancement factor) of an encased liner associated with one- and two-lobe modes was determined by an iterative numerical procedure. They concluded that the enhancement factor is "simply a function of the gap size ratio," i.e. gap-size/host-pipe-radius, and is almost free from the geometry of the liner-pipe system. In this context, the gap size Δ was the sum of the initial gap Δ_1 (induced by contraction due to temperature drop after the curing process) and the gap increase Δ_2 (induced by hydrostatic pressure during the test). When correlating the analytical predictions to observed buckling pressures reported in Lo et al. (1993), a good agreement was found as shown in Fig. 2.6: test data scattered within and all over the range bounded by the lower and higher extremes predicted by the one- and two-lobe modes, respectively.

Based on analyses of experimental buckling pressure data obtained by Aggarwal and Cooper (1984), Lo et al. (1993), and Guice et al. (1994), Omara et al. (1997) suggested that the critical pressure of a constrained liner can be related to the *D/t* ratio as follows

$$P_{cr} = \frac{aE}{(1-\nu^2)}\left(\frac{t}{D}\right)^m \qquad (2.10)$$

The fitting parameters a and m, obtained by a regression analysis of Aggarwal and Cooper's data, were determined to be 1.07 and 2.17, respectively, which were very close to 1.0 and 2.2 as in Glock's equation (2.5).

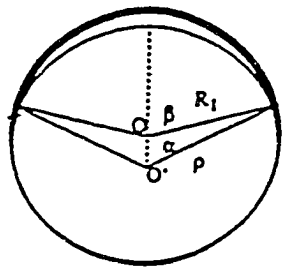

a. Asymmetrical mode

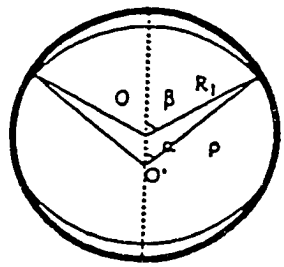

b. Symmetrical mode

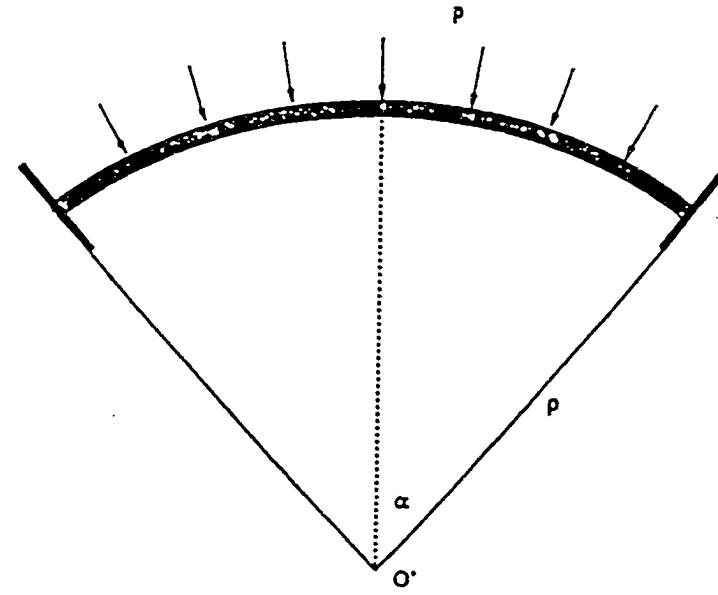

c. A clamped circular arch model

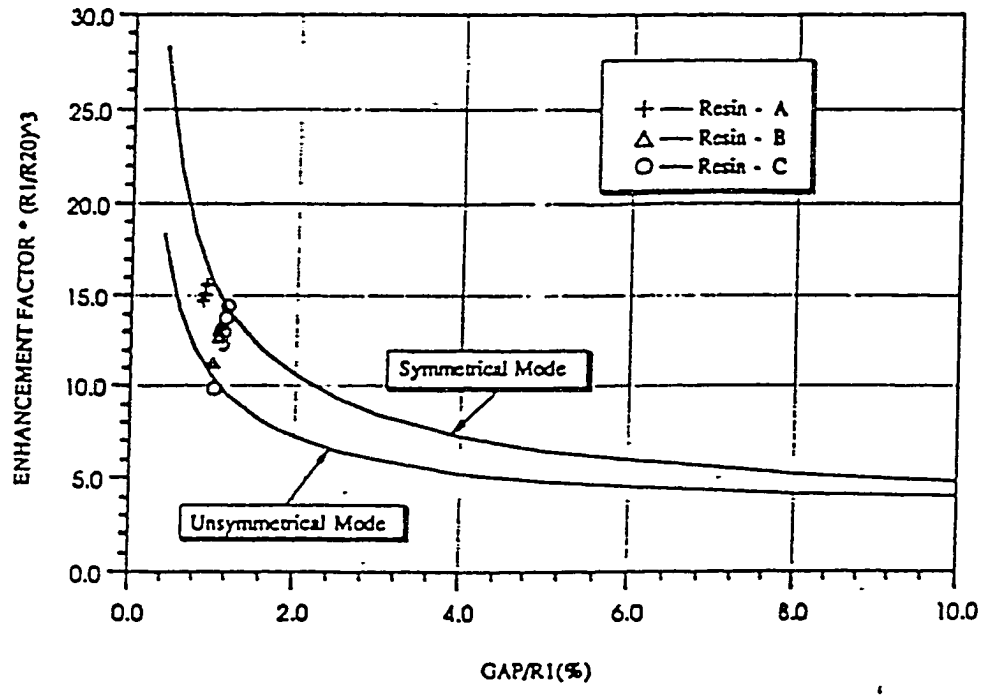

d. Predicted versus buckling test results

Fig. 2.6 Schematic of model used by Lo and Zhang (1993)

El-Sawy & Moore (1997) investigated the effect of liner geometry and imperfections on liner buckling strength. Parametric studies were conducted to quantify the effects of liner diameter to thickness ratio, initial liner imperfection (defined as a wavy intrusion), loose fitting (uneven gap) between a liner and its host pipe, and ovality of host pipe. Empirical formulae for reduction factors accounting for various imperfections were proposed to be used in design practices.

More practical considerations were included in Falter (1997) which may be important in a rehabilitation design. Criteria based on both material failure and structural stability requirements were emphasized to be consistent with bursting failures observed in buckling tests conducted by Wagner (1992). The snap-through pressure of an encased liner was given by multiplying reduction factors concerning initial imperfection and initial gap with the Glock's solution. His reduction factors, adopted from parametric studies conducted earlier (Falter, 1994), led to very conservative predictions of test results reported by Boot and Welch (1996).

2.5 Summary

Unique features of constrained creep buckling of CIPP liners are highlighted by a structural instability problem, which is entangled with liner-hostpipe interactions and complex creep behaviors of polymeric materials. Research interests in this problem have been invoked by the demanding needs for this advanced rehabilitation technique during the past 15 years. However, theoretical models appropriate for liner life prediction are still yet to come.

As can be concluded from the brief review of existing approaches to similar

problems, a closed-form analytical solution, which considers all sources of nonlinearity arising from both material and geometrical aspects, is very hard to realize. Therefore, a numerical approach is considered appropriate in the current study. The philosophy is to conduct numerical simulation so as to reveal the fundamental structural behavior of constrained CIPP liners subject to external pressure and to quantify the effects of different factors discussed in this chapter. From these simulation results, models for accurate and efficient prediction of CIPP liner life can be established.

CHAPTER 3

MECHANICAL PROPERTIES OF CIPP MATERIALS

In this chapter, the mechanism and mechanics of material properties of cured-in-place plastics will be discussed, with close reference to a typical commercial product, Insituform Enhanced (polyester) resin. After explaining test observations available at the TTC and from other resources via a contemporary material science point of view, a visco-elastoplastic constitutive model appropriate for CIPP liner short- and long-term buckling analysis will be presented.

It is common knowledge that the mechanical behavior of polymers is greatly influenced by temperature. The normal ambient temperature, under which the material was characterized and the liner will be working, will be used as default throughout this chapter and the whole dissertation. The temperature effect will therefore not be mentioned in the sequel for simplicity.

3.1 Thermosetting Polymers Formed by Curing

The formation of thermosetting plastics by means of curing usually takes a two-stage reaction. In the first stage, the starting materials (usually two or more monomers) are inter-combined to form a resin, which contains the high polymer molecules with a

heterochain structure. In the second and curing stage, an additional monomer called curing agent is added into the liquid resin to crosslink the original chain-like polymer molecules into a random network. The preparation and curing of unsaturated polyesters are illustrated in Fig 3.1 (as quoted from Hall, 1981)

Once set by heating, the crosslinked structure cannot be melted and exhibits a good stiffness and resistance to creep. These desired qualities make polyester popular in sewer rehabilitation applications.

Because of the irregularity of the random molecular structure, the cured polyester behaves more like an amorphous substance than crystalline polymers. Unfortunately, the mechanical behavior of thermosetting polymers is "rather nondescript" (Courtney, 1990), and the mechanisms are usually poorly understood. The uncertainty of the concentration and configuration of the crosslinked structure may contribute to the differences of mechanical properties of materials from different batches, which makes the problem even more complicated. However, network polymers actually possess some mechanical characteristics common to many long-chain polymers, such as linear elasticity and viscoelasticity at ordinary temperature. Imagining a mixture of amorphous and long-chain mechanisms co-resident and competing to each other will help to understand the unique features of thermosets (or CIPP materials).

3.2 Time-Independent Properties

Conventionally, the total strain is divided into elastic (recoverable) and inelastic (permanent) components. The inelastic portion can still be divided into plastic (time-independent) and creep (time-dependent) parts. The classification can be expressed as

Typical starting materials:

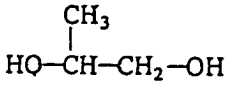

propylene glycol

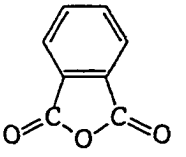

phthalic anhydride

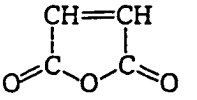

maleic anhydride

We represent these molecules by the symbols

Polymerisation produces a linear unsaturated polyester with a structure like this:

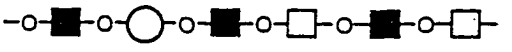

The addition of a vinyl monomer such as styrene makes a liquid resin which can be crosslinked by a free-radical initiator (*curing agent*)

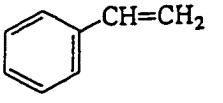

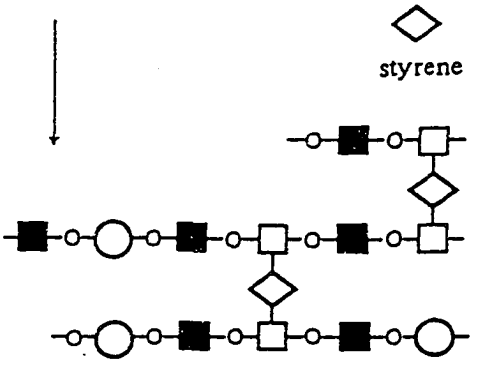

styrene

Schematic crosslinked polyester structure

Fig. 3.1 Crosslinked polyester formed by curing
(From Hall (1981), Table 1.9)

$$\varepsilon^T = \varepsilon^E + \varepsilon^I \tag{3.1}$$

$$\varepsilon^I = \varepsilon^P + \varepsilon^{CR} \tag{3.2}$$

The elastoplastic behavior is discussed in this section, while the creep phenomenon and pertinent numerical models are to be discussed in the section that follows.

3.2.1 Linear Elasticity

As have been observed from material characterization tests of typical Insituform resins (Guice et al, 1994; Boot and Javadi, 1998), for small deformation, typical CIPP materials exhibit linear elasticity. The elastic modulus is in the range of $10^5 \sim 10^6$ psi ($10^3 \sim 10^4$ MPa) and is about the same in compression as in tension. As compared to metals and ceramics for which deformation involves primary bond stretching, the lower modulus of thermosets reflect that small strain involves relative movement of atoms or molecule segments which are not directly bonded (in the van der Waals' force fields) (Hall, 1981).

3.2.2 Yield and Fracture--axial

Polymeric materials can exhibit either brittle or ductile behavior under different loading conditions. Under normal room temperature and at a low strain rate (e.g., 1 in/min), a typical stress-strain curve of a Insituform product sample subject to tensile loading is shown in Fig 3.2a (Omara, 1996). As reported by various resources (Guice et al., 1994; Boot and Javadi, 1998), the failure process with no significant necking is characterized by "clearly audible stable fracturing" (Boot and Javadi, 1998) and can be modeled by an ideal elastic-plastic law, with a yield strength of about 3,500 psi.

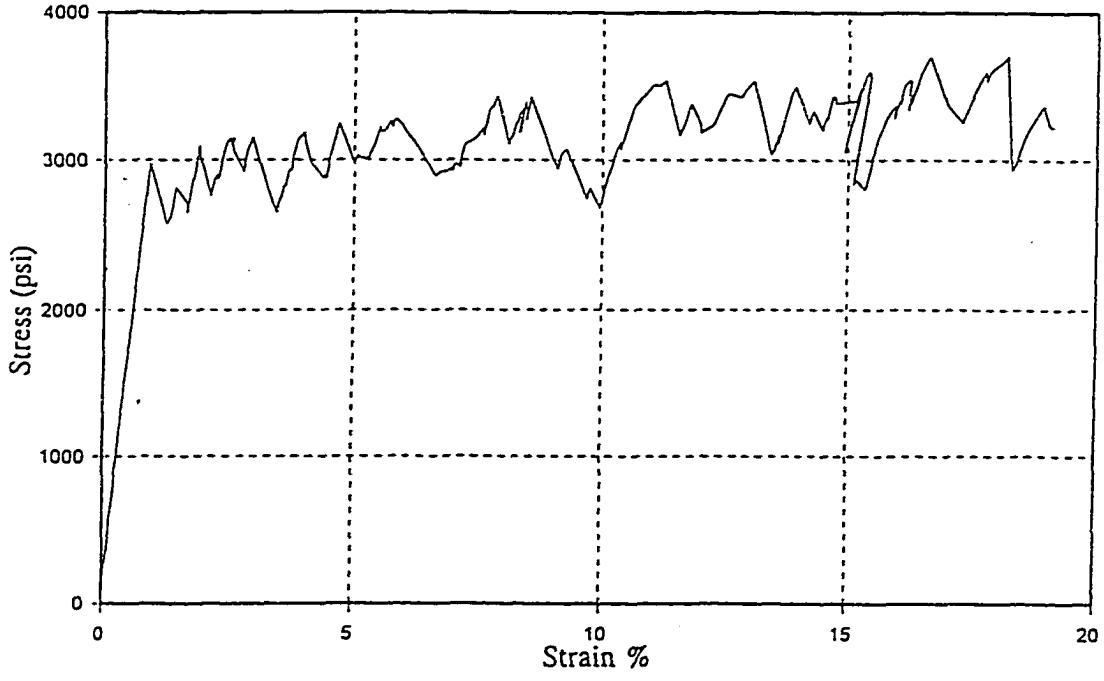

a. tension test

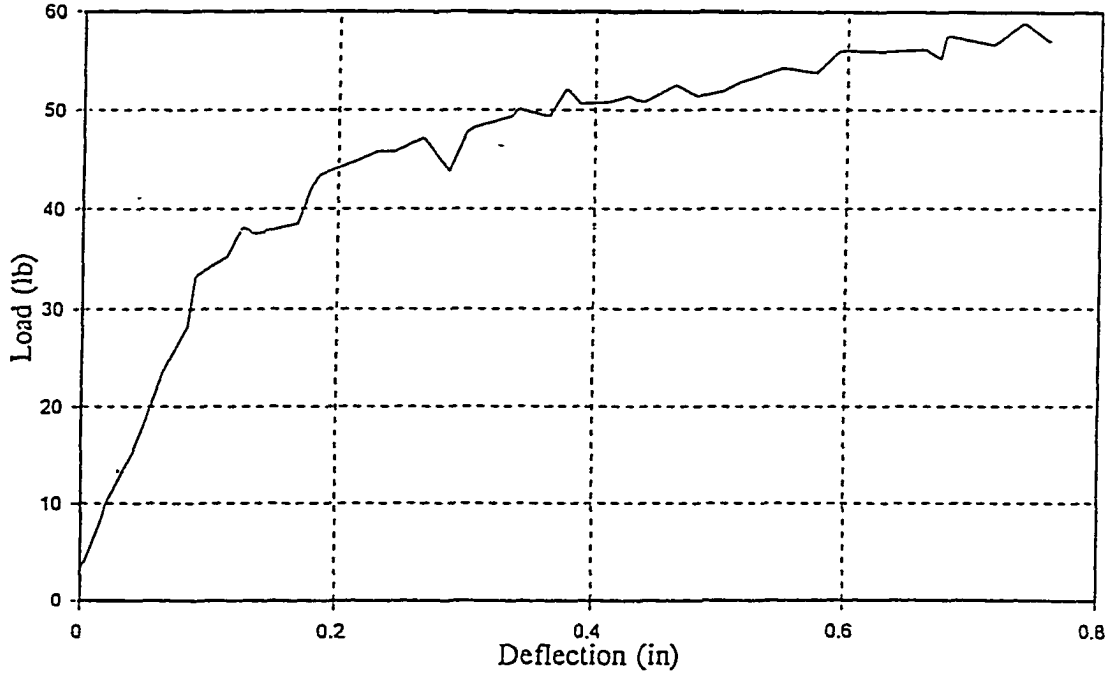

b. bending test

Fig. 3.2 Typical material test results
(From Omara (1996), Appendix A)

In the competition between yielding and fracturing, the heterogenous mass of amorphous molecules tends to nucleate cracks or voids all over the volume to allow for a considerable strain of 3% before the final breakage, yet no necking is noticeable.

The compressive failure behavior has not been reported yet, but the "yield" strength under compression is known to be more than twice the tensile strength. The reason can be explained as follows: compressive fracture may occur (in brittle and some ductile materials) as the result of cracks induced by heterogenous yielding, and the crack nucleation and propagation stresses are higher in compression than in tension. Therefore, unlike metals whose yield strengths are almost independent of hydrostatic pressure, in polymers, pressure does affect the yield condition in the following way: tensile components of stress promote yielding while compressive components delay it. According to Courtney (1990), the following yield criterion can be used for glassy polymers under multiaxial stresses

$$S + \alpha_p p \geq \tau_y \tag{3.3}$$

to replace the von Mises criterion for general uses.

$$\frac{1}{\sqrt{6}}[(\sigma_1 - \sigma_2)^2 + (\sigma_2 - \sigma_3)^2 + (\sigma_3 - \sigma_1)^2]^{1/2} = S \geq \tau_y \tag{3.4}$$

In the equations, τ_y is the yield stress in pure shear, $p = (\sigma_1 + \sigma_2 + \sigma_3)/3$ is the mean pressure affecting volume, and σ_1, σ_2 and σ_3 are the principal stress components.

3.2.3 Yield and Fracture--flexural

The deformation and failure behavior of Insituform Enhanced resin under (three- and four-point) bending conditions has also been tested. The fracturing mechanism is the

same, but the stress-strain curve shows a rather different phenomenon: the plateau beyond the yield point in the tensile curve is now replaced by a ramp (Fig. 3.2b).

Applying the discussion on the difference between tensile and compressive yield limits, this ramp can be explained as follows: the strain increases proportional to the stress with a slope equal to the axial modulus until the tensile yield limit is reached at the extreme fiber in the tensile region. After that, the slope of the curve drops with the propagation of the yielded area in the stretched side. The compressive yield limit will then be reached in the opposite side, and the sample under bending stresses will finally fail when a plastic hinge forms at the mid-span point. The nominal bending stress (determined by the moment over the specimen inertia) at failure should be lower than the compressive yield limit (when ideal elastic-plasticity assumed).

Therefore, the flexural behavior is primarily a structural phenomenon rather than an essential material property. The bending-till-failure behavior will be simulated in the next chapter by using a specially designed composite beam element incorporating specific material properties observed in tests.

3.3 Creep Properties

The concept of creep, or time-dependent deformation under constant stress, can be phenomenologically illustrated by Fig. 3.3. A typical creep strain development curve is usually divided into three stages: primary (rapidly growing), secondary (steady), and tertiary (rupture). The division is rather arbitrary. Constant strain rates are rarely found in real test data. In addition, the tertiary stage may not occur when the stress (rather than the load) is kept constant (Conway, 1965). In creep-induced buckling analyses, the major

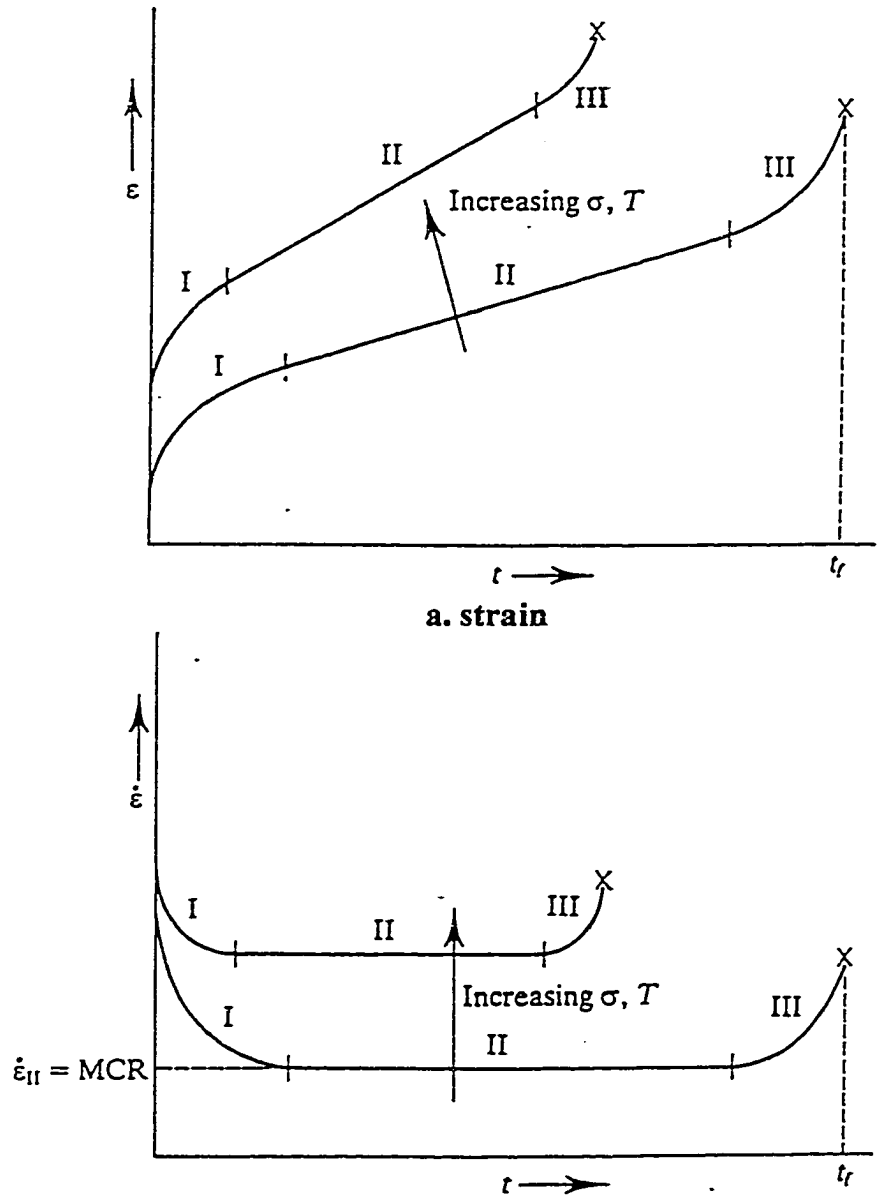

Strain (a) and strain rate (b) vs. Time in a constant-stress creep test. The creep curve can be divided into three stages. In Stage I (transient creep), the strain rate decreases until it attains a steady-state, minimum value (Stage II). Tertiary creep (Stage III), characterized by an increasing strain rate, precedes fracture at t_f. Increasing stress and/or temperature raises the overall level of the creep curve and also results in higher creep strain rates.

Fig. 3.3 Phenomenological description of creep
(From Courtney (1990), Fig. 7.2)

concern is focused on the second stage, which may last for decades under certain stress levels. The typical way to model the primary and secondary creep strain is by employing an empirical expression based on specific test data.

3.3.1 Creep Mechanisms

In crystalline materials such as metals, dislocation glide along arrays of lattices plays an important role in creep under certain temperature ranges. In amorphous substances like thermosetting plastics, whose irregular microstructures prevent the likelihood of dislocations, creep is induced mainly by thermal diffusions.

One diffusional mass transport mechanism, Nabarro-Herring creep, originally used to explain creep of metals under temperatures where dislocations are not active, is also observed in amorphous materials. The idea can be adopted to help understand the creep phenomena in thermosets.

As illustrated in Fig. 3.4 (Figure 7.5 of Courtney, 1990), Nabarro-Herring creep results from the tendency of mass flux toward and vacancy (or void among lattices or granular microstructures) flux away from the areas subject to tensile stresses. In crystalline substances, these fluxes are because of the changes of atomic volume in accordance to stresses. In crosslinked polymers, it can be considered as (partial) alignment of chain segments (especially where crosslinked networks are incomplete) along the direction of tensile stresses or perpendicular to the direction of compressive stresses.

Another closely related concept is stress relaxation, which is based on the same mechanism as creep but occurs in different situations. Creep and relaxation can be

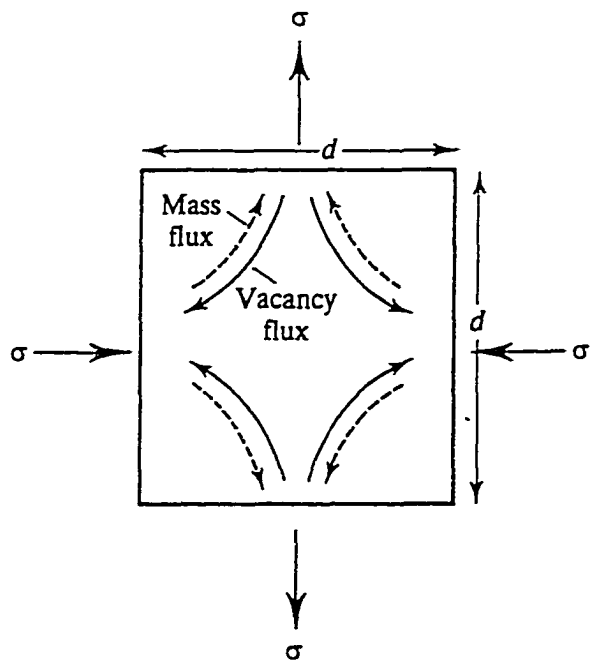

a. mass and vacancy flux

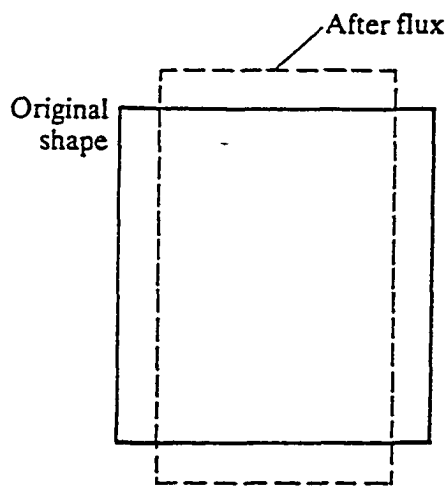

b. deformation due to flux

Nabarro-Herring creep results from a higher vacancy concentration in regions of a material experiencing a tensile stress vis-a-vis regions subject to a compressive stress. This results in a vacancy flux from the former to the latter areas, and a mass flux in the opposite direction (a). The resulting change in the grain dimensions (b) is equivalent to a creep strain.

Fig. 3.4 Nabarro-Herring creep mechanism
(From Courtney (1990), Fig. 7.5)

thought of as two sides of the same sheet of paper. When the material is subject to a sustained load (as in the case of creep buckling), stress may redistribute along with uneven deformation rather than decrease (or release) over the whole volume.

Creep recovery is also significant in polymers. Even large strains can be recovered almost completely after loads are removed for a certain period of time. For thermosetting plastics, recovery can be explained as the crosslinked structure influences the time-dependent deformation and the changes in this structure induced by stress or strain are "remembered" in some sense (Finnie and Heller, 1959). Once again recovery may be negligible in creep buckling processes in which stresses change (redistribute) gradually rather than release completely, as under the assumption of constant pressure.

For long-term CIPP liner buckling where the external pressure on the liner changes due to variation in the groundwater level, recovery may play an important role in the evolution of the stresses, strains, and deflections in the liner. Further investigations are needed to include the effect of recovery into the modeling.

3.3.2 Creep Under Various Loading Conditions

Another important aspect that needs to be addressed is that the creep rates of the Insituform resin is a strong function of the loading condition. For a specific nominal stress level, the tensile strain rate is significantly larger than the compressive strain rate, with the flexural strain rate residing in between. In addition, the steady creep stage for compression can last thousands of hours at stress levels under which tensile samples will break instantaneously or rupture within a few days.

Although the mechanism for this phenomenon is not yet clearly known, analogue can be made to the yield and fracture situation where the influence of hydrostatic pressure has been used to explain the difference between tensile and compressive yield strengths. Under a negative pressure (as in compression), the same magnitude relative movement of polymer segments where crosslinked networks are incomplete will need greater stresses or longer time, whereas under a positive pressure (in tensile regions), it is comparatively easier to stretch in alignment to the stress. This type of movement has been considered the main reason for creep strains in space (crosslinked) polymers (Findley, 1960).

The randomness of imperfect spatial structures leaves a great deal of room for variations among creep curves from different samples. However, consistency has been found for specimens from the same batch for which the concentration of crosslinks can be considered as a constant in a statistical sense.

The creep of specimens under bending is considered here as a structural behavior in which the concave side suffers compression and the convex side suffers tension. The overall (nominal) creep rate should be in the range bounded by tensile and compressive rates. With the occurrence and propagation of plastic yield region in the stretched side, the specimen is actually undergoing a visco-elastoplastic deformation. This case will also be simulated by using finite element analysis in Chapter 4.

3.3.3 Creep Models

Although rational models such as Maxwell's or Voigt's and the Boltzmann's Principle are frequently used in literature to depict viscoelasticity, empirical models are widely used in structural analyses involving creep to allow for specific test data. Early

empirical creep models were reviewed by Convey (1965), and a more extensive list is available in Skrzykep (1993). Interested readers can refer to them for more details.

Under constant stresses, creep phenomena are found primarily dependent on time, stress, temperature, and other factors (such as moisture). Many researchers assumed that the effects of various factors are separable. In the present study, the creep strain is assumed to be a function of time t and stress σ as follows

$$\varepsilon^{CR} = f(t)g(\sigma) \tag{3.5}$$

A Norton-type creep law (Norton, 1929) has been widely used for metals under high temperature, where (nearly) constant creep strain rate was found under constant stresses.

$$\dot{\varepsilon}^{CR} = \kappa\sigma^{m} \tag{3.6}$$

The equation has also been extended to include the primary phase, by combining a Bailey (1928) law, in which $g(\sigma)$ is also a power function, to provide more variability.

$$\varepsilon^{CR} = \kappa\sigma^{m}t^{n} \tag{3.7}$$

The concise form allowed close-formed solutions being obtained for creep-buckling of rectangular plates and cylindrical shells when the stress exponent was odd numbers (Hoof, 1957, 1959; Ellington, 1960).

For plastic materials, Findley (1962) suggested a simple expression based on his 1900-hour creep tests

$$\varepsilon^{CR} = \varepsilon_{t}t^{n} \tag{3.8}$$

in which ε_{t} is test constant dependent on σ. The equation was proved later to give a good fit to test data obtained over a continuous time span of as many as 26 years (Findley, 1987).

Although a hyperbolic-sine function was proposed for some plastics (Findley and Khosla, 1955), it is also possible to relate ε_t to stress σ by a power function. In the current study, based on a re-analysis of Lin's (1995) data, the Bailey-Norton type creep model (Eqn.. 3.7) is used. Different constants are used for creep strain under tensile and compressive stress. The fit curves and test data are compared in Fig 3.5, with the corresponding creep constants listed in Appendix A (Table A.1).

3.3.4 Creep Under Changing Stresses

The stress is subjected to change (or redistribution) in the creep buckling process, even when the load is kept constant. Time and strain hardening theories are two possible ways to determine the accumulated creep strains under changing stresses. Despite the convenience associated with time hardening expressions when analytical approaches are used, it has been known for a long time that they may lead to incorrect predictions, especially in creep buckling analyses (Shanley, 1952). The strain hardening law is hence adopted according to Findley and Khosla (1955), as expressed in the following equation where the time-dependent strain rate is described as a function of strain ε^{CR}

$$\dot{\varepsilon}^{CR}\Big|_{\sigma=const} = \frac{n(k\sigma^m)^{1/n}}{\left(\varepsilon^{CR}\right)^{(1/n)-1}} \tag{3.9}$$

The integration of strain rate allows creep strain being accumulated as shown in Fig. 3.6. The strain hardening law is applicable to plastic materials when no stress decreases will occur. In the case of a constrained liner undergoing constant external pressure, stresses mainly increase monotonically, as will be shown in later chapters.

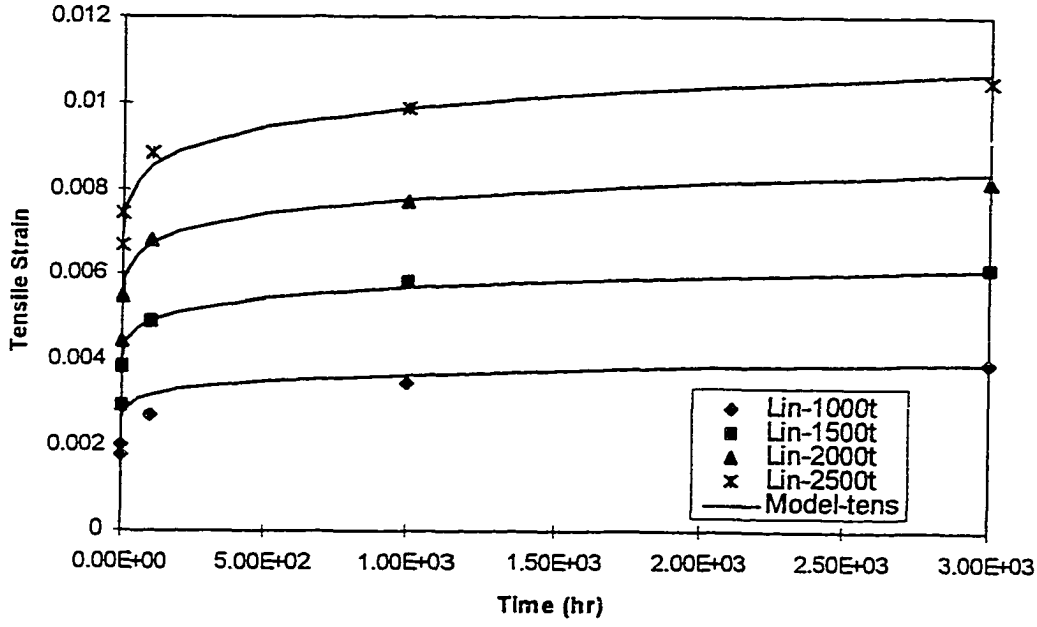

a. creep under tension

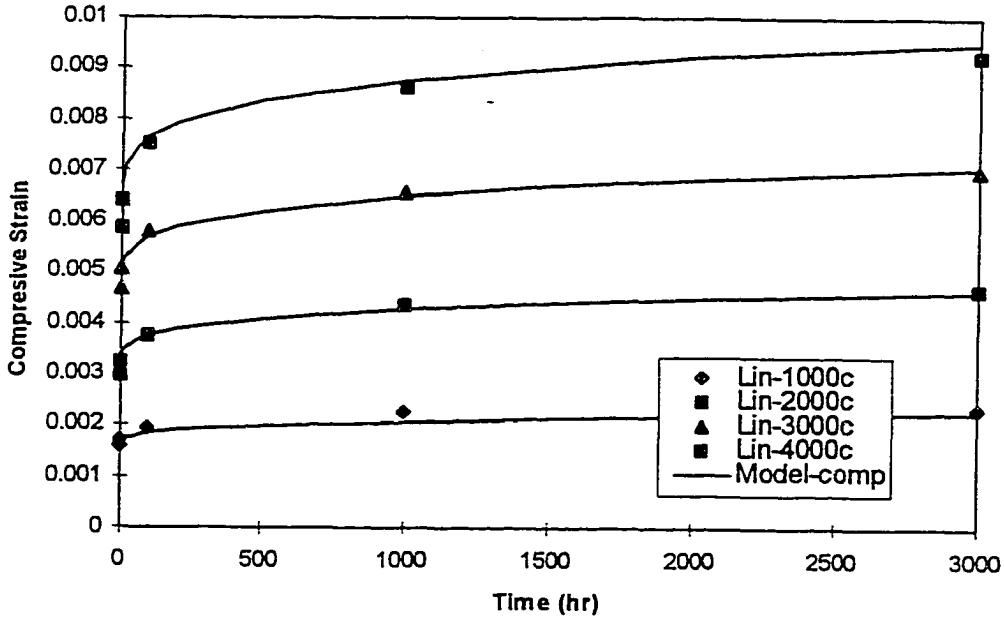

b. creep under compression

Fig. 3.5 Proposed creep model versus Lin's (1995) tests

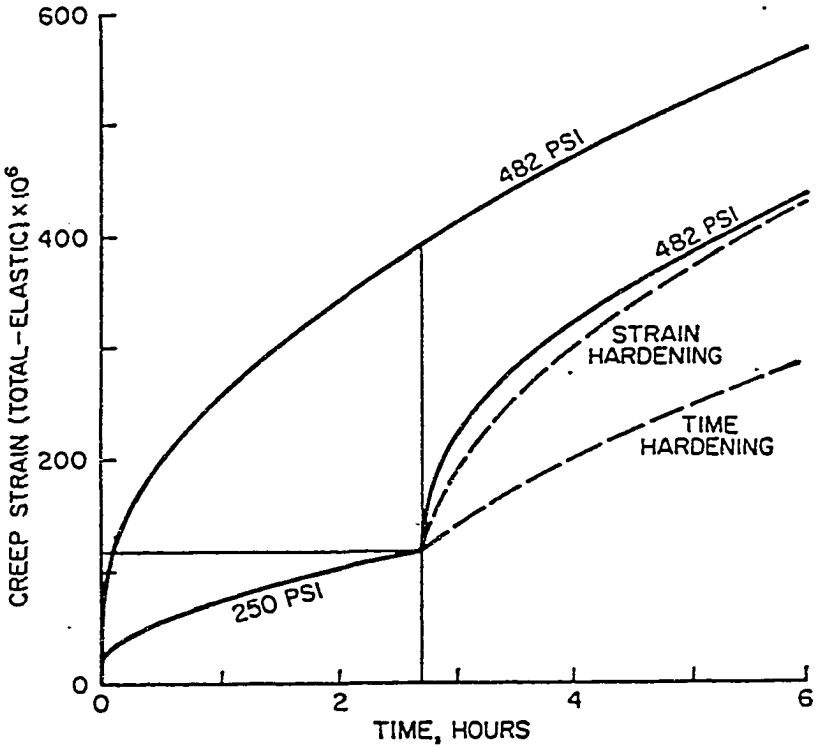

Fig 3.6 Time- and strain-hardening predictions for a varying-stress tension test on a lead at 120°F (From Finnie and Heller(1971), Fig. 6-2)

3.4 Summary

The constitutive model used in the present study can be summarized as follows:

1) The conventional division of total strain, as expressed by Eqns (3.1) and (3.2), will be adopted.
2) Linear elasticity before yield and ideal plasticity beyond yield is assumed.
3) The same modulus (obtained from tensile tests) is used for tensile and compressive elastic deformations.
4) Different yield strengths are used for tensile and compressive deformations in accordance with test observations.
5) The Norton-Bailey creep law (Eqn. 3.7) is adopted, with two different sets of parameters (k, m, and n) associated with tensile and compressive deformations.
6) The strain hardening law is used to determine creep strains subject to stress redistribution.

Creep under bending is considered as a structural phenomenon, which should be determined by applying the essential properties obtained in axial tests.

Based on specific characterization tests, this model reflects all the major features of the mechanical behavior of a typical CIPP material, and hence is considered appropriate for both short- and long-term buckling analyses of CIPP liners. Incorporation the model into the finite element representation will be detailed in the next chapter.

CHAPTER 4

FINITE ELEMENT MODEL AND ANALYSIS

A finite element approach is employed to model the liner-pipe configurations and provide the necessary solution procedures. With the aid of a sophisticated finite element package, ABAQUS, the intrinsically nonlinear problem can be handled with ease so as to focus on the simulation of long-term behavior of the encased liners in which we are most interested.

The assumptions made in this study are addressed first in this chapter. These assumptions are followed by the finite element model design and implementation to bring these assumptions into reality. The ABAQUS features used in the modeling are also described where necessary.

4.1 Essential Assumptions

Rigidity of Host Pipe. The host pipe, though deteriorated, is assumed rigid because its stiffness is typically much higher that that of a CIPP liner. In addition, it is also assumed that the pipe-soil system is still strong enough to resist all the loads transferred from the surrounding soil. The case in which the host pipe is still (nearly) circular or slightly oval is considered in this dissertation.

Loading Condition. To really focus on the liner, the panorama of the soil-pipe-liner system under all possible environmental loads will be reduced to an idealized situation in which the liner is subjected only to hydrostatic pressure as the result of underground water and interacts with its host pipe. The hydrostatic pressure induced by underground water inflows through the cracks on the host pipe is assumed constant throughout a liner's service life.

2-D (Ring) Configuration. In a typical rehabilitation application, the length of a liner will be much greater than the diameter of the liner. Along longitudinal direction, the fitting condition between the liner segment and the sewer pipe into which the liner is installed would be roughly the same, and the hydrostatic pressure will be, in the worst case, uniformly distributed. To simplify the solution procedure, the original problem concerning a cylindrical shell is reduced to a commonly used ring configuration (with the plane strain condition adopted), assuming a single cross-section of the liner (with a width of unity) can be used to represent the whole liner.

Ring/Beam Model. The ring structure will be modeled with 2-D beam elements (B21) in the finite element simulations. Actually, the beam model has been widely used by previous investigators as reviewed in Sections 2.2 and 2.4. In the present study, the use of beam elements is also based on the consideration of specific CIPP properties.

Material Properties. A particular CIPP product, the *Insituform Enhanced* resin, is chosen as the object of the study because both the material and physical test data necessary for use are available. The trend revealed from the study based on a specific

material is considered applicable to many others.

The Insituform Enhanced product is made of polyester, a thermosetting plastic. Its inelastic properties, such as yield limits and creep rates, associated with various loading conditions have been found quite different. This phenomenon reflects that the inelastic behavior of the material depends not only on effective stress (or the second stress invariant) but also on hydrostatic pressure as well (Chapter 3). The inclusion of this specific feature is considered essential to the accurate prediction of the buckling behavior of CIPP liners in both short and long time scales. However, sophisticated constitutive models for the polymeric materials have not been well established.

For the simplified thin ring configuration and throughout the buckling process, the stress state through the liner thickness is dominated by circumferencial components: compression plus bending in the deflected part(s); and pure compression in the remaining part(s). Therefore, it can be assumed that any fiber within the liner thickness is subject to uni-axial stresses: either compressive (on the concave side) or tensile (on the convex side). The effect of an actual multi-axial stress state can be taken into account by introducing proper adjustment factors to relevant material properties, e.g. multiplying the Young's modulus E by a factor of $(1-\nu^2)$ to account for the plane strain condition.

It is assumed in this study that the liner material can be phenomenologically divided into two parts: one part can resist tensile stress only, and the other part can resist compressive stress only. The constitutive relations can then be modeled by using experimentally determined properties under uniaxial tension and compression tests. The tensile and compressive behaviors can be modeled as concluded in Section 3.5.

4.2 Incorporating CIPP Properties into Finite Element Model

The specific mechanical properties of the polymeric material as discussed in the prior section can be incorporated into the finite element model by employing the ABAQUS features as detailed next.

4.2.1 "Composite" Beam Element

To simulate the different material properties with respect to tensile and compressive deformations, a composite beam element is implemented by using two B21 (2-node beam) elements back to back as one. One of the elements is assumed "NO-TENSION," and the other "NO-COMPRESSION," using the capability provided by the ABAQUS (HKS, 1995) material library. The "composite" beam element makes it convenient to incorporate different modulii, Poisson's ratios, yield limits, and creep properties associated with tensile and compressive stresses into the analysis. This feature allows the analyst adhere to specific material properties observed in tests.

Material Properties. Different CIPP materials may exhibit quite different mechanical properties under short- and long-term loading conditions. Even for the same product used in this study, *Insituform Enhanced*, considerably different short- and long-term properties have been reported by several resources because specimens from different batches have been used (Guice et al., 1994, and Lin, 1995; Boot and Javadi, 1998). While each resource presents a very similar elastic modulus, E, and a single Poisson's ratio, ν, different yield limits and creep rates are listed for tension and compression. The compression yield limit has not been characterized. However, it has been noticed that it

should be slightly higher than twice the value of the tensile yield limit.

Three sets of material properties will be used in this dissertation for different purposes:

1) LONG (Guice et al., 1994, and Lin, 1994) This set of data is associated with the CPAR tests which gives the most comprehensive long-term buckling database until now. LONG will be used wherever long-term properties are needed.
2) SHT1 (Boot and Javadi, 1998) This set gives a complete spectrum of yield limits which can be used to validate the performance of the proposed composite beam elements.
3) SHT2 (Stokeld, 1998) This set is associated with the latest short-term tests conducted at the TTC. It will be used in Chapters 5 and 6 to verify short-term FEA predictions against test rests.

The material properties (instantaneous and creep) with appropriate adjustments as the result of the plane strain assumption are listed in Appendix A.1.

4.2.2 Performance Validation

The performance of the proposed "composite" beam element under various loading conditions will be verified in this subsection.

Axial Loading. Only one composite beam element with a length of unity is used in the simplest loading condition. SHT1 data (from Boot & Javadi, 1998) is used because they gave the most complete set of properties. The element is completely constrained at one end and loaded by the application of forced displacement at the other end (See the

original ABAQUS input file AXLYLD.inp in Appendix B.1 for details) . The stress-strain curve is given in Fig. 4.1. The material deforms and yields in a way exactly as defined.

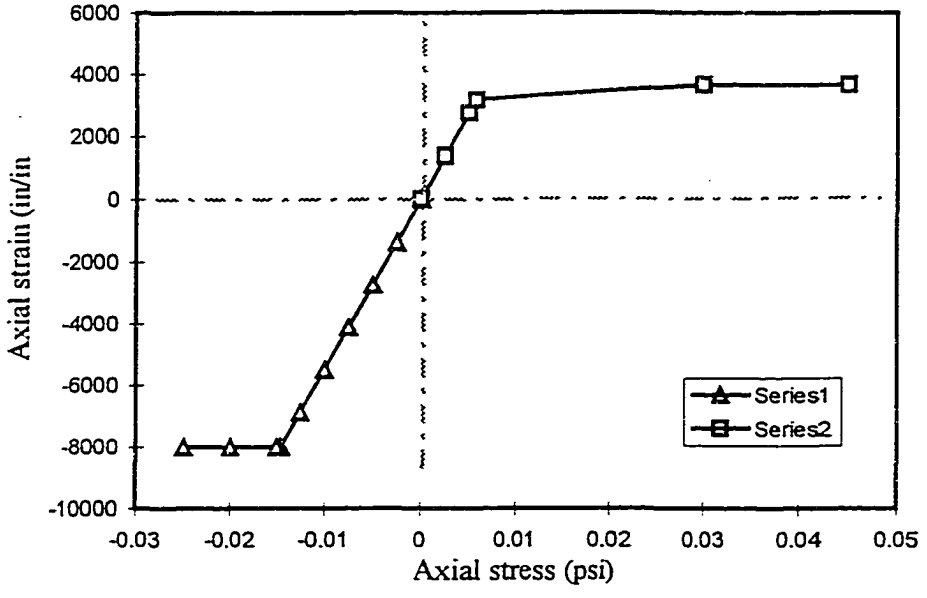

Fig. 4.1 Finite element simulation of axial loading

Flexural Loading. This simulation is a real test for the performance of the new element. The SHT1 data is also used here. A three-point bending test is simulated, in accord with the ASTM D 2990-77 (1977) standards: the specimen under bending is .21 inches in width (b) and depth (h), and the span ($2L$) between supports is 3.36 inches, sixteen times of the depth. Only half of the test setup is modeled with 20 composite beam elements. The axial and flexural displacements are constrained at mid-span for symmetry, and the lateral DOF is constrained at the end node to simulate a simple support condition (cf. FLXYLD.inp in Appendix B.2). The response curve for the lateral displacement Δ at mid-span node to the applied load P (on the half beam model) is converted to the nominal stress-strain curve for the outermost fibers at the mid-span.

$$\varepsilon = 3h\Delta / 2L^2 \tag{4.1}$$

$$\sigma = 6PL / bh^2 \tag{4.2}$$

The stress-strain curve is given in Fig. 4.2, showing a "ramp" similar to a real flexural test curve (as reported in Omara, 1996, Fig. 3.2b).

There is no significant yield point on the flexural stress-strain curve. It can be traced from the tensile stress history that when the outermost fiber on the tensile side starts to yield at 3150 psi, the nominal "flexural" stress is about 3800 psi, coinciding with the yield stress of 3700 psi (25.7 MPa) by Boot and Javadi (1998). The flexural curve then grows at a gradually decreasing rate until it stops at 7684 psi when a plastic hinge is formed at the mid-span node.

The predicted breakage stress (7684 psi) shows good agreement with the reported values, 7350 psi, while the predicted nominal strain at break, 3.43%, shows less agreement. Besides the possible influence from the artificially assigned yield limit (8000 psi) associated with the compressive deformation, the differences may be induced by the absence of the fracture mechanism in the finite element model. An ultimate tensile strain of 3% was reported by Boot and Javadi (1998), which was proposed as a failure criterion. In the simulation, when this ultimate strain is reached at the outermost fiber under tension, the nominal flexural stress is 7100 psi with a nominal strain of 1.89%. After that point, local breakage should have occurred which tends to reduce further stiffening of the beam and to enlarge the lateral deflection.

The simulation of fracturing during the bending test is not intended in this study. This example shows that the composite beam element can accurately simulate the short-term behavior of CIPP materials (represented by the *Insituform Enhanced* resin) subject to

various loading conditions when observed tensile and compressive properties are used. The simulation of long-term behaviors will be verified next.

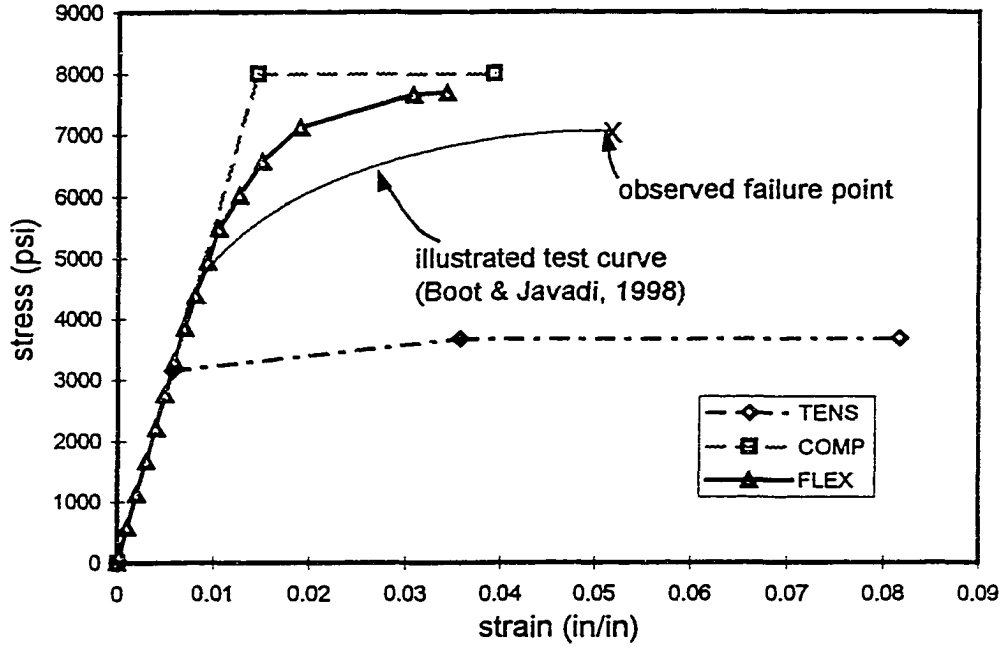

Fig. 4.2 Finite element simulation of flexural loading

Axial Creep. The same geometry as used in the short-term axial test is used, with the material properties from LONG (Guice et al., 1994; and Lin, 1995) because of the availability of long-term properties. Four stress levels have been used for tensile and compressive creep, as done by Lin (1995) in his characterization tests. The corresponding ABAQUS input file, `AXLCRP.inp` is listed in Appendix B.3, and the simulation results are shown in Fig. 3.5. The predicted creep curves agree well with the observed test data.

Flexural Creep. The three-point bending model and the material property set LONG are used in this example. The four nominal stress levels used in Lin's (1995) tests, 1000, 2000, 3000, and 4000 psi, are applied. The load P in each case is determined by an

alternative form of Eqn. (4.2), as

$$P = \sigma b h^2 / 6L \tag{4.3}$$

The simulations are accomplished by four ABAQUS runs. Each time, the applied load in the line following the `*CLOAD` command in `FLXCRP.inp` (Appendix B.4) is adjusted accordingly. The predicted creep curves are shown in Fig. 4.3, with Lin's test data for comparison.

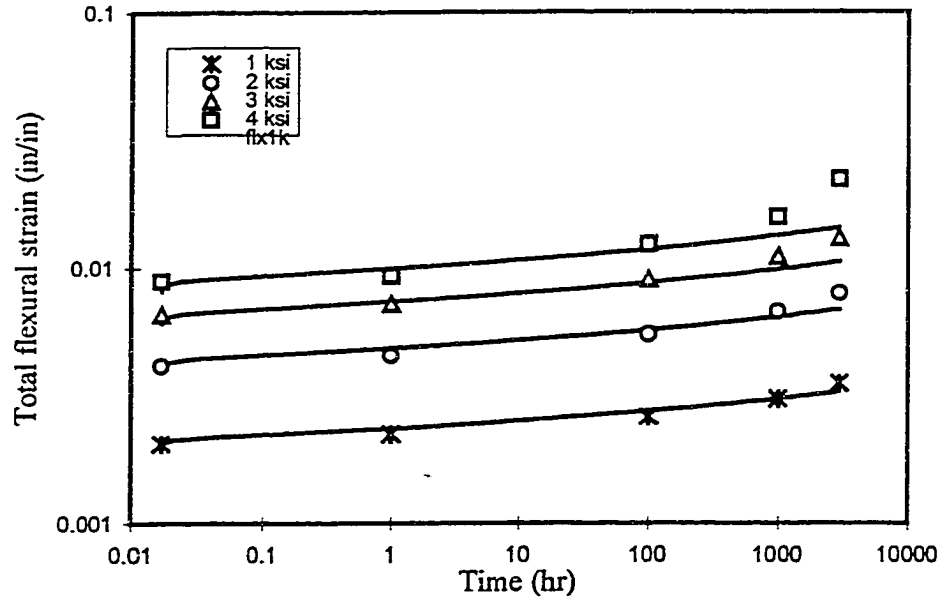

Fig. 4.3 Finite element simulation of flexural creep strain

From the comparison, the predicted total strains show good agreement with the observed values at the beginning, but this agreement decreases at longer times and higher stress levels.

To investigate the reason for this discrepancy, the stresses at the outermost fibers for both tensile and compressive sides are plotted in Fig. 4.4 for all four stress levels, together with the nominal flexural stress histories. The maximum tensile stress under each

case decreases with time, while the maximum compressive stress increases. This phenomenon may occur because material in the tensile side creeps at a faster rate than in the compressive side. This mismatch in creep rates would lead to partial release of the tensile stress and stress redistribution across the beam thickness. This phenomenon might be happening in real bending tests, yet the detail is not known. From the numerical analysis standpoint, the predicted curves might be able to fit the test data if the stress is constant during the entire time span. Hence, constant stress assumption is the cornerstone of the creep model established in this study.

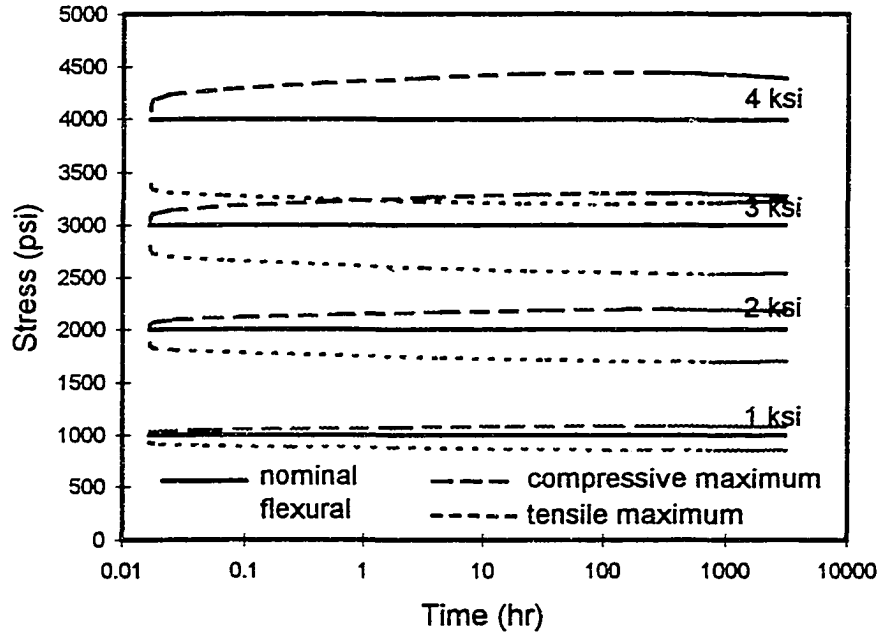

Fig. 4.4 Finite element simulation of flexural stress history

Unexpected differences between simulated and experimentally observed flexural creep rates may indicate some unknown mechanisms in CIPP material properties. More thorough experimental investigations and analytical modeling are recommended.

4.3 Finite Element Model Setups

As discussed earlier, the buckling behavior of constrained CIPP liners depends strongly on both material and geometric parameters. An appropriate methodology to define the typical geometric configuration of the liner-pipe system is another cornerstone of the present study.

4.3.1 Constraint from Host Pipe

First of all, the liner deflection should always be constrained within the confines of its host pipe. During the constrained buckling process, a liner interacts with its host pipe through the contact area(s) which may change in size and position with the evolution of liner deflection. This contact condition is simulated by employing the surface contact capability in ABAQUS.

In the finite element model, the host pipe, assumed to be rigid, is modeled with a set of R2D2 (2-node two-dimensional rigid body) elements. The set is then defined as a rigid body, whose translational and rotational displacements are represented by a "master" or reference node. All the degrees of freedom of the reference node are then constrained so as to fully constrain the host pipe against any motion.

The inner surface of the rigid pipe and the outer surface of the liner are defined appropriately by using the "*SURFACE DEFINITION" command, and then defined as a "CONTACT PAIR," indicating the potential contact between the two surfaces.

Contact elements internal to ABAQUS will be generated automatically at run time to deal with the contact condition. Any liner nodal displacement attempting to penetrate the rigid body surface will be cut back, and the iteration will be repeated until an allowable

liner profile is reached or the number of iterations exhausted. The contact pressure is positive at an individual node whenever the gap between the pair of surfaces is closed; otherwise, the contact pressure will remain zero.

The flexible liner surface, or the "slave" surface in the pair, is allowed to slide along the rigid ("master") pipe surface, and the relative sliding can be "finite." The tangential interactions or frictional forces can also be assumed by the definition of an appropriate friction coefficient. For simplicity and to be conservative, the friction coefficient between the liner and pipe is usually defined as zero in the present study. However, nonzero tangential frictional coefficients and the resulting forces are included in simulations of the evolution of deflected shape of the liner (Chapter 5). The coefficient value is varied from 0 to 0.2 (Hall, 1981) to investigate the consequences.

4.3.2 Definitions of Geometric Parameters

The geometric configuration of the liner-host pipe system can be characterized by parameters from the following three categories: liner dimension ratio, annular spacing or gap between the liner and host pipe, and imperfections on liner-pipe geometry. These parameters will be defined as follows in dimensionless forms to extend the applicability of the FEA results.

Liner Dimensional Characteristic. The cross-section of a liner is first idealized as a perfect circular ring. The "slenderness" of the ring is conventionally described by its dimension ratio

$$DR = D/t \tag{4.4}$$

in which D and t are the mean diameter (measured at the mid-surface of the liner) and the thickness of a liner, respectively. When any imperfection, e.g. variable thickness or ovality, is taken into consideration, an equivalent perfect cross-section can be thought of which will provide the *DR* ratio for comparison.

Annular Gap between Liner and Host Pipe. The existence of gap in the liner-pipe system is inevitable. In the idealized case, the gap is the annular space between two perfect circles, one of which is encased in the confines of another. Although the relative position of the two circles may vary, the total space depends only on Δ, the difference of the inner diameter of the host pipe and the outer diameter of the liner. The size of gap, *g*, is then defined as one half of the diameter difference, or as a uniform gap, when it is evenly distributed along the liner circumference.

$$g = \Delta/2 \qquad (4.5)$$

The relative or dimensionless gap is defined as

$$G\,(\%) = g/D^{*}100 \qquad (4.6)$$

On the other extreme, when the annular gap is unevenly distributed, a G (%) gap describes the maximum gap 2g (or Δ) at one side and no gap at the opposite side.

Imperfections in Liner and/or Host Pipe. Since the liner stiffness is much smaller as compared to that of its host pipe, the liner deflection will be influenced greatly by the shape of its host pipe. Therefore, the ovality of the (damaged) host pipe is a major influencing factor which should be taken into account. In the present study, the ovality of the liner is always assumed to be the same as that of its host pipe.

$$OV(\%) = (D_{max} - D_{min})/(D_{max} + D_{min})*100 \quad (4.7)$$

Other imperfections of liner geometry, such as thickness variation and noncircular (wavy) shape local to a certain ring segment (Fig. 4.5), are also considered, especially in liner life prediction. Thickness variation, V, and a relative local dent, W, are expressed as

$$V(\%) = v/t*100 \quad (4.8)$$

and

$$W(\%) = w/D*100 \quad (4.9)$$

These localized imperfections should also be related to an angle ϕ defining the range of imperfection as shown in Fig. 4.5..

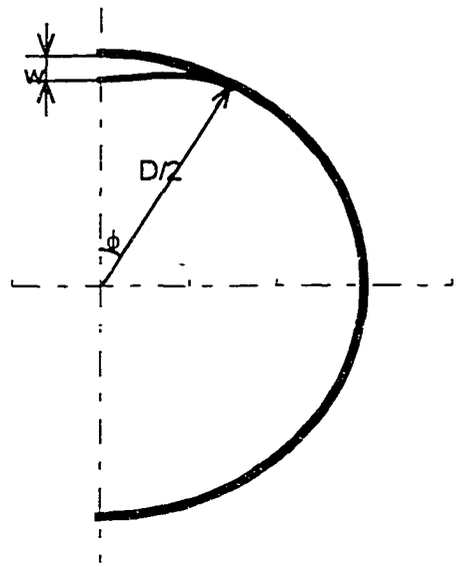

Fig. 4.5 Schematic of local imperfection

4.3.3 Model Setups

By using the definitions in the prior subsection, the geometry of the liner-pipe system can be determined by the selection of D, the mean diameter of the liner. Other dimensions necessary in the finite element model definition can be determined as

$$D_{pipe} = D*(1 + 2G);$$

$D_{pipe} = D^*(1 + 2G)$;

$D_{min} = D^*(1 - OV)$, $D_{max} = D^*(1 + OV)$ for oval pipes, and

$t = D/DR$.

When any local imperfection is present, the range angle ϕ is also needed.

Three types of finite element models are used in this study for different purposes: one- and two-lobe, and transition models. Although each type relates to different conditions, they all share a single assumption that the liner will buckle in the vertical axis. In reality, an encased liner may tend to snap through along the short axis of the ovalized host pipe or at an imperfect locality where the liner is thinner or dented. The vertical axis of the finite element model is assumed to align with that direction.

One-Lobe Model. This type of model is characterized by a one-lobe buckling mode and is most frequently used throughout this study. In the one-lobe model, gap is assumed unevenly distributed (the gap is $2g$ at the top and 0 at bottom). The radial displacement at the bottom node where the liner touches the host pipe is constrained for simplicity. In this case, only one half of the liner and host pipe is modeled with composite beam elements (as discussed in the prior section) and rigid body elements (R2D2), respectively. Symmetrical boundary conditions are applied to both end nodes of the half liner (Fig. 4.6).

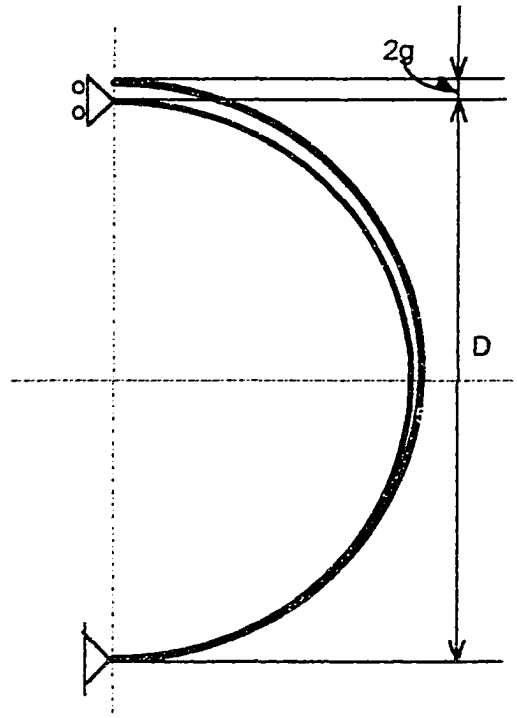

Fig. 4.6 Schematic of the one-lobe model

Two-Lobe Model. In this type of model, the gap is assumed even, and the resultant buckling mode is symmetric with respect to the horizontal axis. Therefore, only a quarter of the liner-pipe system is meshed up, with symmetric boundary conditions being applied at the end nodes (Fig. 4.7). This model is be used to provide "upper bound" predictions where comparisons are needed.

Transition Model. This kind of model is used mainly in Chapter 5 to investigate more realistic deflection evolution of an encased liner other than the conventional one- and two-lobe assumptions. One half of the liner-pipe system is modeled as in the one-lobe model, yet the boundary conditions at the end nodes are different: only the rotational degree of freedom is constrained. The liner is thus allowed to "float" within the confines

of its host pipe. Logical connector elements, i.e. spring and dashpot elements (HKS, 1995), will be used to provide a small stiffness to resolve the numerical difficulty which will otherwise be induced by a singular system stiffness matrix. The setup of this kind of model will be described in further detail in Section 5.4.

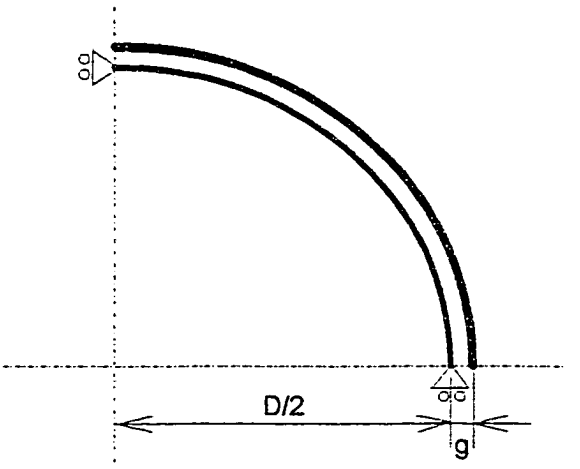

Fig. 4.7 Schematic of the two-lobe model

4.3.4 Solution Procedures

The deflection of an encased liner can be driven either by an increasing external pressure or by the accumulation of creep strain with time under a sustained constant external pressure. The final collapse will occur when the critical value corresponding to the increasing pressure (critical pressure) or elapsed time (critical time) is reached. The physical processes involved can be idealized as elastoplastic deformation under loading and visco-elastoplastic deformation under constant pressure, which are time-independent and time-dependent, respectively.

Two different solution procedures in ABAQUS can be used to simulate the two

different processes: *STATIC for time-independent loading, and *VISCO for time-dependent creeping. Both procedures can deal with the geometrical nonlinearity resulting from finite displacements of the liner during liner buckling.

ABAQUS allows the user to divide the solution of a complex nonlinear problem into a sequence of "steps," and to choose different procedures in different steps. If the geometrical nonlinearity effect is considered, i.e. NLGEOM is selected in a specific step, the final state of the model (displacements, stresses, strains, etc.) can be included in the response in the step that follows.

Instantaneous Buckling Solution Procedures. A typical finite element analysis of the short-term buckling of an encased liner includes two *STATIC steps.

1) Application of an initial disturbance: the gravity force (assuming a specific weight of $.0361\, lbf / in^3$) is loaded upon the liner, to distort the perfect circular configuration and introduce initial deflections.
2) Loading: The uniformly distributed external pressure is applied on the liner and increased until the onset of buckling is reached.

Creep Buckling Solution Procedures. A typical finite element analysis of long-term buckling induced by creep is composed of three steps. The first two are *STATIC steps similar to the ones described above. An additional *VISCO step is needed to solve the creep problem.

1) Application of the initial disturbance.
2) Loading: Applying and increasing the pressure until the desired load level (lower than the critical load) is reached.

3) A *VISCO step in which the deflection of the liner grows with time under a constant external pressure as a result of the creep phenomenon. The solver can automatically assign appropriate time increments according to the error tolerance on creep strain defined by the user. The solution stops at the onset of liner collapse. At that point, no convergent solution satisfying the error tolerance can be reached when the attempted time increment is equal to or smaller than its lower limit.

4.4 Summary

Finite element models incorporating specific mechanical properties of CIPP materials and simulating representative liner-pipe configurations are discussed in this chapter. The performance of the proposed composite beam element has also been validated against characterization test data. After an appropriate mesh refinement study (as detailed in Appendix C.2), the models employing 144 equal length (composite) elements can be used.

CHAPTER 5

FUNDAMENTAL BUCKLING BEHAVIOR OF CONSTRAINED PIPES

The fundamental structural behavior of encased CIPP liners during the short term buckling process will be simulated in this chapter by using the finite element model incorporating experimentally observed material properties as discussed in Chapters 2 through 4.

The constrained buckling analyses based on the conventional one- and two-lobe models are first conducted. The validity of the proposed method based on a composite beam element is calibrated by comparing the predicted results against buckling pressure data observed from the latest short-term tests at the TTC (Hall, 1998a). The effects of plastic yield and buckling mode on the prediction accuracy are discussed. Also, the mechanism for possible deflection evolution patterns of buckled liners is discussed.

5.1 Fundamental Buckling Behavior

A typical liner-pipe configuration is used here to demonstrate the basic buckling behavior of a constrained CIPP liner under external pressure. The dimension ratio DR = 50, a relative gap G = 0.4%, and both the even and uneven gaps are used. The predicted ultimate pressures corresponding to one- and two-lobe modes are 78.17 and 106.0 psi,

respectively. Compared to an unconstrained liner, the critical pressure from the Timoshenko's Equation (2.2) is predicted to be 9.91 psi

5.1.1 Stress Distribution and Evolution

Curves showing the stress distribution along the liner for both models are given in Fig. 5.1. In the figure, maximum stresses can be found at the middle and at the border of the buckled part(s), which are denoted as points I and II, respectively.

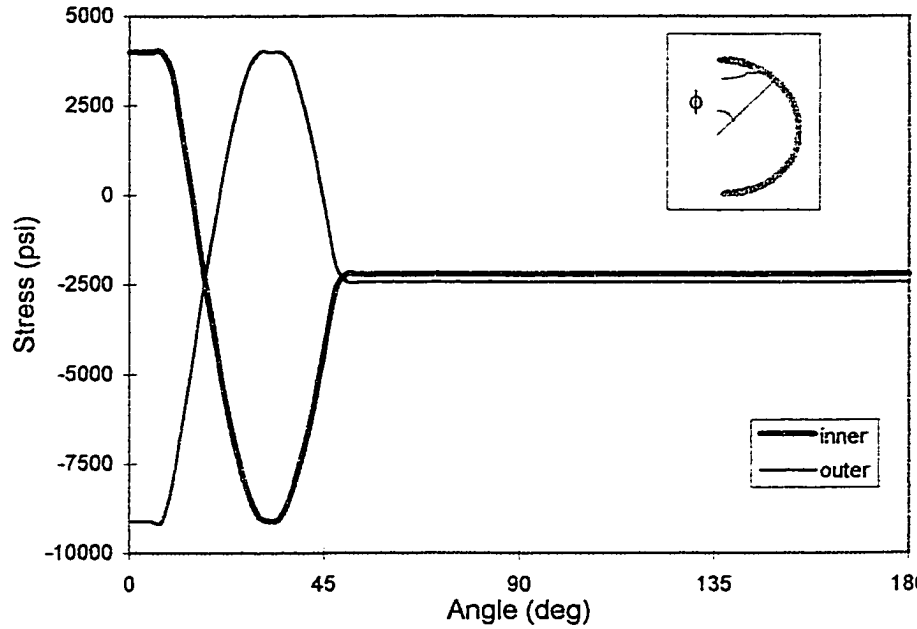

Fig. 5.1 Stress distribution for a one-lobe model

As compared with a free-standing pipe, the constrained ring sustains a much higher pressure, and the deformation of the buckled part(s) is much more severe. A stress-pressure plot is given in Fig. 5.2. The plastic yield limit is first reached at the inner fiber at point I. After that, the outer fiber yields (at point I) which is under compression. Thereafter, the material at point II (both inner and outer fibers) yields. The liner collapses when plastic hinges are formed at both points I and II, making the buckled portion a

three-point mechanism. Without the incorporation of material failure, a significantly higher critical pressure, 93.7 psi, will be predicted.

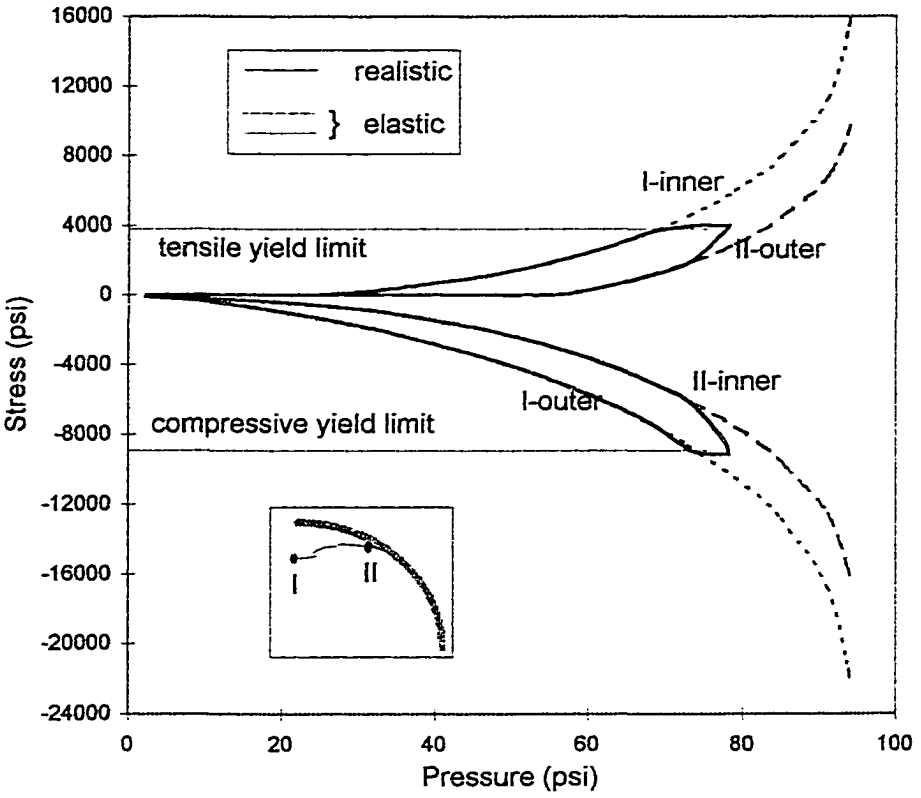

Fig. 5.2 Stress history for a one-lobe model

The ultimate pressure for the two-lobe model (predicted as 100.6 psi) is higher than that for the one-lobe model. The higher pressure can be explained as follows: in the two-lobe model, more of the ring undergoes high stresses resulting in more strain energy storage.

A structure is expected to deform along a path associated with the lowest possible potential energy level. This is the reason why the one-lobe mode is the most frequently observed buckling mode of constrained (steel and plastic) liners. The concept of possible buckling paths will be discussed in detail later.

5.1.2 Effect of Plastic Yield

The constrained ring suffers a structural instability problem. However, for the reasons discussed in the prior subsection, the plastic yield strengths (associated with tensile and compressive stresses) are reached before the critical pressures predicted by elasticity can be approached. Therefore, an elastic model tends to overestimate liners' buckling resistance when they are externally constrained.

The dashed curve in Fig 5.2 shows the critical pressure prediction obtained by adopting an elastic stress-strain relation throughout the buckling process. When the purely elastic model is used, maximum stresses at Point I went far beyond the yield limits for tensile and compressive conditions. These stresses were 13942 psi in the tensile region and -19323 psi in the compressive region for the one-lobe model. A similar finite element run reveals that the maximum stresses are 14000 and -20000 psi for the two-lobe model. However, the corresponding tensile yield limit was found to be 3600 psi. The compressive yield limit was known to be higher than twice that of the tensile limit, and is assumed as 8000 psi in the present study (See Table A.3 for more detail) .

5.2 Model Verification with Short-Term Tests

A new buckling test program was carried out at the TTC in 1998, to investigate the short and long term buckling behavior of CIPP liners encased in circular and oval pipes. The short term test results (TTC, 1998) will be used here and in the next chapter to verify the validity of the proposed model before the simulation of creep-induced constrained buckling is carried out.

5.2.1 Test Summary

Results from two series of short term tests, conducted with nominal 12"ID and 8"ID round pipes, are used here. Each series had three sets each has a different nominal thickness as 5.5, 6.5, and 7.5 mm (or 0.217, 0.256 and 0.295 in) for 12", and 4.5, 5.5, and 6.5 mm (0.177, 0.217 and 0.256 in) for 8". Each set had 5 samples. Liner thickness and outer diameter values were measured at both ends of each specimen, and the average values were recorded as listed in Appendix A.2. The total volume of the annular spacing was also measured to estimate the gap magnitude in each test.

Material properties used in these tests were characterized by Stokeld (1998) as listed in Appendix A.1, under SHT2.

As can be seen from the observed buckling pressures listed in Appendix A.2, the liner buckling resistance increased with a decrease in the *DR* ratio.

5.2.2 Predicted Results and Comparison

Finite element analyses were conduced based on the one- and two-lobe models to give theoretical predictions. To compare with the test data, liners with dimension ratios of 35, 40, 45, 50, 55, 60, and 65 were used. According to the annular volume measurements, an average total gap $g = 0.05$" was used. The nominal diameter of the rigid surface (host pipe) was set as 12". For the 8" case, the thickness and gap values were adjusted accordingly to obtain the desired *DR* ratios.

Critical pressure predictions based on one- and two-lobe models are listed in Table 5.1.

Table 5.1 FEA Predictions of critical pressure

D/t	P_{σ}^{I} (psi)	P_{σ}^{II} (psi)
35	177.7	230.3
40	133.7	177.6
45	102.9	138.9
50	80.5	110.2
55	64.1	88.8
60	52.0	72.5
65	42.9	60.1

Both test and FEA results are plotted in Fig. 5.3 for comparison. It can be seen that numerically determined critical pressure predictions exhibit excellent agreement with experimental results. The majority of test records fall in a band bounded by the lower and upper extreme lines predicted by the one- and two-lobe models, respectively. Outlying points, such as the fifth specimen from the 12"OD 5.5mm set, can be found below the lower bound. Deviation of these experimental results from the numerical results can be caused by a number of factors, such as local variations in liner thickness, gaps, and material properties.

These results show a phenomenon extremely similar to what was reported by Lo and Zhang (1993) as discussed in Subsection 2.4.3. They suggested a "combined effect of these two competing collapse mechanisms" (i.e., one- and two-lobe buckling models) to explain the fact that the observed enhancement factors were bounded by upper and lower bounds. The author proposes that this phenomenon may be caused by a transition from the two-lobe configuration to the one-lobe configuration before the higher pressure associated with two-lobe buckling is reached. The concept of deflection mode transition will be discussed in the following section.

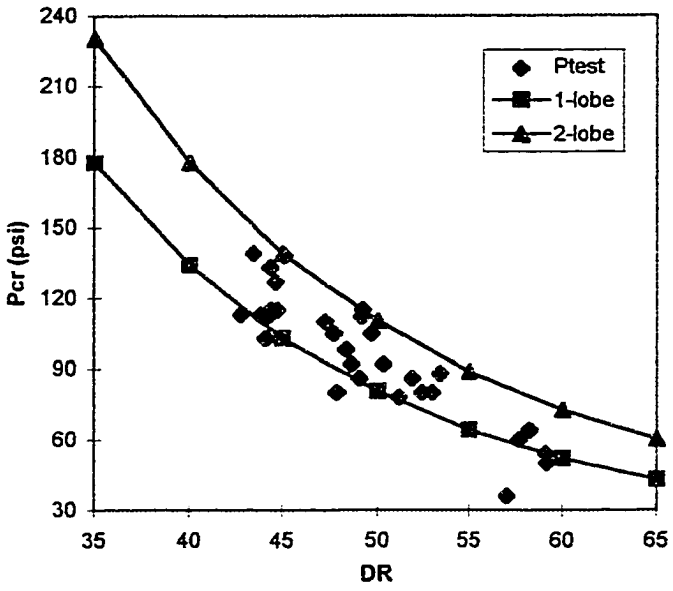

Fig. 5.3 Comparison of predicted and observed buckling pressure

5.3 Experimental Observations of Liner Deflections

The deflection evolution of CIPP liners during short-term and long-term (creep-induced) buckling tests have been investigated by a number of researchers (Lo et al., 1993; Guice et al., 1994; and Boot and Welch, 1996). The vast majority of liner buckling tests conducted at the Trenchless Technology Center (TTC), Louisiana Tech University, indicated that the deflection of the constrained liners starts with the two-lobe mode, and undergoes roughly symmetric lobe development during the majority of the tests (Guice et al., 1994). Figure 5.4 shows a typical deflected liner profile recorded during recent liner buckling experiments at the TTC. The deflection of the liner was amplified by a factor of 10 to make it easy to be observed, and hence some part of the liner appears erroneously to have moved out of its host pipe. A two-lobe deflection pattern remained in effect as the pressure approached the buckling pressure. However, at the onset of buckling, one of

the lobes became dominant (in all tests), resulting in a one-lobe collapse (Fig. 5.5). The other lobe either remained stationary or was released during buckling.

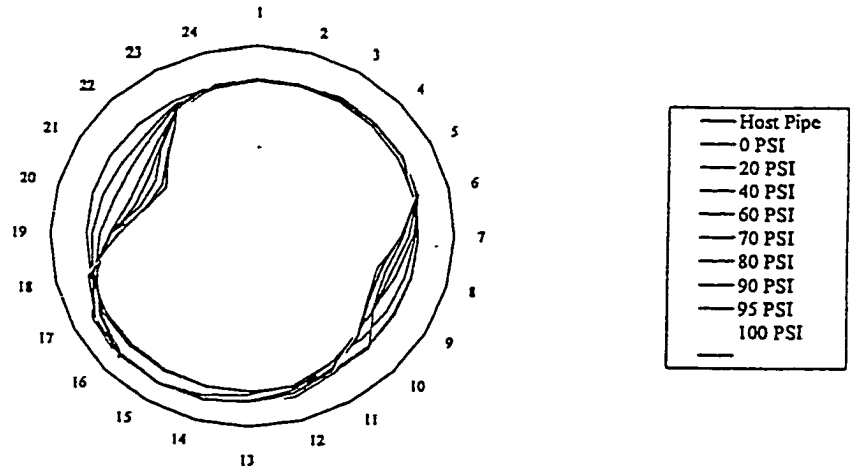

Fig. 5.4 Typical deflected profiles observed in test (TTC, 1998)
(Note: Measured deflections are amplified by a factor of 10)

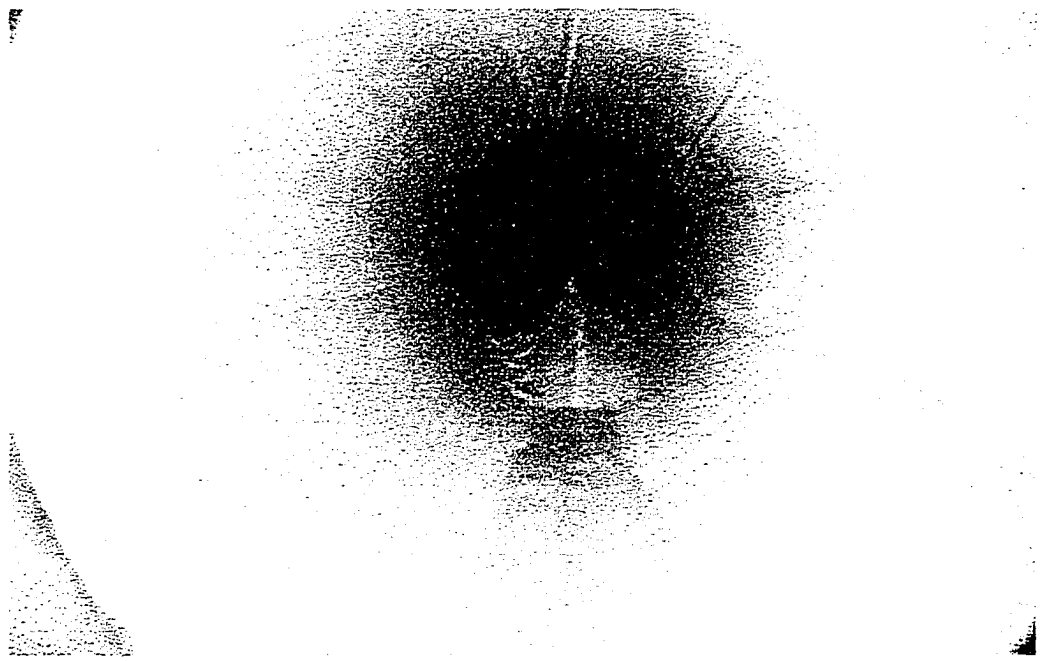

Fig. 5.5 Typical post-buckling profile

Lo et al. (1993) report a similar single-lobe collapse phenomenon for buckling tests on encased CIPP pipe liners. Boot and Welch (1996) report a two-lobe deformation

history leading up to buckling, but do not report the mode of final collapse; one of their 14 specimens exhibited a one-lobe deformation history. Based on several experimental studies, Gumbel (1997) indicates that snap through will occur on one lobe or the other even when the deflection begins in a two-lobe mode.

Experimental results suggested that liner deflection may undergo a transition from the two-lobe mode to the one-lobe mode. Because there is no predominant preference in the distribution of annular spacing, it seems reasonable to assume a symmetric initial gap distribution which favors the two-lobe deflection. Yet, the development of symmetrical deformation will be distorted by any initial asymmetries (in pipe shape, liner thickness, and/or gap distribution), which will be amplified with the external pressure increment. When the asymmetry becomes so great that the support (from the diminishing contact area between the liner and the host pipe) can no longer arrest its development, the buckled liner configuration tends to transition from the two-lobe mode into the one-lobe mode which corresponds to a lower critical pressure. The phenomenon is rather natural, since any structural behavior always tends to proceed along the path which associates with the lowest possible potential energy level, which is the lowest critical pressure in the case of liner buckling.

5.4 Simulating Mode Transition by FEA

When simulating mode transitions, the liner is initially located at the center of the cavity within its host pipe. A single dashpot (`DASHPOT1`) element links the top node of the liner to a virtual fixed point, and a spring (`SPRING1`) element links the bottom node to another, so as to provide a nontrivial stiffness associated with the vertical DOF at the

two nodes (Fig. 5.6). A small perturbation force is applied at the middle node to ensure that the liner initially deforms in a two-lobe configuration.

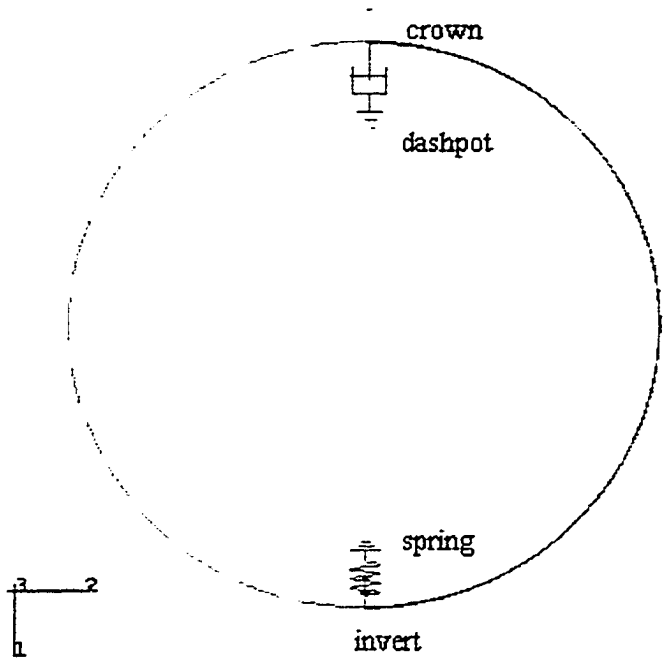

Fig. 5.6 Finite element model for mode transition analysis

The spring and the dashpot elements provide a small resistance to sudden liner movements and are essential for computational stability. The spring applies resistance at low liner velocities while the dashpot limits the velocity from becoming too large. The spring element also produces a slight asymmetry in the vertical direction. As discussed later, the small nodal forces induced by these elements are much smaller than the forces induced by the applied pressure or the liner-host pipe frictional forces and produce little or no change in the final buckling pressure,.

According to buckling theory, the deflection of a constrained liner may have components of both the one- and two-lobe modes, and possibly those of other higher order modes.

The model configuration as used for this simulation can be summarized in as $DR = 50$, $g = 0.025$ in, $D = 12$ in, $k = 0.01$ lbf/in, and $\eta = 0.0001$ lbf/(in/sec). The upper and lower bound predictions are known to be 110.24 and 80.51 psi, respectively. The slight asymmetry induced by the two weak connector elements is enough to activate mode transition. To introduce the initial deflection, a small concentrated load pointing outwards is applied to the middle node in the disturbance step.

A typical mode transition process is illustrated in Figure 5.7. To emphasize the evolution of the liner profile, the displacement has been magnified by a factor of 10 (the apparent extension of the liner outside of the host pipe is a consequence of the initial gap and this magnification). The initial configuration (Fig. 5.7a) quickly deforms into a roughly symmetric pattern after the pressure is applied (Fig. 5.7b). The slight asymmetry in Fig. 5.7b is caused by a small initial shift of the liner toward the spring as the inward deflection at the lobes begins. This slight asymmetry is natural in applications and can be caused by small variations in liner thickness and material properties as well as by buoyancy forces. Figure 5.4 verifies that such asymmetries occur experimentally.

The deflection continues to develop in a two-lobe mode but becomes increasingly asymmetric as the pressure rises (Fig. 5.7c). The larger of the two lobes will generate higher liner-hostpipe contact pressures near the location where the lobe departs from the host pipe. This difference between contact pressure on the upper and lower portions of the liner is the driving force for mode transition (in the absence of other effects such as buoyancy forces). When the asymmetry in liner profile becomes so severe that the liner and the frictional force between the liner and the host pipe can no longer withstand the imbalance in the net vertical contact forces associated with the opposite

lobes, one lobe will become dominant and snap through, and the other lobe may be released, resulting in a shape as shown in Fig. 5.7d and 5.7e. The mode transition as shown in Fig. 5.7d and 5.7e may not always occur; it is possible that one lobe will simply become dominant and buckle while the opposite lobe remains fixed in a stable unreleased configuration.

The load-deflection history of the extreme upper and lower nodes is plotted in Fig. 5.8. Here, it appears that the sudden release of the lower lobe, which occurs when the deflection of the lower node returns to zero, corresponds to snap-through buckling of the upper lobe. Other possible deflection paths are described in the following section.

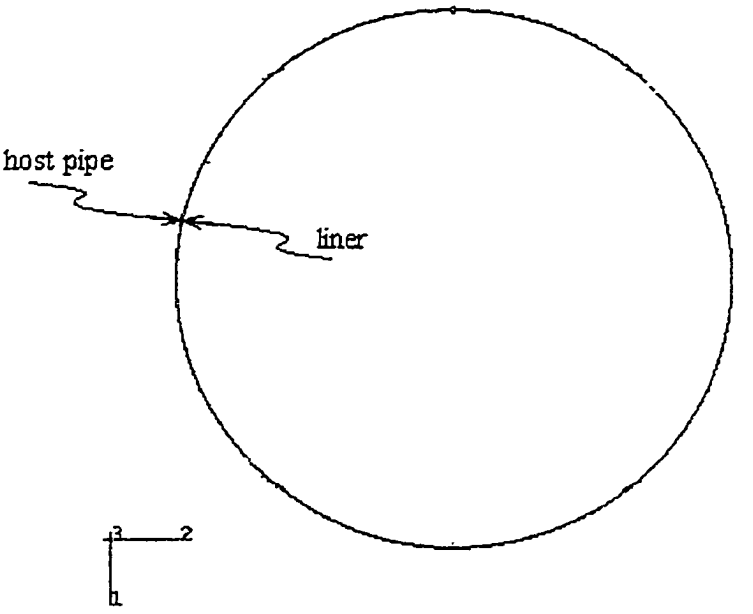

a.initial configuration
(the small initial gap between the liner and host pipe is not visible)

Fig 5.7 Typical deflection evolution process

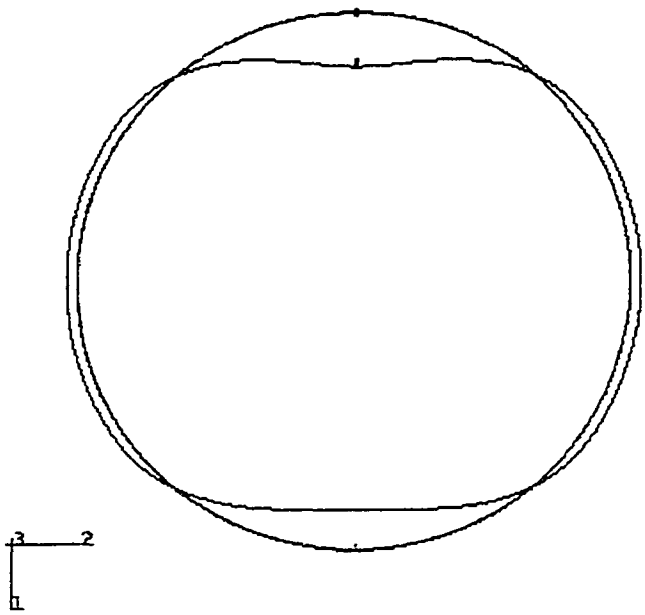

b. initial two-lobe deflection mode

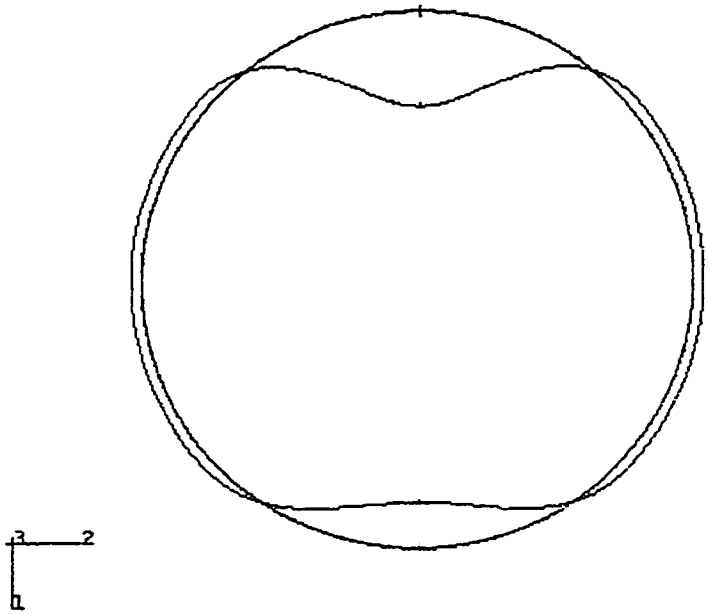

c. increasing asymmetry

Fig 5.7 Typical deflection evolution process (cont'd)

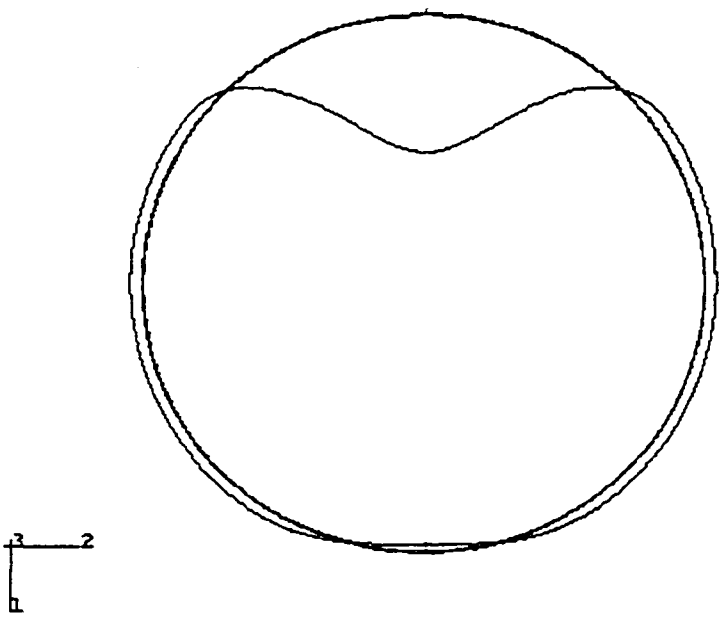

d. mode transition

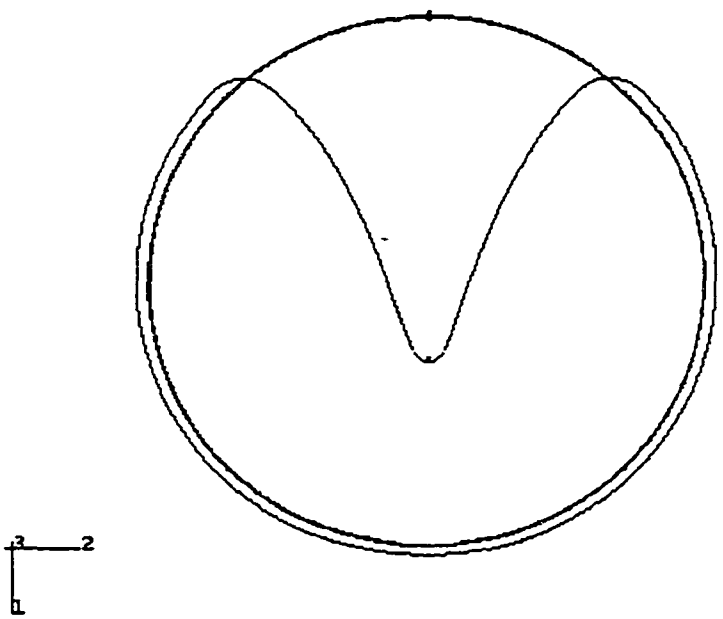

e. one-lobe mode collapse

(Note: The displacement has been magnified by a factor of 10, therefore parts of the liner seem outside of the pipe)

Fig 5.7 Typical deflection evolution process (cont'd)

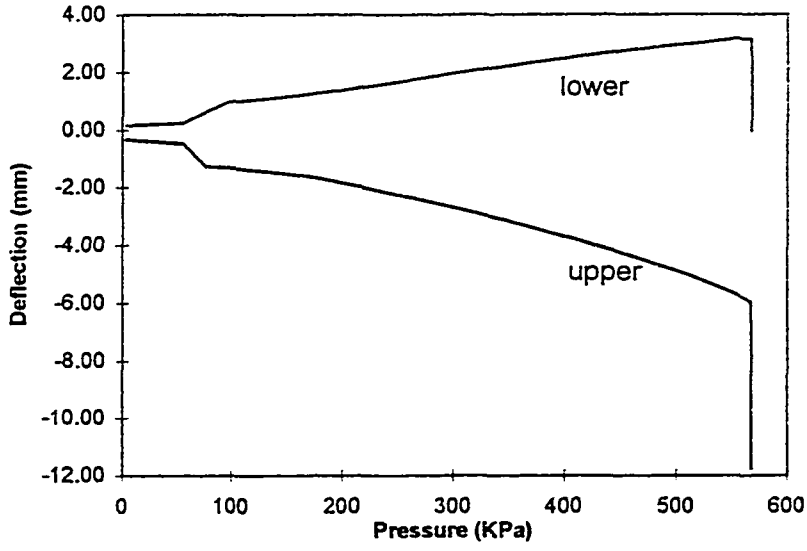

Fig. 5.8 Load-deflection history for upper and lower nodes

5.5 Possible Load-Deflection Paths

The deflection evolution of a liner depends on a number of factors including variations in liner and host pipe geometry, frictional conditions, and material properties. Figure 5.9 shows the deflection evolution of the extreme upper and lower nodes for six cases of liner buckling. As discussed below, changes in the frictional coefficient between the liner and the host pipe may cause the liner to transition from two-lobe to one-lobe buckling at different pressure levels.

Path A: The deflection evolution for a free liner (no host pipe constraint) is given for comparison.

Paths B and C: Path B and Path C correspond to conventional one- and two-lobe buckling modes, respectively. Path C coincides with Path A until the deflected liner begins to receive support from the host pipe. Path B for the upper side (or crown) takes a

slightly different course because liner-hostpipe contact begins at a lower pressure; notice that the deflection at the lower side (or invert) is restricted to zero. Path B and C correspond to lower and upper bound buckling pressures of 558 and 764.0 KPa (80.5 and 110 psi), respectively.

Path D: When there is little or no friction between the liner and the host pipe, the transition from a two-lobe to a one-lobe deflection pattern can occur in an early stage of lobe development. Notice that for Path D, the deflection evolution suddenly transitions to the conventional one-lobe pattern, thereafter following Path B to failure.

Path E: The presence of significant friction between the liner and the host pipe will prevent early transition from a two- to a one-lobe pattern. Path E shows that with friction present, the liner snaps through at a pressure slightly greater than the lower bound pressure. Here, snap-through corresponds to collapse of the crown and the simultaneous disappearance of the lobe at the invert.

Path F: As the friction between the liner and the host pipe increases, the pressure level at which the dominant lobe snaps through also increases. Path F indicates that increased friction results in snap through at a pressure level closer to the conventional two-lobe buckling pressure. The invert lobe may stay stationary or completely release after snap-through from the crown lobe. The post-buckling behavior was not attempted in the present study.

Paths D, E, and F above correspond to liner-hostpipe friction factors of 0, 0.14, 0.20, respectively. Buckling mode transition may be initiated by a number of other

factors including variations in liner thickness and material properties as well as in host pipe geometry variations. Finite element simulations of mode transition caused by liner thickness variations and initial eccentricity of the liner-pipe system have been undertaken in this study.

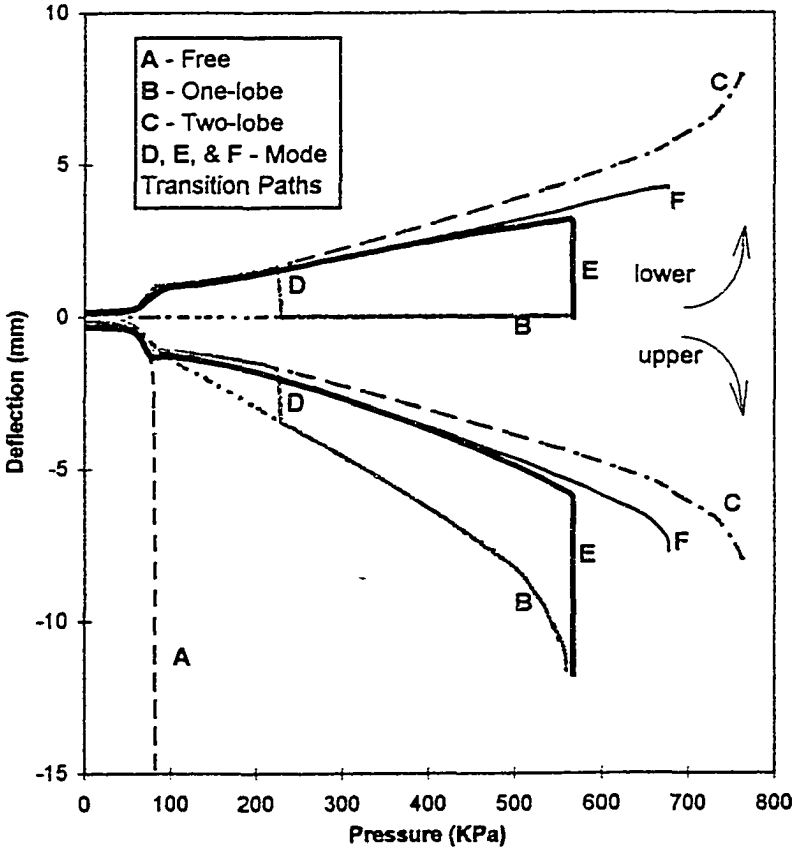

Fig. 5.9 Possible transition paths

In summary, variations in liner-hostpipe geometry and material parameters result in liner buckling at pressures between the lower bound (one-lobe) buckling pressure and the upper bound (two-lobe) buckling pressure. As a result of the complex nature of this buckling phenomenon and the lack of precise data in field applications, it is

recommended that liner design be based on the lower bound buckling pressure associated with one-lobe buckling models.

5.6 Conclusions

Experimental results showing the load-deflection evolution of liners constrained within rigid host pipes indicate an initial two-lobe buckling mode which eventually leads to a single-lobe collapse. The phenomenon whereby the buckling mode transitions from a two-lobe mode to a one-lobe mode is not well understood. This chapter helps to clarify this issue through finite element simulations of buckling mode transition, resulting in the conclusions listed below.

1) The conventional one- and two-lobe buckling modes are found to give lower and upper bounds for all possible critical pressures. The finite element predictions show excellent agreement with experimental data, with most of the experimental data falling between the predicted lower and upper bounds.

2) Experimentally observed load-deflection paths are characterized by transitions from the two-lobe mode, which corresponds to a higher critical pressure, to the one-lobe mode. A finite element approach has been used to simulate the possible deflection evolution paths.

3) The load-deflection paths determined from finite element analysis are seen to fall between the paths corresponding to the conventional one-lobe and two-lobe buckling modes, depending on the specific conditions of the liner system (e.g. friction factor, initial gap, liner thickness variations, etc.).

4) Because these conditions are not controllable in many engineering

applications, the design of such liner systems should be based on one-lobe buckling models corresponding to a conservative lower-bound buckling prediction.

CHAPTER 6

BUCKLING PRESSURE OF CIPP LINERS IN CIRCULAR AND OVAL PIPES

The effect of geometric parameters on accurate prediction of buckling pressure of CIPP liners will be discussed in this chapter. An empirical model will be used to relate the buckling pressure, based on the one-lobe mode (Chapter 5), to the dimension ratio (DR) of liners and to coefficients that depend on geometric imperfections of the liner-host pipe system. These coefficients can be determined by a small number of finite element runs over a range of the geometric parameters and by numerical analysis techniques such as the Lagrange interpolation and least-squares.

6.1 Parametric Study

Since buckling resistance of an encased liner is highly enhanced by the interaction with its host pipe, any factor which causes a certain change (or degradation) from the ideal fitting between a liner and its host pipe may lead to a reduction in the enhancement, and hence to reduction in the liner's buckling pressure. The effect of each factor can be determined by a parametric study.

6.1.1 Influential Parameters

The dimension ratio (*DR*) is the first parameter to be included in the study, since is

is essential to any pipe design where buckling is involved. In the context of constrained CIPP liners, the most influential factors are the geometric imperfections of the liner-pipe system as a whole, most important of which is the gap (annular spacing) between a liner and its host pipe. When the deteriorated pipe loses its original circular shape, the ovality of the host pipe should be considered. These three factors (gap, *DR*, and ovality) are considered essential for accurate prediction of buckling pressure, and will be included in the following study in order to develop an empirical model for liner design based on short term buckling criterion. Other factors, such as variation of liner thickness and local imperfections will be discussed in the long-term buckling case (Chapter 8).

Of the parameters, *DR* and host pipe ovality (OV) are dimensionless. To enhance the applicability of the model and the ability to compare its results with those available in the literature, an effective gap parameter, which is the ratio of the total gap to the mean diameter of the liner, is used.

Because of the thermal contraction after the curing process, a gap between a liner and its host-pipe cannot be avoided in the liner-pipe system. In Guice et al. (1994), gap was measured by using feeler gages and thus limited to the ends of the specimens. Total annular spacing volume was included in the latest test program at the TTC (1998a) as a measure of average gap size. According to the volume measurement data, an effective (uniform) gap size g can be determined by averaging the volume uniformly over the whole outer area of the liner. A dimensionless gap parameter G is defined as the ratio of the uniform gap size g to the liner mean diameter D.

As discussed in Chapter 5, in a practical design process, the one-lobe model can be used to give a lower bound on the prediction of critical pressure of an encased CIPP

liner. Therefore, in this chapter, gap is assumed to be unevenly distributed along the circumference, which implies that the one-lobe model will be used. In the one-lobe model, the gap size is $2g$ at the *crown*; at and is zero at the *invert*.

The ranges of interest of the dimensionless parameters are defined as follows:

1) Dimension Ratio (*DR*): This parameter is defined as the ratio of the mean diameter (measured at the middle surface) to the thickness of a liner. Three levels (35, 50, and 65) were chosen over a moderate range of *DR*, to ensure that meaningful empirical formulas can be derived.
2) Dimensionless Gap (*G*): Three levels for even gap ratio *G* were chosen as 0.1, 0.4, and 0.7%, based on test conditions which are considered representative in real applications.
3) Host Pipe Ovality (*OV*): The ovality levels of 0, 3, and 6% were selected to compare with experimental data, in which nominal ovality values of 2 and 5% were used. An ellipse shape for both pipe and liner were assumed.

6.1.2 Results and Analysis

Based on the following considerations, only three levels were chosen for each parameter and the finite element analyses were run over the 27 combinations:

1) The dependency of ultimate pressure on each parameter is rather monotonous. Ultimate pressure decreases when any or all of *DR*, *G*, and *OV* increases.
2) The response surface of P_{cr} is smooth enough over the selected region to allow accurate interpolation by employing simple numerical techniques, such as the Lagrangian polynomial.

3) It is convenient in the design environment if only a few finite element runs will help to set up adequate design criteria.

The short term buckling analysis procedure, as discussed in Chapter 4, was employed to give ultimate pressure predictions. The material properties were from Stokeld's (1998) test (see Appendix A.1). The 27 ultimate pressure values are listed in Table 6.1.

Table 6.1 FEA predictions of critical pressure

	OV=0			OV=3%			OV=6%		
	G=.1%	G=.4%	G=.7%	G=.1%	G=.4%	G=.7%	G=.1%	G=.4%	G=.7%
DR=35	190.8	146.3	118.9	163.8	123.9	99.1	142.6	105.1	82.7
DR=50	89.9	61.9	48.1	77.2	52.0	40.1	65.8	44.1	33.7
DR=65	49.3	31.8	24.1	42.1	26.8	20.2	36.1	22.5	17.0

6.2 Empirical Model

As mentioned in Chapter 2, Omara et al. (1997) suggested that Glock's model for constrained pipes (Eqn. 2.5) and the Timoshenko's equation (Eqn. 2.2) can be expressed in the same form (Eqn. 2.10) as a power function of the D/t ratio. Equation (2.10) can be rewritten in the following format

$$P_{cr} / E^{*} = aDR^{-m} \tag{6.1}$$

where the effective modulus E^{*} is the Young's modulus E for plane stress and $E/(1-\nu^2)$ for plane strain. In Glock's model, a and m are 1 and 2.2, while in the Timoshenko's equation, a and m are 2 and 3, respectively. Equation (6.1) may be used as an empirical model, with the coefficient a and exponent m to be determined for various geometric parameters.

6.2.1 Effect of Dimension Ratio

The effect of *DR* is visualized by log-log plots for each {*G*, *OV*} combination, as illustrated in Fig. 6.1. As can be clearly seen from the figure, each curve, corresponding to a specific {*G*, *OV*} combination, looks very close to a straight line,

$$\lg(P_{cr} / E^{*}) = \lg a - m\lg(DR) \qquad (6.2)$$

which verifies the proposed expression in Eqn. (6.1).

By employing the least-square regression technique, the *a* and *m* values were determined for each of the 9 {*G*, *OV*} combinations, as listed in Table 6.2. Of the 9 regression analyses, the lowest R-squared value is 0.9997, very close to the highest possible value 1. This R-squared value indicates that Eqn. (6.1) is a good model expressing P_{cr} as a function of *DR*. Results listed in Table 6.2 show that the values vary approximately from 0.55 to 1.65 for *a* and 2.15 to 2.55 for *m*.

As can be seen from Eqn. (6.2), *m* is the slope and lg(*a*) the intercept of the linear regression equation. One feature of the *a* and *m* pair is that a smaller *m* tends to accompany a smaller *a*, since a less inclined line tends to intersect the vertical axis at a lower point.

Table 6.2 Fitting constants *a* and *m*

a. intercept factor *a*

a	OV = 0	OV = 3%	OV = 6%
G = .1%	0.626380	0.541558	0.544630
G = .4%	1.328110	1.191958	1.038094
G = .7%	1.643238	1.349973	1.197897

b. slope *m*

m	OV = 0	OV = 3%	OV = 6%
G = .1%	2.1506	2.1526	2.1934
G = .4%	2.4369	2.4532	2.4607
G = .7%	2.5552	2.5512	2.5661

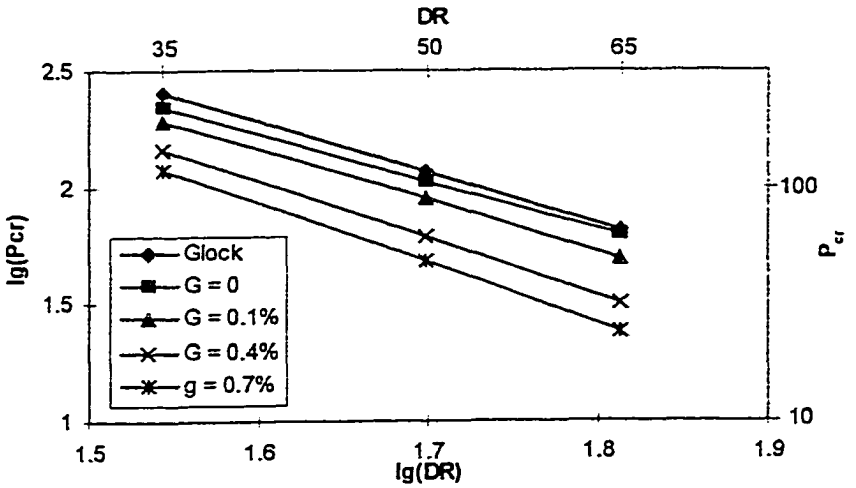

a. $OV = 0$

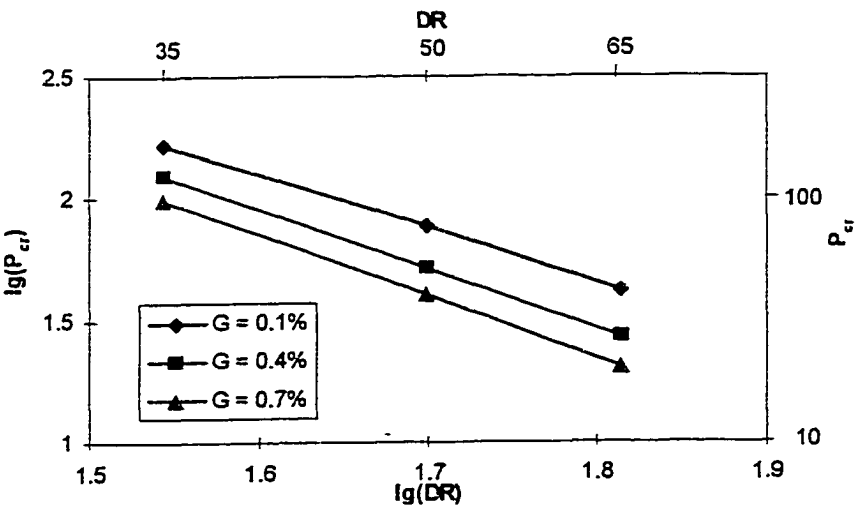

b. $OV = 3\%$

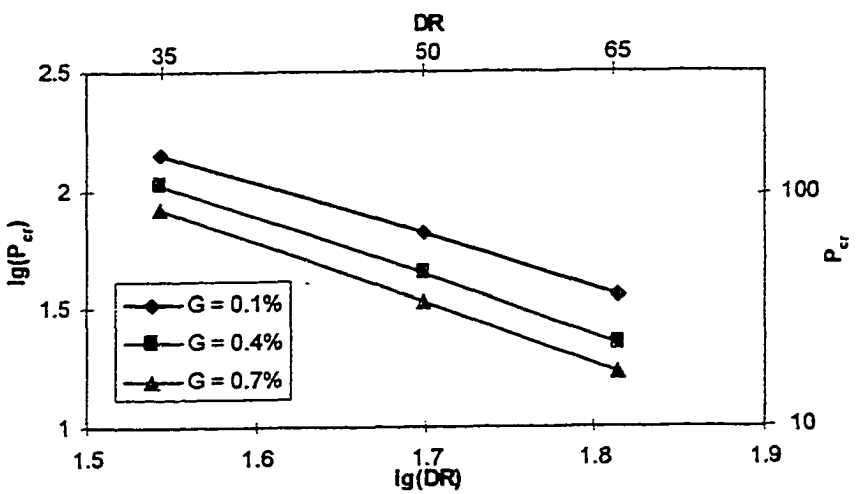

c. $OV = 6\%$

Fig. 6.1 Effect of *DR*

6.2.2 Effect of Gap

As illustrated in Fig. 6.1, ultimate pressure drops with an increase in G for any given pair of $\{DR,OV\}$. It can also be seen from Fig. 6.2 and Table 6.2b that the slope m value increases with an increase in G. This implies that P_{cr} decreases faster with an increase in DR under a large dimensionless gap G.

The effect of gap, especially when combined with DR, on the enhancement factor K, is investigated by using Eqn. (6.1) and the Timoshenko's equation (2.2). Here, K may be expressed as

$$K = \frac{a}{2} DR^{3-m} \tag{6.3}$$

Table 6.3 gives the K values thus obtained for a circular pipe and liner over the region of interest, which vary from 3.95 (for $DR = 35$ and $G = 0.1\%$) to 14.94 (for $DR = 90$ and $G = 0.7\%$). The variation shows that the validity of assuming $K = 7$ depends on both the dimension ratio DR and liner-pipe fitting condition achieved in a rehabilitation application. The accuracy of predictions for K listed here will be verified shortly in the model validation section.

Table 6.3 Predicted enhancement factor *K*

DR	*G*=0.1%	*G*=0.2%	*G*=0.3%	*G*=0.4%	*G*=0.7%
35.0	6.27	5.71	5.24	4.83	3.95
39.0	6.92	6.23	5.65	5.17	4.16
44.0	7.74	6.86	6.15	5.57	4.40
49.0	8.54	7.48	6.64	5.96	4.64
50.0	8.70	7.60	6.73	6.03	4.68
52.5	9.10	7.91	6.97	6.22	4.79
58.5	10.05	8.63	7.52	6.65	5.05
65.0	11.08	9.39	8.09	7.10	5.31
90.0	14.94	12.19	10.18	8.69	6.21

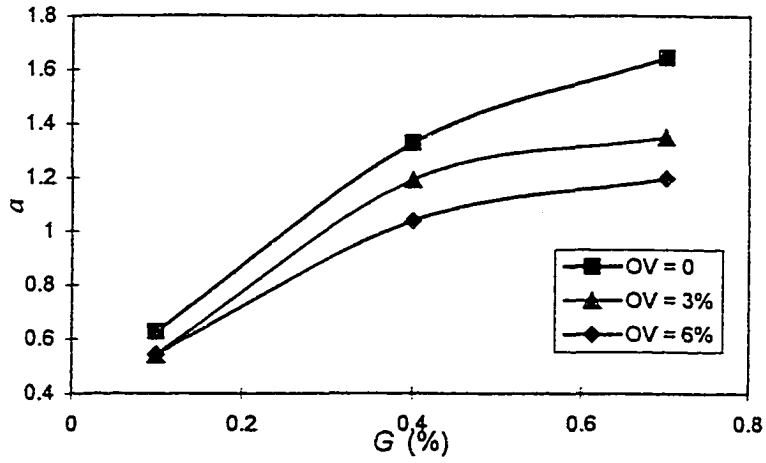

a. intercept factor *a*

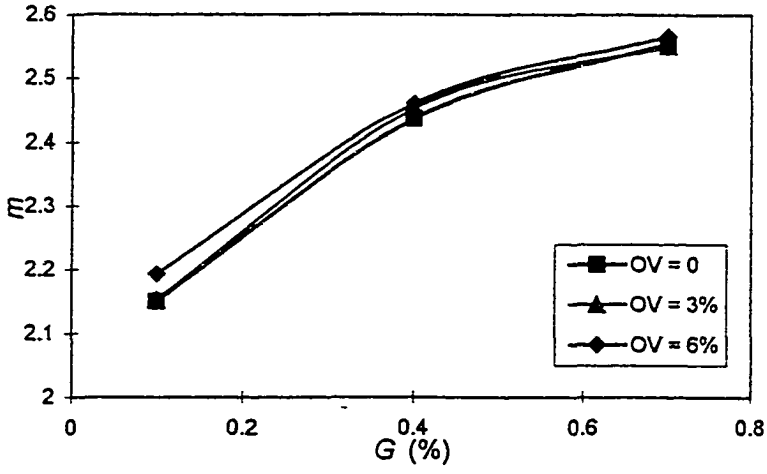

b. slope *m*

Fig. 6.2 Effect of *G*

6.2.3 Effect of Ovality

As can be seen from Fig. 6.2 and Table 6.2b, the slope m does not vary much for different ovality levels. This means that the reduction factor as the result of pipe ovality, $P_{cr}^{OV} / P_{cr}^{CIR}$ is almost independent of the DR ratio. An equation for the reduction factor based on the lower bound developed from FEA results listed in Table 6.1 can be written as

$$\alpha = \exp\{-OV / 15\} \tag{6.4}$$

which is lower than the equation proposed by El-Sawy and Moore (1997). This difference is because in the present study, the effects of plastic yield and gap between the liner and its host pipe were taken into account.

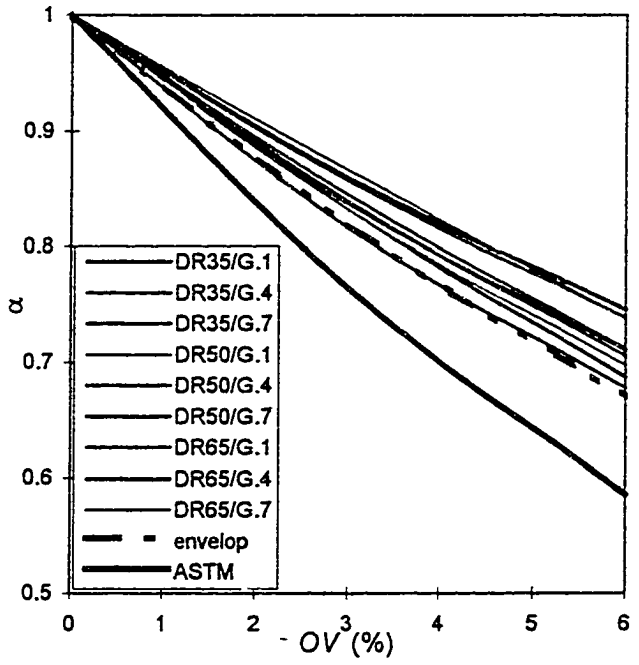

Fig. 6.3 Reduction factor due to pipe ovality *OV*

6.3 Model Verification

The ultimate pressure predictions given in the prior section will be checked against analytical and experimental results to verify the validity of the proposed model.

6.3.1 FEA Results versus Glock's Model

A number of FEA runs were conducted for the case of $G = 0$, i.e. the no-gap case, in order to compare with the analytical solution given by Glock (1977). Both elastic and elastoplastic constitutive relations were used in the finite element runs. It can be seen

from Fig. 6.1a that the elastic solutions agreed well with Glock's, as was also observed by El-Sawy and Moore (1997). The corresponding elastoplastic analyses gave lower predictions since material failure did accelerate the final collapse of the liner. The slope of the elastoplastic solution curve (m = -1.9388) was lower than that in Glock's model because the thicker the liner (corresponding to a lower DR ratio), the higher the influence of the plastic yield. Consequently, the a coefficient (a = .3199) was also lower, indicating that the less inclined line intersects with the lg(P_{cr}) axis at a lower point than that associated with Glock's solution.

6.3.2 FEA versus Experimental Results

The latest physical test data available at the TTC, Louisiana Tech University, were used to validate the FEA results presented in earlier sections. In addition to the data for the two circular pipe series (12"ID and 8"ID) mentioned in Chapter 5, results from a series of oval pipe tests with a nominal (equivalent) diameter of 12" were also used. The recorded dimension ratio, ovality and gap measurements were used to generate the parameters necessary for interpolating the predictions of ultimate pressure from FEA results given in Table 6.4. The FEA results gave lower bound predictions as expected because the one-lobe mode is used.

It can be seen from Fig. 6.4a that a majority of the observed buckling pressures were above the G = 0.2% curve, which is the average gap as determined by the gap volume measurements. The curves corresponding to G = 0.1, 0.3, and 0.4% are also presented. Only one of the test data points fell below the range, and may therefore be deemed as an outlier.

In the oval pipe tests, the average gap magnitude was 5%. It can be seen from Fig. 6.4b that for 0 and 2% ovality, most of the test data were above the $G = 0.5\%$ curve. For OV = 5%, the observed buckling pressures were closer to the 5% curve. This phenomenon may be explained by the fact a liner is more ready to buckle in the one-lobe mode when ovality of its host pipe is large.

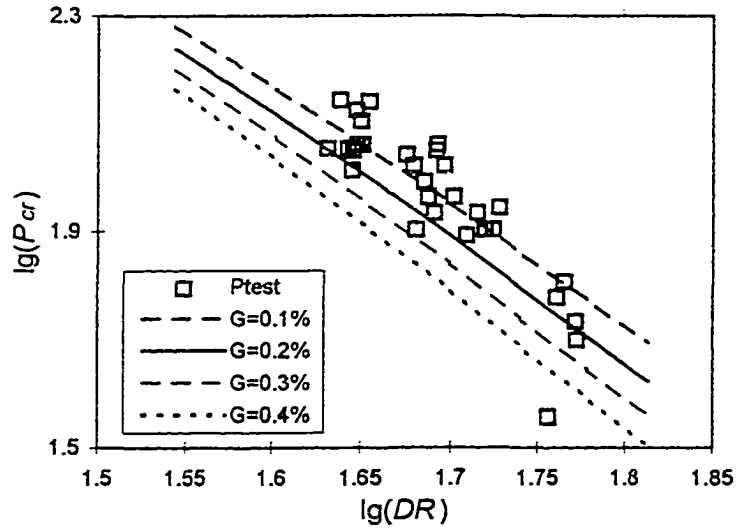

a. Circular pipes

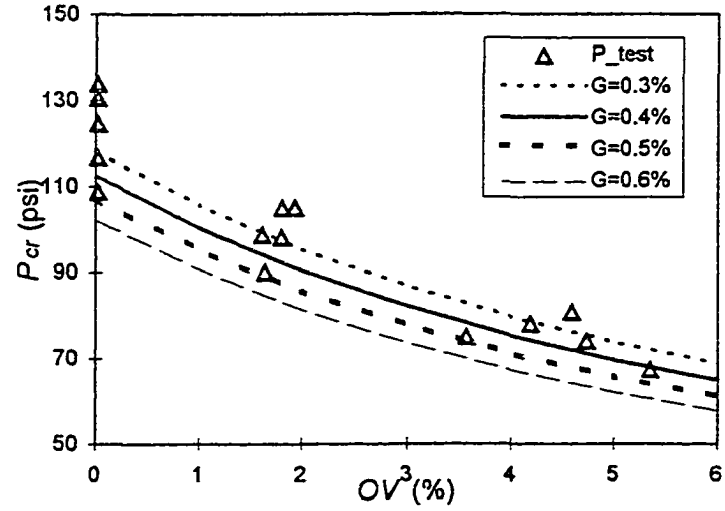

b. Oval pipes

Fig. 6.4 Predicted versus test data

6.4 Conclusions

From the results presented in this chapter, the following conclusions can be drawn:

1) The finite element simulation revealed the fundamental structural behavior of constrained CIPP liners subjected to external pressure. Accurate prediction of ultimate buckling pressure depends greatly on knowledge of material properties and the geometrical factors of the liner-pipe system.
2) By using an appropriate finite element approach, the effects of specific mechanical properties (e.g. yield limit), gap, and ovality were determined. Excellent agreement between analytical and test results were found.
3) The critical pressure at which a liner buckles can be determined by Eqn (6.1). The dependency of the a and m on the ovality, DR, and gap was determined from finite element runs and standard interpolation techniques.
4) The enhancement factor K (frequently referred to in CIPP design guidelines and in the literature) depends greatly on parameters including the dimension ratio, gap, ovality, and yield limits. The suggested $K = 7$ value may not be suitable for design purpose. Predictions by means of the methodology presented in this paper will lead to conservative designs.
5) A comparison between predicted and test results show that in the case of oval pipes, buckling pressures tend to be close to the lower bound predicted by the one-lobe buckling mode.

CHAPTER 7

CREEP BUCKLING OF CIPP LINERS

Finite element simulation of creep-induced buckling behavior of encased CIPP liners will be discussed in this chapter. The similarities between long- and short-term buckling will be addressed first, especially the stress and strain evolution curves. Emphasis will then be focused on models used to correlate the critical time to the external pressure level.

Creep property characterization results from Lin (1995) will be used to predict the critical time. Finite element results will be checked against long-term test results from Guice et al. (1994) to calibrate the proposed model.

7.1 Similarities to Instantaneous Buckling

The one- and two-lobe models are again used here to illustrate the typical long-term buckling behavior of a constrained CIPP liner. The pipe inner diameter is set at 12". The liner geometry is taken from the average of the 39 *Instituform Enhanced* samples (D-series) reported by Guice et al. (1994) with a liner mean diameter D_{mean} = 11.729", and thickness t = 0.221". The mean gap, g = 0.025", is determined as one half of the difference between pipe inner and liner outer diameters. The dimension ratio DR and the relative gap G can then be determined as 53.07 and 0.213 %, respectively (Fig. 4.6).

A free ring as specified above is known to buckle at a critical pressure of 9.91 psi (assuming the plane strain condition) based on the well-known Timoshenko's equation (2.2). The buckling pressure predictions associated with the one- and two-lobe models have been calculated by employing the same short-term buckling procedure as in Chapter 5, as 78.17 and 105.07 psi, respectively.

The finite element models used in creep buckling analysis are not different from the ones used in the instantaneous analysis, except for the additional information of creep property. As introduced in Chapter 4, in the loading step, the external pressure is applied to the liner and increased until a desired level (lower than the instantaneous buckling pressures given above) is reached. A `*VISCO` step is then used to simulate the time-dependent deformation induced by creep under constant pressure. The solution step stops when one of the strain rate components is infinitely large, which is the indication of the onset of buckling.

7.1.1 Stress Distribution and Evolution

A sustained pressure of 65.236 psi, or 80% of the critical pressure of the one-lobe model, is used here as an example. The buckling mode and stress distribution are identical to those discussed in the previous section. Figures 7.1 and 7.2 show the curves of maximum deflection (at Point I) and maximum stresses (at Points I and II) versus time for the one-lobe model, respectively.

The stress history shows that the compressive yield limit is reached at the middle of the lobe (Point I), after the pressure (of 62.536 psi) is loaded for about 70 hours. The ring then becomes weaker than the elastic model, and buckles soon after the tensile stress

at the middle of the lobe and the compressive stress at the end of the lobe reach their limits at the same time, 250 hours after the pressure is applied.

When material failure is not taken into account, the predicted critical time increases greatly, from 250.39 to 1153.63 hours.

For comparison purposes, critical times (visco-elastic and visco-elastoplastic) predicted for the two-lobe model under the same pressure (65.236 psi) are also presented in Table 7.1. As can be seen, they are much greater than the corresponding one-lobe predictions. Therefore, to be on the conservative side, only the one-lobe model will be used in the sequel to investigate liner life-time prediction.

Table 7.1 FEA predictions for the example

	P_{cr}(psi)	d_{cr}(in)	T_{cr}(hr)	d_{cr}(in)
Free model				
realistic	9.97	--	--	--
One-lobe model				
realistic	78.17	0.4048	250.39	0.4840
elastic	93.74	0.6119	1153.63	0.7912
Two-lobe model				
realistic	105.07	0.2511	84133.4	0.4707
elastic	127.61	0.4343	106465.0	0.6950

As shown in Fig 7.1, the effect of plastic yield is not so significant in the two-lobe model as in the one-lobe model. This phenomenon can be explained by the fact that the external pressure applied was only 61.9% of the instantaneous critical pressure for the two-lobe model. The maximum stresses (Fig. 7.3) start at low levels and reach the yield limits just before the elastic snap-through time is approached.

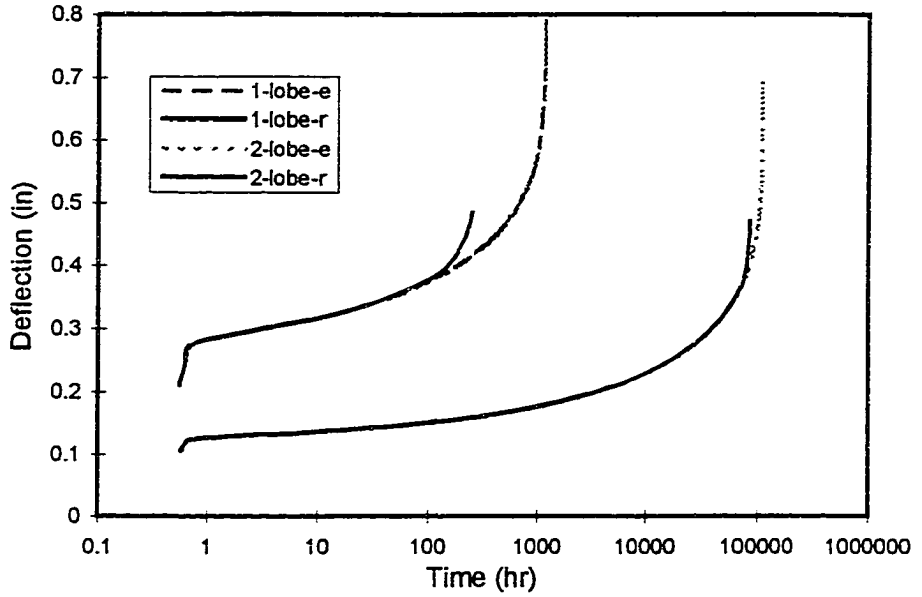

Fig. 7.1 Typical time-deflection curves

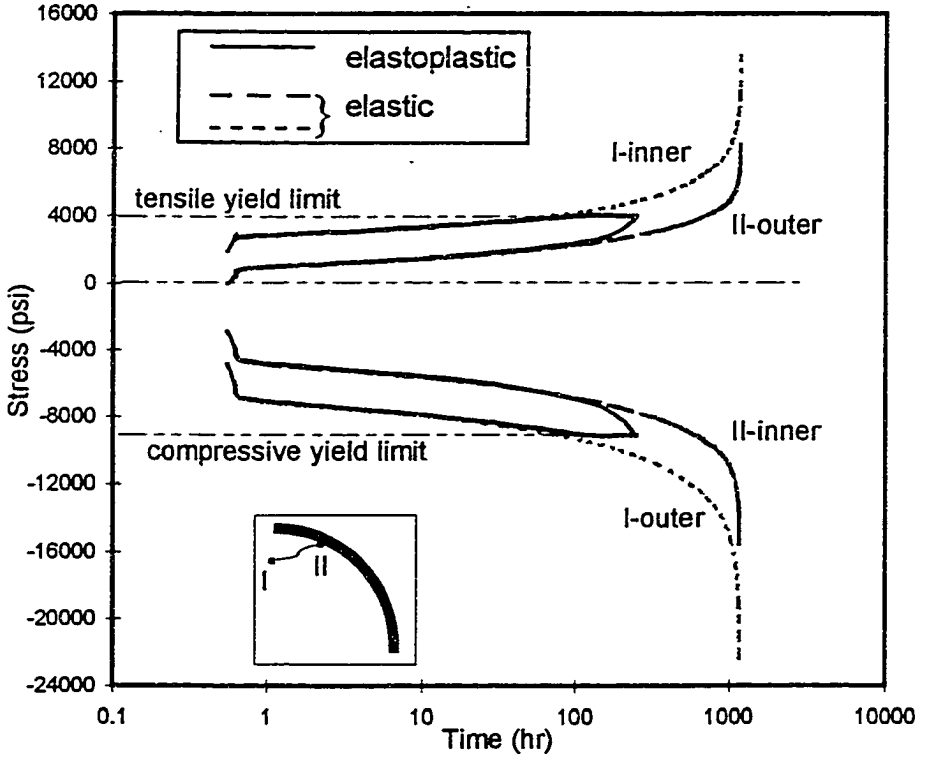

Fig. 7.2 Typical maximum stress history for the one-lobe model

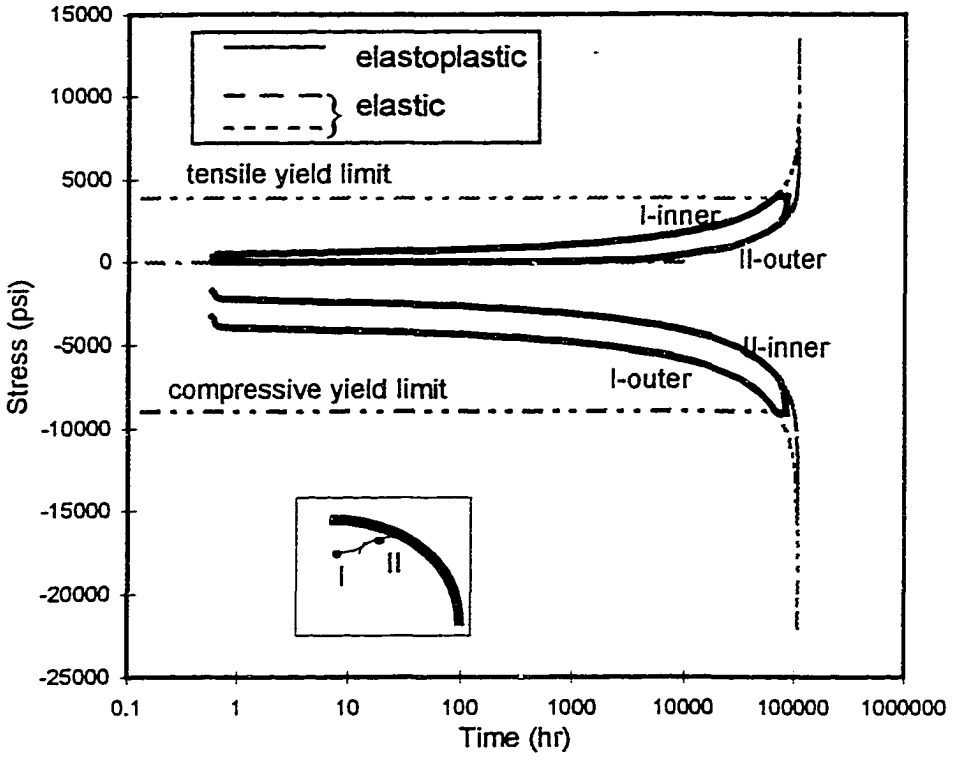

Fig. 7.3 Typical maximum stress history for the two-lobe model

7.1.2 Time-Deflection Curves for Various Pressure Levels

As mentioned earlier in the analysis of creep-induced buckling, there are two critical parameters used in pairs: the critical time associated with a specific load which is a fraction of the critical load for instantaneous buckling. Sometimes the applied sustained load is also called critical load in the sense that the structure is in the critical state (for buckling) under that specific load which lasts for a certain period of time.

It is reasonable to assume that the critical time will decrease with an increase in external pressure. This trend has been observed in long-term buckling tests by Guice et al. (1994), although the data scattered considerably because of the variation in liner geometry. With the aid of finite element simulation, the geometric parameters of the liner-

pipe system can be precisely controlled, and the buckling behavior of an encased liner under various pressure levels (denoted by dimensionless pressure ratio $PR = P/P_{cr}$) can be studied systematically.

Typical time-deflection curves for the present example under various pressure levels (i.e. PR = 0.1, 0.3, 0.5, 0.6, 0.7, 0.8, 0.9) are plotted in Fig. 7.4. It can be seen that the critical time decreases when the external pressure level increases (Table 7.2).

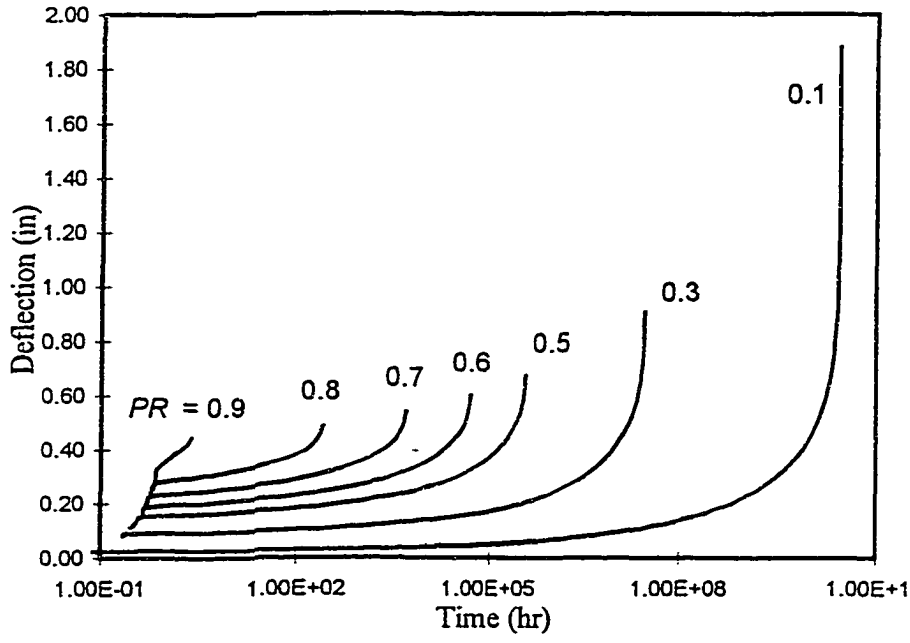

Fig. 7.4 Typical time-deflection curves for various pressure levels

The effect of plastic yield in the liner material can be seen by examining the critical deflection against associated pressure level: when pressure is high, i.e. $PR \geq 0.6$ in the specific example, material yields before deflection is fully developed and buckling occurs immediately thereafter. By contrast, when pressure is low, material may not yield until the deflection is very large.

7.2 Models for Predicting Critical Time

The correlation between the critical time and the applied compressive load is desirable in designs based on creep buckling criteria. Empirical models used in the literature to fit buckling test data will be first discussed, followed by a presentation of a model to be used in the present study.

7.2.1 Models for Fitting Test Data

Several empirical models have been used in the literature to depict the monotonic descendent relation between buckling time T and compressive load P.

A two-parameter power function was used by Guice et al. (1994) to fit the 10,000-hour buckling test data. For the purpose of determining design pressure with regard to the expected service life of CIPP liners, external pressure P was expressed as a function of time T as follows.

$$P = aT^{-b} \qquad (7.1)$$

A least-square regression analysis was used to calculate the constants a and b, based on the $\{P, T\}$ pairs observed in long-term buckling tests. This simple formed model was shown to give good fit to the test data.

An exponential function was used by Cohen and Arends (1989a) to fit critical time data obtained from creep buckling tests of plastic bars. In their experiment, the geometry of the high-density polyethylene (HDPE) bars could be controlled more precisely by means of machining, and there were no such uncertainties as those induced by gap and external rigid constraints. The data could be best fitted by the following exponential function

$$T_{cr} = T_0 \exp(-P / P_0) \tag{7.2}$$

where T_0 and P_0 are constants. The time constant T_0 was a very large number, intended to reflect the infinitely large critical time when no compressive load was applied; and P_0 was much smaller than the critical pressure of the plastic bar. This equation was modified later (Cohen and Arends 1989b) to the following form in order to force T_{cr} to be infinite when $P = 0$.

$$T_{cr} = T_0 (P_0 / P) \exp(-P / P_0) \tag{7.3}$$

7.2.2 Proposed Model

Precisely controlled numerical tests conducted in the present study allow for a more rational model to be specified based directly on knowledge of critical pressure. The relationship between critical time T_{cr} and the external pressure P can be expressed as

$$T_{cr} = \tilde{T}_0 (1/P - 1/P_{cr})^n \tag{7.4}$$

By introducing the dimensionless pressure ratio $PR = P/P_{cr}$, the model can be rewritten as

$$T_{cr} = T_0 (1/PR - 1)^n \tag{7.5}$$

This model intends to reflect the following intuitions to the T_{cr} - P relation:

1) When PR = 1, i.e. the critical pressure is applied, a liner will buckle instantaneously, i.e. $T_{cr} = 0$;

2) A liner will not buckle ($T_{cr} = \infty$) when no pressure is applied, i.e. $PR = 0$;

3) The critical time T_{cr} increases monotonically with a decrease in PR;

4) The time constant T_0 is the nominal life of a constrained liner (with a specific DR and G) when the applied pressure is one half of the corresponding critical pressure ($PR = 0.5$).

A parameter b, slightly less than 1, may be needed in fitting

$$T_{cr} = T_0(b / PR - 1)^n \tag{7.6}$$

in order to give better agreement over the whole PR range. Furthermore, a purely dimensionless relationship can be reached by introducing the time ratio $TR = T_{cr} / T_0$ into Eqn. (7.6) to yield

$$TR = (b / PR - 1)^n \tag{7.7}$$

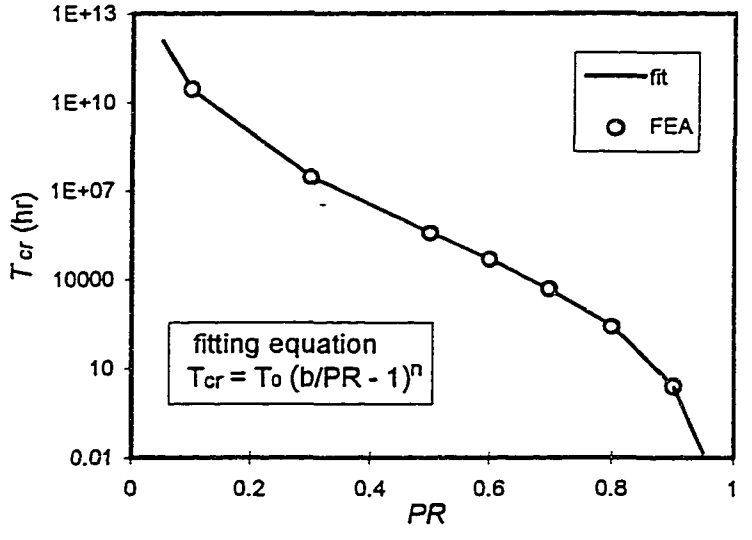

Fig. 7.5 Typical critical time-pressure ratio curve

The critical times for various pressure ratios (as listed in Table 7.2, column FEA) are plotted in a linear-log coordinate system in Fig. 7.5 together with the least squares fitting curve based on Eqn. (7.6). (See Appendix D for the source code of the computer program used for this purpose.) The curve shows that the model fits extremely well with

FEA results over the whole range of *PR* (from 0.1 to 0.9). A standard regression analysis gives the value of 1.0 for the correlation between predicted (by Eqn. 7.6) and FEA results.

Table 7.2 Critical time versus pressure ratio

PR	FEA	Eqn. (7.6)	Eqn. (7.2)	Eqn. (7.3)	Eqn. (7.1)*	Eqn. (7.1)**	Eqn. (7.1)
0.95	--	1.42E-02	2.31E+00	2.21E+00	2.85E+01	6.53E+03	9.77E+01
0.90	2.43E+00	2.44E+00	8.86E+00	8.00E+00	6.54E+01	9.45E+03	1.63E+02
0.80	2.50E+02	2.58E+02	1.30E+02	1.06E+02	3.99E+02	2.11E+04	4.97E+02
0.70	4.82E+03	4.66E+03	1.90E+03	1.44E+03	3.10E+03	5.27E+04	1.76E+03
0.60	4.86E+04	4.71E+04	2.79E+04	1.98E+04	3.31E+04	1.51E+05	7.55E+03
0.50	3.78E+05	3.83E+05	4.09E+05	2.80E+05	5.43E+05	5.27E+05	4.23E+04
0.30	2.82E+07	2.91E+07	8.80E+07	6.52E+07	1.39E+09	1.74E+07	5.31E+06
0.10	2.74E+10	2.71E+10	1.89E+10	2.73E+10	2.94E+16	3.19E+10	1.73E+11

The parameters T_0, n, and b are dependent on material properties and liner-pipe configuration. The determination of these parameters by means of finite element analysis will be presented in detail in Chapter 8.

7.2.3 Evaluation of Models

The same set of critical time data are then fitted (by using least squares) to the models given in Eqns. (7.1) to (7.3). The results are compared in Table 7.2 and Fig. 7.6.

The two exponential functions (Eqns. 7.2 and 7.3) do not differ significantly from each other, except for $PR < 0.1$. They both fit well with the finite element results within the moderate *PR* range, from 0.3 to 0.7. For lower *PR* ratios, i.e. $PR < 0.3$, they tend to give conservative predictions for critical time. On the other hand, they tend to give higher predictions when *PR* is higher then 0.7. This trend is usually acceptable, since CIPP liners will rarely be designed to work under *PR* greater than 0.3.

The power function (Eqn. 7.1) represents a straight line in a log-log plot, which does not resemble the curvature characteristic depicted by the finite element results over the whole *PR* range (from 0.1 to 0.9). Two separate fits have been performed by using Eqn. (7.1) over *PR* ranges of [0.1, 0.5] and [0.5, 0.8], respectively. The latter *PR* range, [0.5, 0.8] is very close to that used in the CPAR tests (Guice et al., 1994). The fit based on the power function over the 0.5 to 0.8 range (labeled as Eqn. (7.1)* in Fig. 7.6) tends to give considerably higher predictions than finite element results. The other fit (labeled as Eqn. (7.1)**) gives better predictions for the low *PR* range, but still is not on the conservative side.

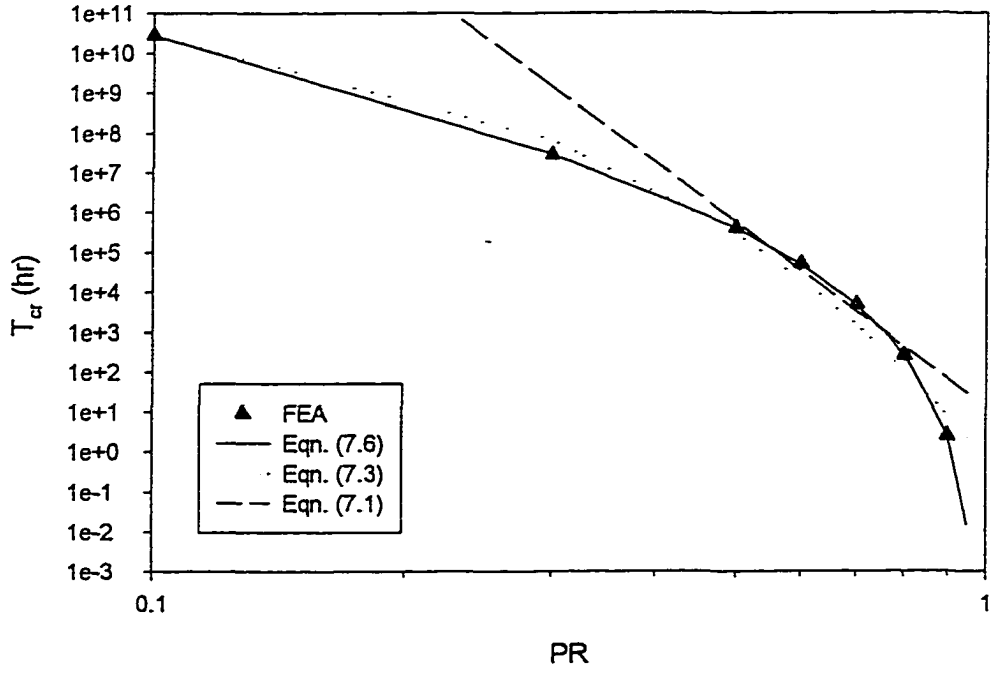

Fig. 7.6 Comparison of models for predicting critical time

Therefore, it seems that the exponential models, especially Eqn. (7.2), are more preferable in fitting long-term buckling test data, because of their conservative predictions.

7.3 Model Verification

Comparison with Models Using 2-D Continuum Elements. To verify the capability of the proposed composite beam element in the analysis of creep buckling of a constrained ring subject to external pressure, the following example has been modeled by composite beam, CPE8 elements (8-node 2-D elements with the plane strain assumption), respectively (Fig. 7.7). The liner mean diameter D_{mean} is set to 25", with a thickness t of 0.5", and a maximum gap $2g$ of 0.5". Therefore, the dimension ratio DR and relative gap G are 50 and 0.2 %, respectively.

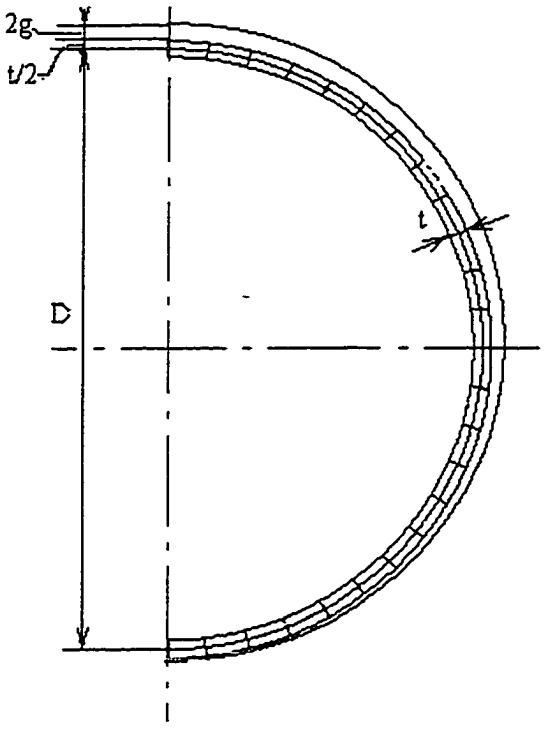

Fig. 7.7 2-D FEA model using CPE8 elements

As can be seen from the results listed in Table 7.3, the two models predict very similar critical results for both instantaneous and long-term (creep-induced) buckling. The beam model is just a little bit stiffer than the 2-D element model.

Table 7.3 Finite element model comparison

	P_{cr} (psi)	d_{cr} (in)	T_{cr} (hr)	d_{cr} (in)
b21	64.11	2.435	2668.0	3.047
CPE8H	64.03	2.389	2504.7	3.120

Comparison with Physical Tests by Guice et al. (1994). Finite element results have also been compared with long-term buckling test results reported by Guice et al (1994). The average *DR* and *G* values (53.05 and 0.2131%, respectively) from all 39 specimens in the D-series are used. The critical pressure under instantaneous buckling condition was determined as 78.17 psi. The critical time values were calculated for *PR* ratios from 0.1 to 0.9. The proposed model, Eqn. (7.6), was used to express the critical time-pressure relation. The original test data and fitted curve are plotted in Fig. 7.8, with the fitting constants listed in Table 7.4.

Equation (7.1) used by Guice et al. (1994) and empirical models suggested by Cohen and Arends (1989), Eqns. (7.2) and (7.3), are also used to fit the same test results. The fitting curves are all plotted in Fig. 7.8 for comparison. The corresponding fitting constants are listed in Table 7.4.

As can be seen from Fig. 7.8, Eqn. (7.1) gives much greater liner life (critical time) predictions than the other models in the lower pressure range (i.e. 10 to 40 psi) which is more likely to occur in practical designs. The straight line model tends to overestimate the durability of CIPP liners. The model proposed in the present study (Eqn. (7.6)) better represents the time-pressure relation in high *PR* range, yet predicts longer life in the design range than the two empirical models by Cohen and Arends (1989a and 1989b). The

difference may be partially attributed to the simplified constitutive relation, or perhaps to geometrical imperfections (e.g. ovality of host pipe and liner, local dents in liner cross-section, and imperfection in liner thickness). The effects of geometric imperfections on liner durability will be discussed in Chapter 8.

Table 7.4 Fit constants for various models

	n or $-a$	T_0	P_0 or b	P_{1h}	P_{10kh}	P_{50y}
Eqn. (7.1)	-0.0532	n/a	81.5	81.5	49.93	40.87
Eqn. (7.2)	n/a	2.300e+08	4.0513	83.67	46.36	31.10
Eqn. (7.3)	n/a	1.638e+09	22.1388	83.11	47.01	32.79
Eqn. (7.6)	5.0428	4.670e+05	0.9807	71.31	52.27	38.63

7.4 Conclusions

Creep-induced buckling of constrained CIPP liners subject to external pressure has been investigated by using a finite element approach. Long term structural behaviors are illustrated by a typical example, and the similarities to corresponding instantaneous behaviors are addressed. The importance of incorporating specific material properties, especially the difference in yield limits and creep rates under tensile and compressive stresses, is emphasized.

A special kind of composite beam element is implemented to incorporate specific mechanical properties of CIPP materials characterized by standard tests. The applicability of the new element is validated by comparing the corresponding results with those from a model using 2-D continuum elements.

A model relating critical time to the dimensionless pressure ratio is proposed. The equation is a monotonical function of pressure ratio, and reflects the rational estimates that

the critical times at the two extremes (zero and the critical pressure) are infinity and zero, respectively. The model gives excellent agreement with the finite element results.

The modeling approach is verified by comparing the predicted results to buckling test data. The sensitivity of the critical time to geometric parameters prevents close specimen-by-specimen matches. However, good agreements are found on the average, especially for lower pressure levels which are more practical in sewer rehabilitation.

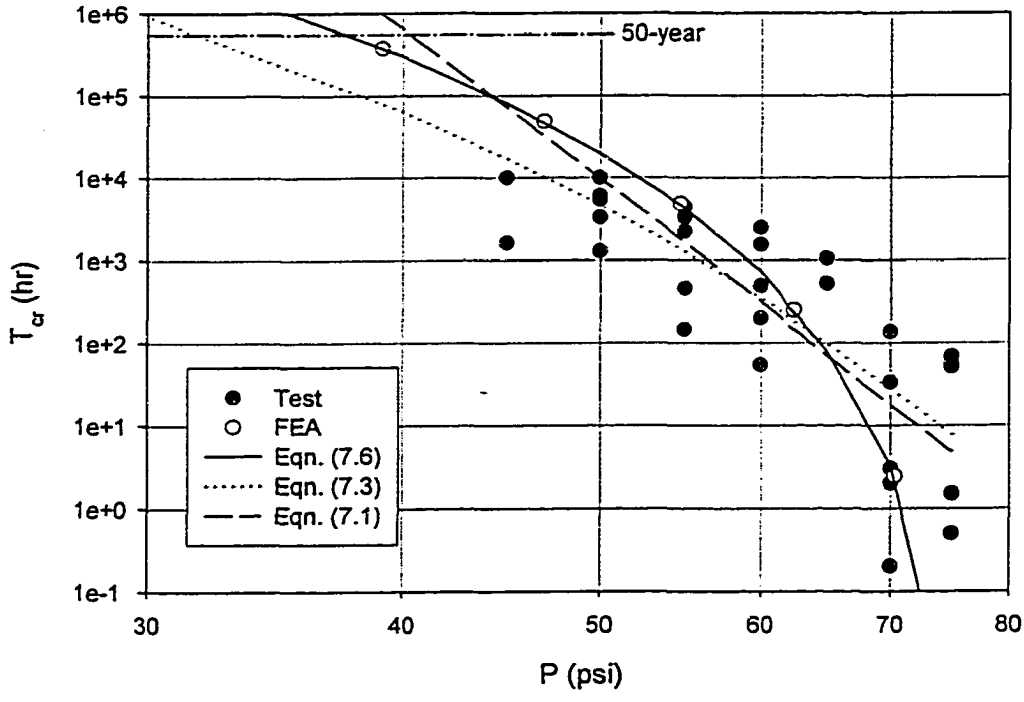

Fig. 7.8 Comparison of predicted and test results
(Note: Test data truncated at 10,000 hr)

CHAPTER 8

FACTORS INFLUENCING LINER LIFE

Generally speaking, the similarity between creep buckling and its instantaneous counterpart can be reflected in the following way: a longer life (or critical time) can usually be expected for a liner with a higher critical pressure, and the critical time depends strongly on material properties and geometric parameters.

The effects of geometric parameters and imperfections on the accurate prediction of long-term buckling resistance are discussed in this chapter. As in Chapter 6, the one-lobe mode is employed here to give lower bound predictions. The material properties used here are from the set LONG.

8.1 Essential Factors

The essential geometric parameters discussed in Chapter 6 are once again used in this section to show the trends of liner life with respect to each parameter. These parameters are dimension ratio (*DR*), gap (*G*), and ovality (*OV*). Three levels are assigned to each parameter. The critical pressure (for instantaneous buckling) results for the 27 combinations are given in Table 8.1a.

The critical times are calculated for 80, 75, 70, 60, and 50% of the critical pressure for each {*DR*, *G*, *OV*} combination. Results are given in Appendix C.

Table 8.1 Effect of geometric parameters on P_{cr}, n, T_0 and b

a. P_{cr} (psi)

DR	OV = 0			OV = 3%			OV = 6%		
	G = 0.1%	G = 0.4%	G = 0.7%	G = 0.1%	G = 0.4%	G = 0.7%	G = 0.1%	G = 0.4%	G = 0.7%
35	216.27	166.85	136.33	185.92	140.91	111.24	161.27	118.68	92.33
50	104.58	72.25	55.75	90.59	60.60	46.37	77.20	50.96	38.29
65	58.31	37.47	28.36	49.95	31.37	23.60	43.06	26.63	19.77

b. n

DR	OV = 0			OV = 3%			OV = 6%		
	G = 0.1%	G = 0.4%	G = 0.7%	G = 0.1%	G = 0.4%	G = 0.7%	G = 0.1%	G = 0.4%	G = 0.7%
35	4.5966	4.6426	4.8417	4.3923	4.6826	4.7259	4.6315	4.5912	4.6705
50	4.7118	4.9257	5.1709	4.8821	4.9418	5.1122	4.8578	5.1387	5.0302
65	4.9096	5.3113	5.4377	4.7196	5.2712	5.4624	5.1891	5.2893	5.4549

c. T_0 (hr)

DR	OV = 0			OV = 3%			O V= 6%		
	G = 0.1%	G = 0.4%	G = 0.7%	G = 0.1%	G = 0.4%	G = 0.7%	G = 0.1%	G = 0.4%	G = 0.7%
35	8.90E+05	1.46E+06	1.89E+06	9.87E+05	1.28E+06	2.07E+06	7.04E+05	1.51E+06	2.61E+06
50	4.88E+05	8.92E+05	1.09E+06	3.66E+05	8.23E+05	1.16E+06	3.83E+05	6.95E+05	1.22E+06
65	3.65E+05	5.03E+05	6.47E+05	4.28E+05	4.98E+05	6.15E+05	2.67E+05	4.55E+05	6.18E+05

d. b

DR	OV = 0			OV = 3%			OV = 6%		
	G = 0.1%	G = 0.4%	G = 0.7%	G = 0.1%	G = 0.4%	G = 0.7%	G = 0.1%	G = 0.4%	G = 0.7%
35	0.99385	0.9626	0.95146	0.97705	0.97061	0.9626	0.9999	0.95928	0.95342
50	0.97568	0.9501	0.9501	0.99209	0.95322	0.95029	0.98662	0.9749	0.95713
65	0.97607	0.9626	0.9501	0.95459	0.95986	0.95615	0.9874	0.95244	0.95576

Predictions of critical time are also correlated to the pressure levels applied, by using Eqn. (7.6). The constants T_0, n and b are listed in Table 8.1. The effects of the three parameters *DR*, *G*, and *OV* on the model constants, and on the liner life are discussed next.

8.1.1 Effect of *DR*

The dimension ratio *DR* is the fundamental design parameter in the CIPP application. The expected life of a liner can be effectively changed by selecting the *DR* value in accord with the external pressure.

The effect of *DR* on liner life is first shown in the $\log T_{cr}$-P coordinate plot in Fig. 8.1. For a given pair of *G* and *OV* values, a higher *DR* value corresponds to a lower critical pressure. The critical time is infinitely large when the external pressure is zero. It decreases to zero when pressure approaches the instantaneous critical value. Therefore, for a liner with a high *DR* value, T_{cr} drops fast with an increase in pressure. For instance, for $G = 0.4\%$ and $OV = 0$, when pressure $P = 30$ psi, the predicted critical times for *DR* = 65, 50, and 35 are 1.04×10^2, 4.41×10^6, and 1.35×10^9 hours, respectively. If the design life is set to 50 years (or 432000 hours), the maximum working pressures are 18, 38, and 95 psi, respectively (Fig. 8.1a).

The critical time should always be discussed with reference to a specific external pressure level. To evaluate the trend of liner life with respect to different geometric configurations, it is convenient to use the normalized form as expressed by Eqn. (7.3), and plot critical time versus the corresponding pressure ratio, *PR*. When $PR << 1$ and $PR > 0$, Eqn. (7.3) can be rewritten approximately as

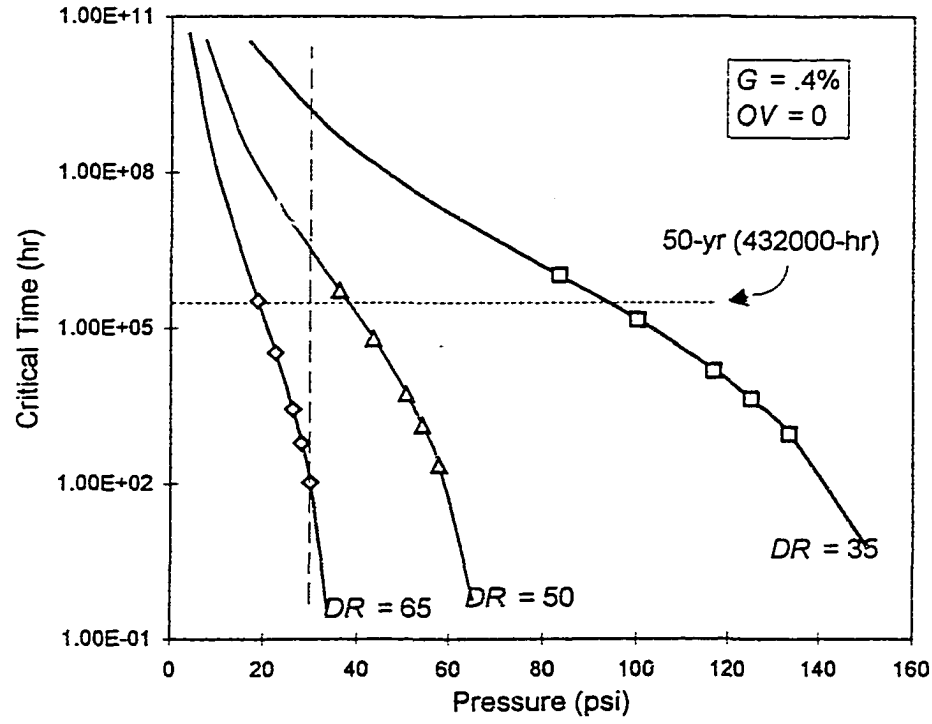

a.

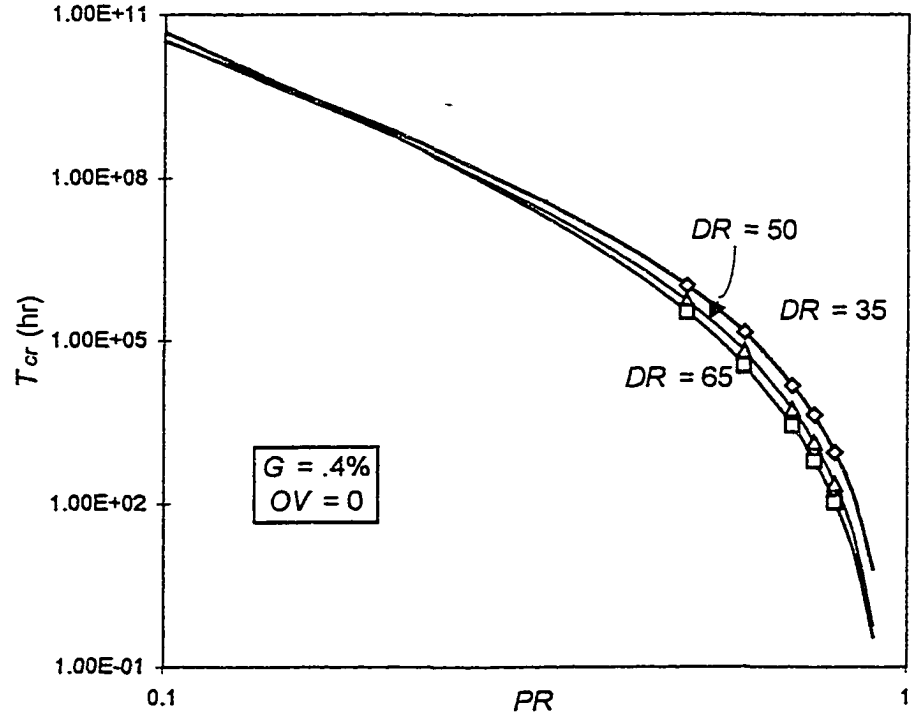

b.

Fig. 8.1 Effect of *DR* on critical time

$$\lg T_{cr} \cong C - n \lg(PR) \qquad (8.1)$$

Therefore, n is the rate at which T_{cr} approaches infinity when PR becomes infinitely small. For a given combination of G and OV, the exponent n increases with an increase in DR, while T_0 decreases. The normalized T_{cr}-PR curves are distinguished from each other only at the high pressure range (Fig. 8.1b).

8.1.2 Effect of Gap

In addition to the DR effect, the buckling resistance of an encased liner is influenced also by geometric imperfections in the liner-pipe system. As has been shown in Chapters 5 and 6, the existence of a gap between the liner and its host pipe can reduce the enhancement greatly with respect to the critical pressure. For the case of $DR = 50$ and $OV = 0$, the predicted critical pressures for G = 0.1, 0.4 and 0.7% are 104.58, 72.25, and 55.75 psi, respectively. The corresponding T_{cr}-P curves are given in Fig. 8.2a. These curves show that the critical time drops faster (with an increase in pressure) in the case of a large gap than in the case of a small gap.

The normalized T_{cr}-PR curves are given in Fig. 8.2b. The three curves can be distinguished from each other only in the low PR range. The exponent n and T_0 increase with an increase in G for a given combination of DR and OV (Table 8.1).

8.1.3 Effect of Ovality

When the deteriorated host pipe is slightly oval, the critical pressure of the encased liner decreases with an increase in pipe ovality. The drop in the T_{cr}-P curve increases with an increase in the OV value. Yet, the T_{cr}-PR curves for $OV = 0$, 3, and 6%

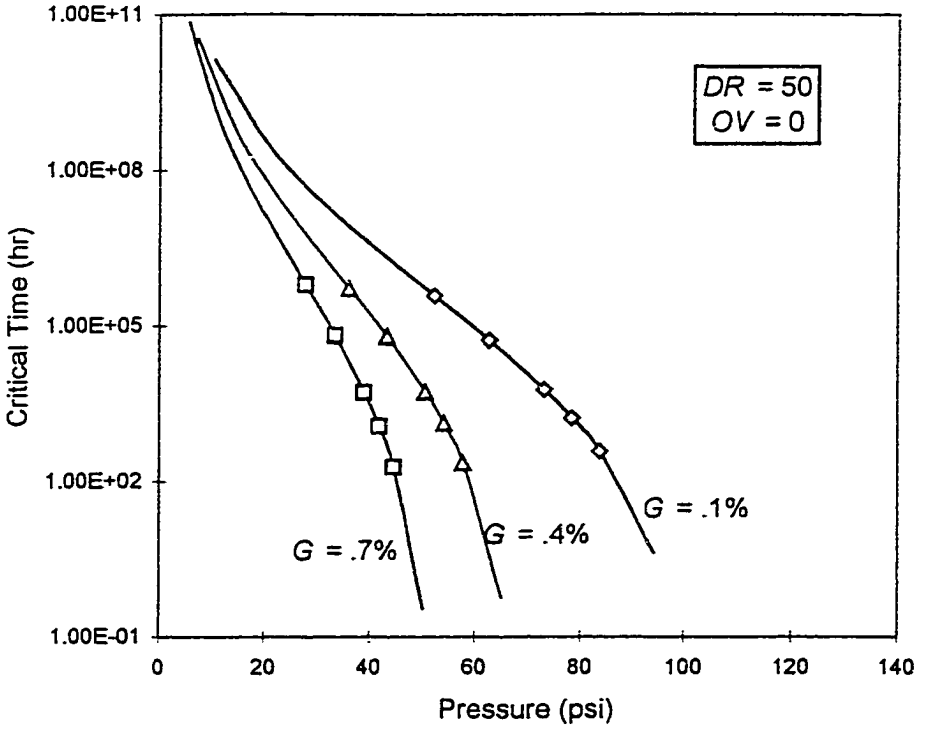

a.

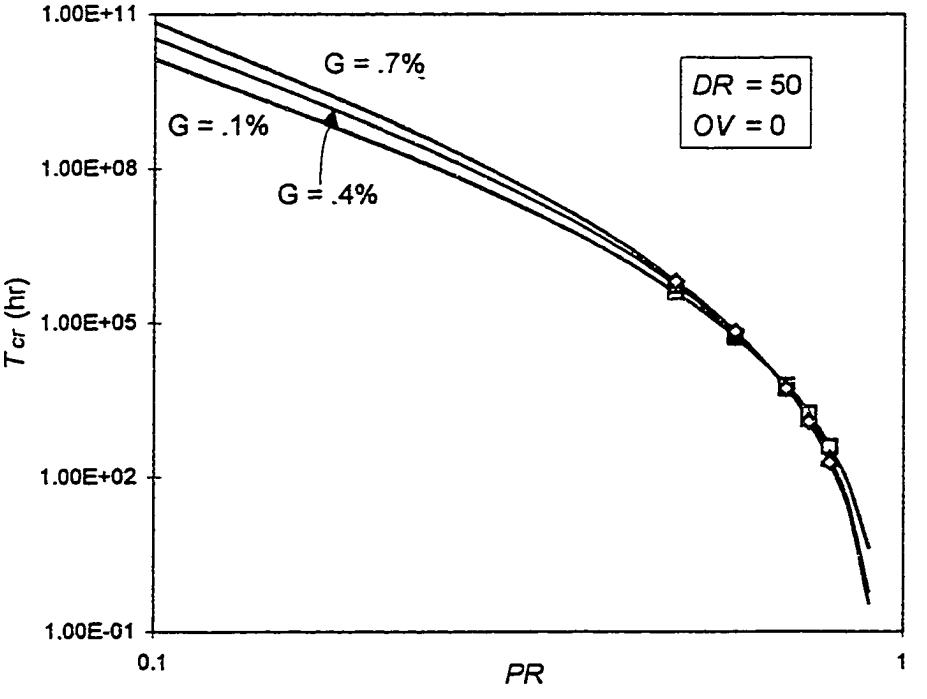

b.

Fig. 8.2 Effect of *G* on critical time

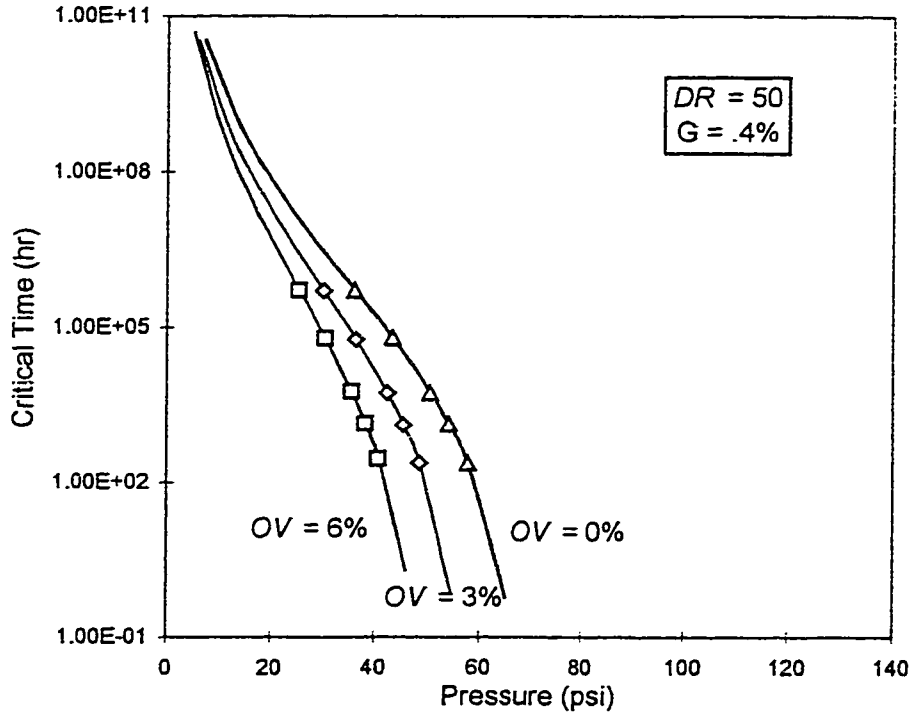

a.

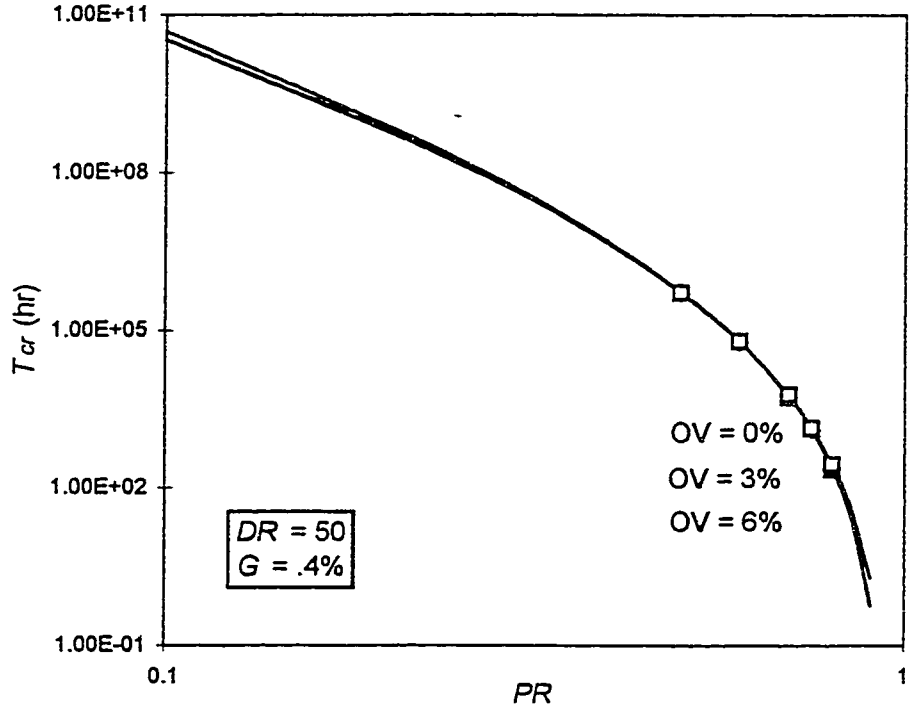

b.

Fig. 8.3 Effect of *OV* on critical time

coincide with each other, as shown in Fig. 8.3b. Therefore, the critical time of a liner installed in a slightly oval pipe can be predicted by using the {n, T_0, b} values for circular pipes and its own P_{cr} value.

8.2 Effect of Variation of Thickness

In addition to the parameters discussed, some other geometric imperfections are also common to CIPP liners. One type of imperfection is the variation in liner thickness, which can be found in any CIPP liner as the result of installation and manufacturing processes. A common practice in buckling tests is to measure the liner thickness at several different locations (at each end of a liner span). The average value over locations will be used as a measure of liner thickness in subsequent analyses. In the present study, *Imperfection in thickness* of a liner will be characterized by the variation in thickness (*VT*), which is defined as

$$VT = [MAX(t_i) - MIN(t_i)] / 2t \tag{8.2}$$

In the equation, t_i refers to the recorded thickness measurements for a liner, and t is the mean value for all t_i's. The variation is usually significant. According to Omara (1996), the highest and lowest *VT* value found in 18 samples were 11.98% and 1.26%, respectively; with an average *VT* of 5.55%. A more detailed study on the variation in thickness can be found in Stokeld (1998).

In the finite element model, the full circumference of a liner is divided into three parts: **average**, **thin**, and **thick**, with corresponding thickness values of t, t-Δt, and t+Δt, respectively. For simplicity, the **thin** part is always at the *top* of the cross section and is adjacent to the **thick** part. Both parts are equal in length so that the average thickness is t

(Fig. 8.4). The deviation of thickness, $\Delta t = VT^{*}t$, is varied from 1% to 15% of the mean thickness t. The ratio of **thin** part to the whole circumference is varied from 1/12 to 1/2 (or the angle ϕ is varied from 15 to 90 degree). As an extreme situation, the circumference of the liner is divided into a **thin** and a **thick** part of equal length, when $\phi = 90^{o}$.

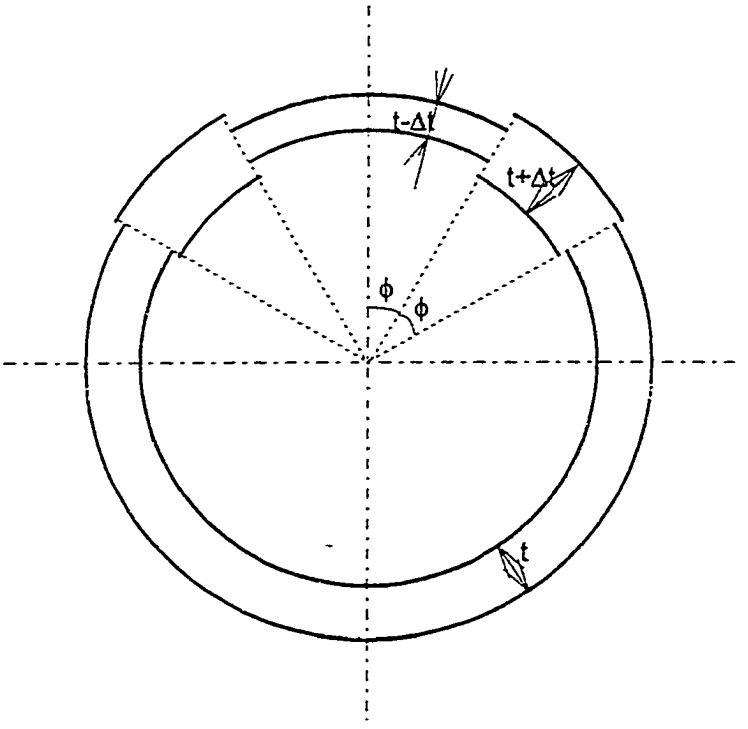

Fig. 8.4 Schematic of model with varying thickness

8.2.1 Instantaneous Buckling

The effect of variation in thickness on critical pressure has been investigated for the case of $DR = 50$, $G = 0.25\%$. Results are listed in Table 8.2.

The critical pressure results corresponding to t-Δt values are also listed in the column under 180^{o}. It can be seen that when $\phi \geq 45^{o}$ or the **thin** part makes up more than

1/4 of the liner circumference, the critical pressure is very close to that of a liner with a uniform thickness equivalent to the **thin** part, t-Δt. Fig. 8.5b shows that the critical pressure P_{cr} decreases at a rate approximately twice that of VT.

Table 8.2 Effect of thickness variation on critical pressure

VT (%)	P_{cr} (psi)					
	$\phi=15°$	$\phi=30°$	$\phi=45°$	$\phi=60°$	$\phi=90°$	$\phi=180°$
0	85.53	85.53	85.53	85.53	85.53	85.53
1	84.80	84.59	83.60	83.74	83.69	83.57
2	84.21	83.56	81.64	81.93	81.93	81.62
5	82.10	79.69	76.13	76.54	76.53	75.87
10	78.91	72.30	67.12	67.82	67.78	66.63
15	75.90	64.63	59.24	59.48	59.40	58.02

8.2.2 Long-Term Buckling

The dependence of critical time on thickness imperfection is investigated by incorporating creep properties discussed in the prior section into the finite element model. Only one pressure level, 50 psi, is used. Results are listed in the following table and illustrated in Figure 8.6.

Table 8.3 Effect of thickness variation on critical time

VT (%)	T_{cr} (hr)			
	$\phi=15°$	$\phi=30°$	$\phi=45°$	$\phi=180°$
0	82825.2	82825.2	82825.2	82825.2
1	75126.4	67779.3	61500.0	60176.2
2	68237.4	54686.2	44833.6	43512.6
5	50950.1	25685.2	15803.6	14067.3
10	31408.2	4593.7	1625.5	1020.1
15	18660.1	334.9	32.1	11.1

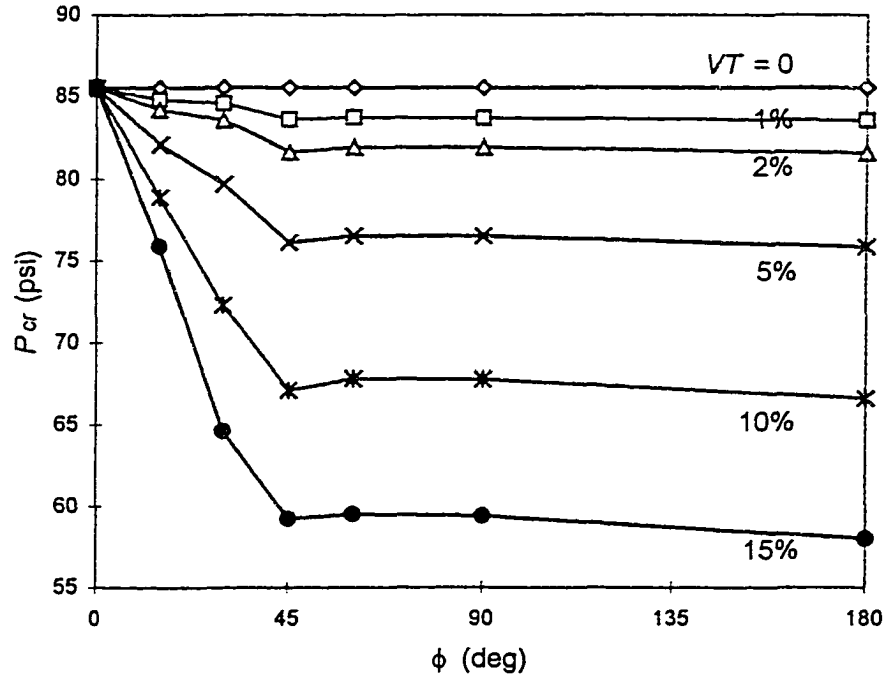

a.

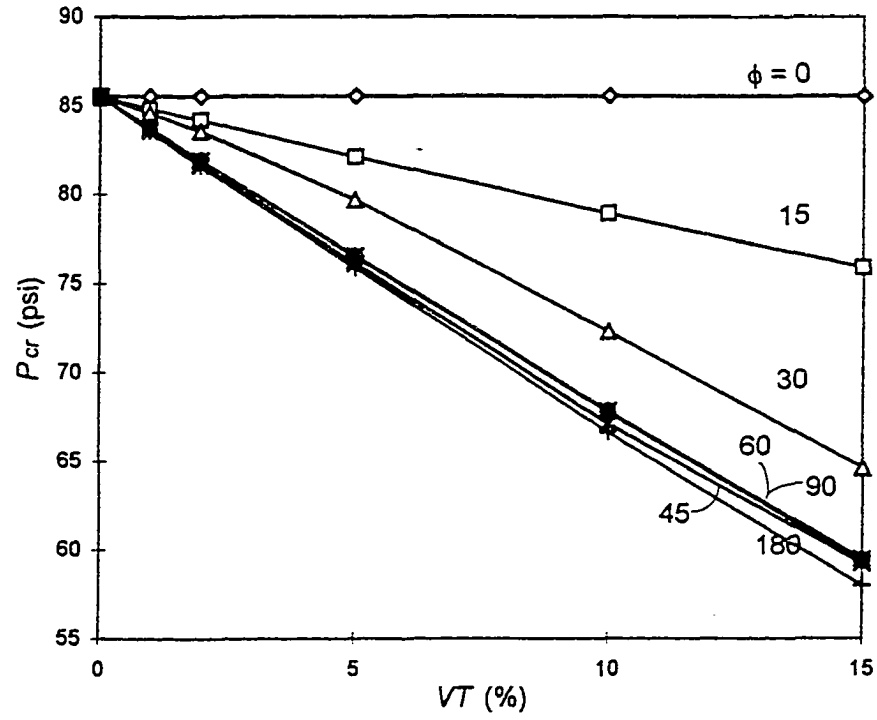

b.

Fig. 8.5 Effect of thickness variation on critical pressure

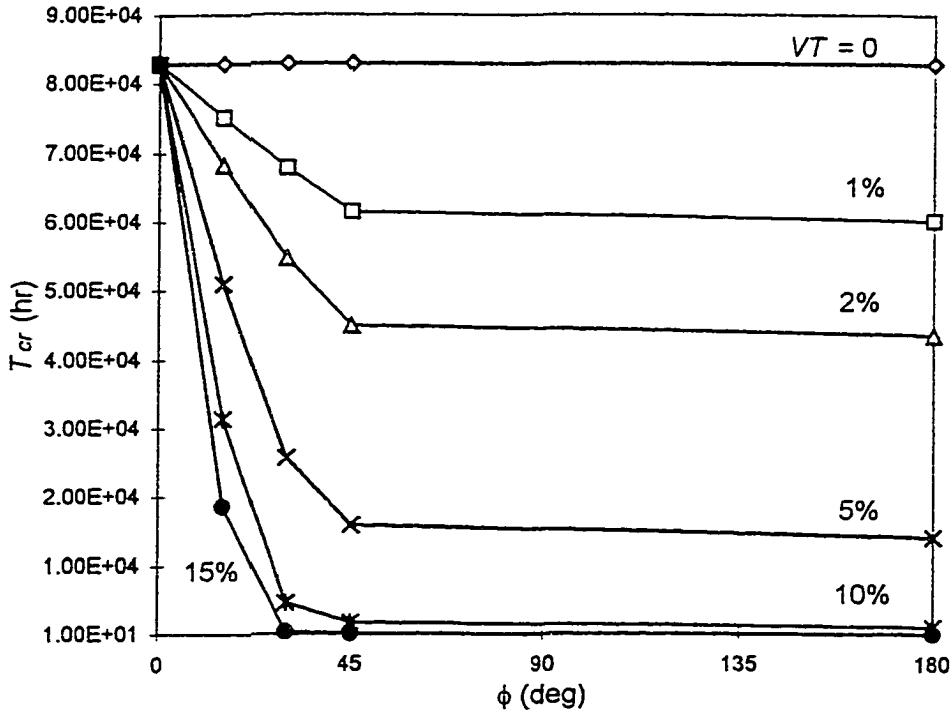

a.

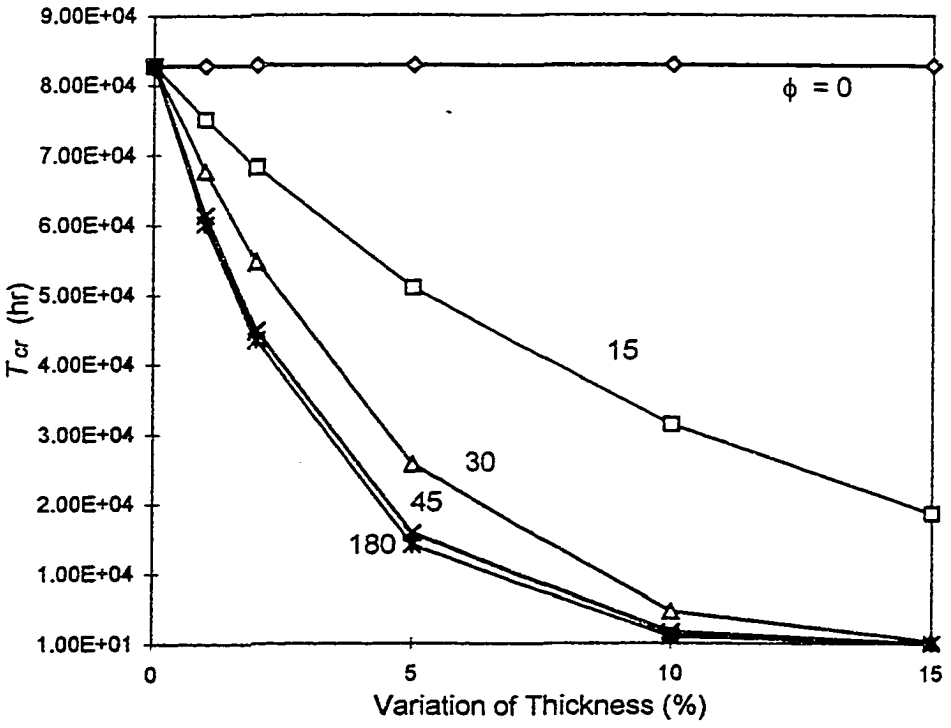

b.

Fig. 8.6 Effect of thickness variation on critical time

It can be seen that a liner with a high short term buckling resistance (i.e., critical pressure) also has a long life (critical time). For the case in which the **thin** part is 1/4 or more of the liner perimeter, the critical time of such a liner is very close to that of a liner with a uniform thickness of t-Δt. As is seen from Table 8.3, the influence of VT on T_{cr} is greater than its influence on P_{cr}. For instance, at $VT = 5\%$, T_{cr} decreases by 38.5%, 69.0% and 80.9% for $\phi = 15^{o}$, 30^{o} and 45^{o}, respectively.

8.3 Effect of Local Imperfection

To model localized imperfections, the shape of the dented cross-section is assumed to follow Eqn. (8.3),

$$u_0 = WD\cos^2\left(\frac{\pi\theta}{2\phi}\right), \quad 0 \le \theta \le \phi \qquad (8.3)$$

with $W = w/D$ being the dimensionless magnitude of the imperfection (in percentage), and 2ϕ being the range of the dented part.

The configuration of DR = 50 is selected, with W varying from 0.5% to 2% and ϕ from 5 to 180^{o}. The dependency of P_{cr} on W and ϕ is illustrated in Figure 8.7.

It can be observed that when $W = G$, the critical pressure value associated with localized imperfection is significantly higher than that associated with uneven gap. The lowest P_{cr} occurs around 10 to 15^{o} for the W values considered. (Larger ϕ values, i.e. greater than 45^{o}, corresponds to free arch configurations, which are not desirable in CIPP applications and therefore not discussed in this study.)

For the case of localized imperfection, the pressure ratio-critical time relationship can also be expressed by equation (7.6).

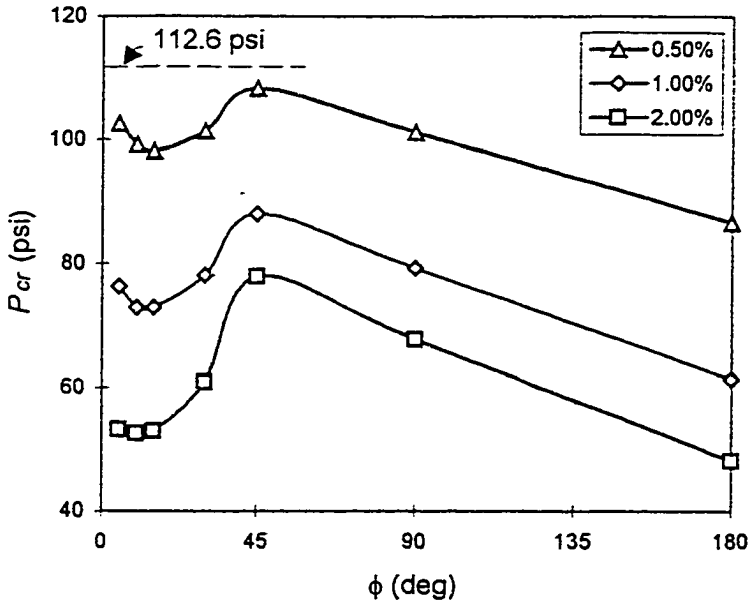

Fig. 8.7 Effect of local imperfection on critical pressure

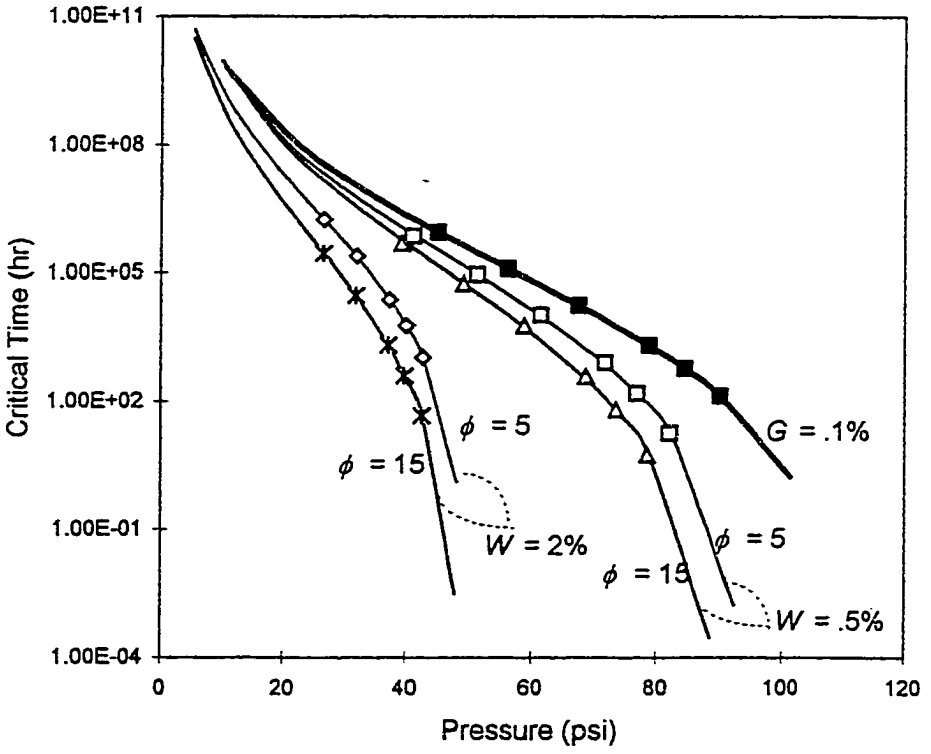

Fig. 8.8 Effect of local imperfection on critical time

8.4 Conclusions

The effects of geometric parameters on critical time of liner are discussed in this chapter. The following can be concluded from the finite element results:

1) The critical time varies with the external pressure, which may not be higher than the critical pressure determined in the instantaneous buckling analysis. Knowledge of critical pressure can be used in the prediction of the liner life duration by using Eqn. (7.6). Under a specific pressure level, a longer critical time can usually be expected for a liner with a higher critical pressure.
2) The parameters n, T_0, and b in Eqn. (7.6) are strongly influenced by the parameters, *DR*, *G*, and *OV*. For a given *G* and *OV* combination, an appropriate *DR* value can be determined to meet the duration requirement.
3) T_{cr}-*PR* curves for various *OV* values are almost identical.
4) The effect of *imperfection in thickness* on liner buckling resistance is shown to be significant. The critical pressure decreases at a rate twice that of *VT* whereas critical time decreases at a rate 8 to 16 times that of *VT*.
5) The effect of local imperfection (wavy dented shape) is most significant when $\phi = 15°$.

Coupling (or interaction) effects may exist among the essential parameters and both types of imperfections. Critical time of a liner can be determined from Eqn. (7.6) by interpolating the dependence of n, T_0, and b on essential parameters *DR*, *G*, and *OV* and then applying appropriate reduction factors with respect to imperfections.

CHAPTER 9

CIPP LINER DESIGN METHODOLGY

This chapter deals with the structural design issues, which an engineer will be facing when the CIPP technique is chosen in a sewer rehabilitation project. General considerations for design criteria common to encased thin-walled liners subjected to creep will be discussed first. The 50-year pressure predicted by using the finite element results presented in the prior chapters will be compared with that determined by the ASTM (1993) guidelines. Design curves and simplified (empirical) formulas based on these results will be proposed for designs using a specific CIPP product, *Insituform Enhanced.*

9.1 General Design Considerations

The basic design decision to make in CIPP application is to choose an appropriate thickness t of the liner for a deteriorated sewer pipe segment of a given diameter D_P, so that the liner can withstand a constant external hydrostatic pressure P and provide separation between the sewer refuse and the surrounding environment for a desired period of time T_D. An efficient yet safe design should predict correctly the time-dependent behavior of the liner material and meet the service life requirement, rather than simply satisfy the conventional instantaneous conditions.

9.1.1 Basics

For a satisfactory rehabilitation, the design durability requirement T_D for the CIPP liner is usually set at 50 years (or 432000 hours), as required by the industry. The hydrostatic pressure P under which a liner will be subjected during its service life may vary with the geographic region. To achieve a tight fit, the outer diameter of the liner, D_o, is nominally chosen to be the same as the inner diameter of the pipe, D_P, which may also change from case to case.

As shown in Fig 8.1, under a given external pressure, a specific liner product can have different time spans when different dimension ratio (DR) values are used. At the same time, a given life span requirement can be met by using different DR ratios under different external pressures. The liner thickness t can then be determined as

$$t = D_o / (DR + 1) \tag{9.1}$$

The effect of gap should also be taken into account, because gap can not be eliminated in the liner-host pipe system. In many rehabilitation cases, the deteriorated pipes may have become slightly oval in shape or dented in certain localities. The pipe ovality and magnitude of local imperfections should be accurately measured or assessed and considered in the design, because they can significantly influence liner service life.

9.1.2 Critical (or Failure) State

It is not clearly defined in the literature or design practices which of the following factors should be used to define the critical or failure state in CIPP liner design:

Final Collapse. As observed in experimental tests and simulated by means of finite element analyses, a liner installed in its host pipe will eventually collapse when the ultimate pressure P_{cr} is reached or with accumulation of creep strain under a certain pressure level which is lower than P_{cr}.

Material Failure. This occurs when the allowable maximum stress (e.g. the yield or breakage stress observed in standard material characterization tests) is reached. This usually happens immediately before the final collapse of the liner structure. When the pressure ratio (PR) is low, e.g. 0.4 or lower, the difference between time until material failure and time till buckling may be negligible.

Maximum Allowable Deflection. The deflection of the liner may become so large that the deformed liner may not take its designed function, e.g. groundwater can actually infiltrate through the annular gap between liner and its host pipe. When the PR ratio is small, the maximum deflection prior to the onset of buckling may be large.

The final collapse is taken in the present study to be the critical state, as implied in the ASTM guidelines (1993).

9.1.3 Safety Factor

There are two ways to apply an appropriate safety factor in structural instability designs in which creep is the main concern.

External Pressure. As recommended by the CIPP design guideline (ASTM, 1993), the usual way is to apply a safety factor N (e.g. $N = 2$) to the 50-year pressure which is determined by the following equation

$$P = \frac{2KE_L}{(1-\nu^2)}\frac{C}{DR^3} \tag{9.2}$$

Referring to Fig. 7.8, for the *Insituform Enhanced* liners, to divide the 50-year pressure by 2 will lead to an increase in critical time by 261.4 and 101.2 times by using finite element predictions (Eqn 7.6) and the exponent regression model given by Eqn. (7.3), respectively. This approach will most likely give highly conservative designs.

Liner Buckling Time. Because the durability requirement is of main concern in CIPP liner design, a safety factor (e.g. 10) can thus be applied directly to the service life requirement (i.e. 50-year). An appropriate liner thickness can be determined according to the finite element results presented in Chapter 8, which will lead to a safe and efficient design.

9.2 The Fifty-Year Pressure

It has been shown in Chapter 8 that the proposed model (Eqn. 7.6) gives a close fit to finite element predictions which take into account the essential design parameters (i.e. *DR*, *OV*) and geometrical imperfections (i.e. *G*, *VT*, and *W*). The model will be reformatted next to show how the fitting constants (i.e. n, T_0, and b) listed in Table 8.1 can be used to determine the fifty-year pressure, P_D, needed for design purpose.

To start with, the left-hand side of Eqn. (7.6), i.e. the critical time T_{cr}, will be assigned as the desired service life T_D. The pressure ratio PR on the right-hand side will be replaced with P_D / P_{cr}. The design equation can thus be expressed as

$$T_D = T_0\left(\frac{b}{P_D / P_{cr}} - 1\right)^n \tag{9.3}$$

Eqn. (9.3) can be rewritten as

$$P_D = \beta P_{cr} \tag{9.4}$$

where the coefficient β is

$$\beta = b\left[\left(\frac{T_D}{T_0}\right)^{1/n} + 1\right]^{-1} \tag{9.5}$$

As such, the 50-year pressure can be determined by using T_D and results from finite element analyses given in Table 8.1. The β and P_D results are listed in Table 9.1.

For comparison, the ASTM guideline (Eqn. 9.2) is used to determine the 50-year pressure. The enhancement factor K is assumed as 7. The long-term modulus is chosen as one half of the short-term value, i.e. $E_L = E/2$. The reduction factor C, which accounts for the effect of pipe ovality is defined as

$$C = \left[(1-OV)/(1+OV)^2\right]^3 \tag{9.6}$$

Results are listed in Table 9.1c.

The 50-year pressures, determined based on finite element results and by using ASTM guideline (Eqn. 9.2), are plotted and compared in Fig. 9.1. Predictions based on the ASTM guideline, which does not explicitly take into account annular gaps between liners and host pipes, happens to give results for fifty-year pressures which are similar to the finite element approach. However, the ASTM predictions for the case of $DR = 35$ are not on the conservative side, especially for the circular pipe configuration. This result may be because plastic yield plays a more important role, when the thickness is large and the enhancement factor is not so large as assumed ($K = 7$). For the cases of $DR = 50$ and 65, the ASTM predictions intersect the finite element solutions within the range of G =

0.2% to 0.5%, which are found to be representative of the liners used in the buckling tests at the TTC (Guice et al., 1994; TTC, 1998a).

Notice that the 50-year pressure corresponding to a single *DR* ratio with a specific pipe ovality *OV* can still vary significantly over the *G* range from 0.2% to 0.5%. For instance, for the case of *DR* = 50 and *OV* = 0%, the 50-year pressure will drop by approximately 25%, from 45 psi to 34 psi, when the gap ratio *G* increases from 0.2% to 0.5%. Therefore, it is desirable that a design equation takes into account a gap parameter. The designer can select a proper gap ratio in liner design, according to the practical limitation in the practicing liner installation techniques. Design curves based on adequate parametric studies, as will be presented shortly, are thus highly recommended.

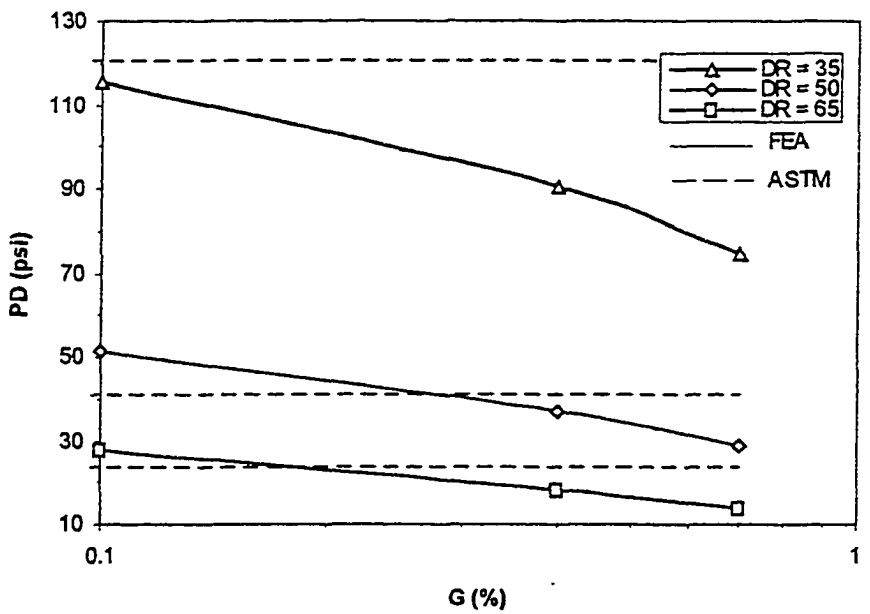

a. *OV* = 0%

Fig. 9.1 Fifty-year design pressure

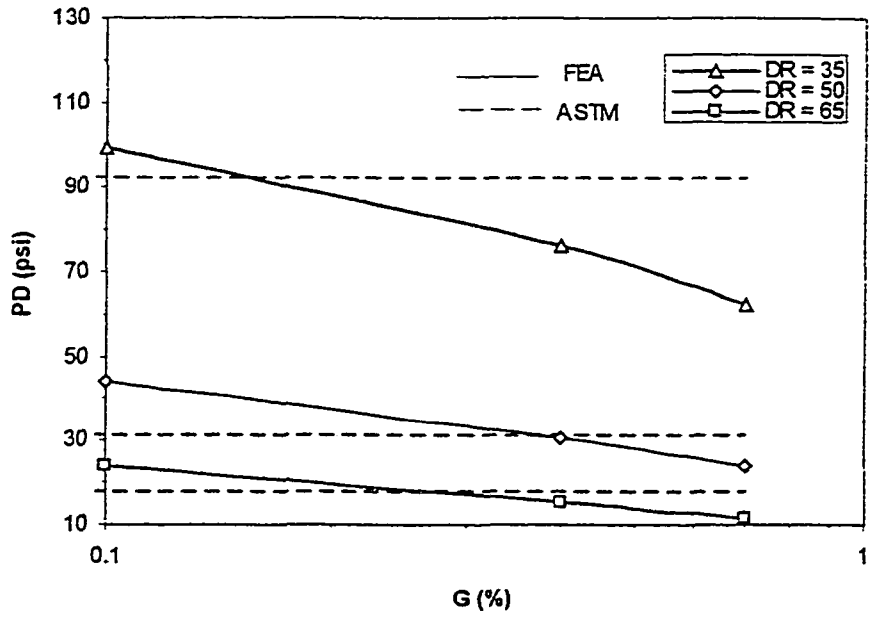

b. $OV = 3\%$

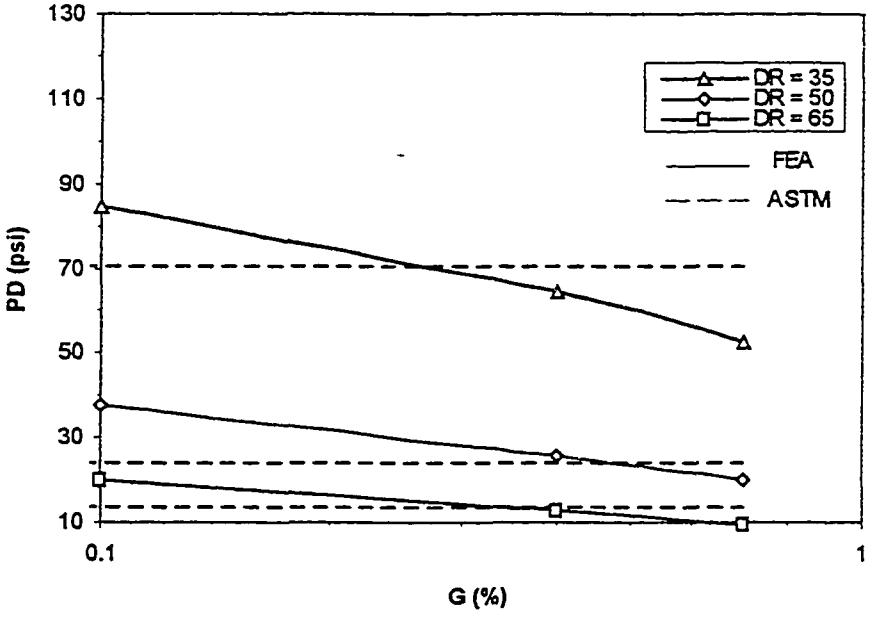

c. $OV = 6\%$

Fig. 9.1 Fifty-year design pressure (cont'd)

Table 9.1 Determination of fifty-year pressure

a. Factor β

	$OV = 0$			$OV = 3\%$			$OV = 6\%$		
DR	$G = 0.1\%$	$G = 0.4\%$	$G = 0.7\%$	$G = 0.1\%$	$G = 0.4\%$	$G = 0.7\%$	$G = 0.1\%$	$G = 0.4\%$	$G = 0.7\%$
35	0.5352	0.5434	0.5470	0.5336	0.5406	0.5597	0.5255	0.5439	0.5667
50	0.4934	0.5093	0.5168	0.4869	0.5070	0.5203	0.4865	0.5093	0.5271
65	0.4790	0.4876	0.4921	0.4761	0.4858	0.4929	0.4702	0.4779	0.4930

b. Fifty-year pressure P_D

	$OV = 0$			$OV = 3\%$			$OV = 6\%$		
DR	$G = 0.1\%$	$G = 0.4\%$	$G = 0.7\%$	$G = 0.1\%$	$G = 0.4\%$	$G = 0.7\%$	$G = 0.1\%$	$G = 0.4\%$	$G = 0.7\%$
35	115.74	90.66	74.58	99.20	76.18	62.26	84.75	64.55	52.32
50	51.60	36.80	28.81	44.11	30.72	24.12	37.56	25.96	20.18
65	27.93	18.27	13.96	23.78	15.24	11.63	20.25	12.73	9.75

c. Fifty-year pressure by ASTM guideline

	$OV = 0\%$	$OV = 3\%$	$OV = 6\%$
35	120.94	92.44	70.81
50	41.48	31.71	24.29
60	24.01	18.35	14.06

A safety factor is always necessary in a practical design to account for any unexpected effects. In a normal structural design methodology, a safety factor is usually applied to the critical design load. The common practice in CIPP liner design is to divide the 50-year pressure (obtained by using Eqn. (9.2)) by a safety factor of two. This treatment is on the safe side, but it may sometimes be too conservative.

Referring back to Fig. 7.8 and Table 7.4, the CPAR data indicate that when the 50-year pressure is divided by a safety factor of two, the resultant pressure corresponds to liner life predictions 46.44, 101.22, and 455440 times greater (than 50 years) based on Eqns. (7.2), (7.3), and (7.1), respectively. The corresponding safety factors on time by the proposed model, Eqn. (7.6), vary from 166.21 to 453.30 times over the range of geometrical parameters discussed (Table 9.2). This factor N_T can be derived from Eqns. (9.3) through (9.5), as

$$N_T = \left(\frac{2b-\beta}{b-\beta}\right)^n \qquad (9.7)$$

Apart from the power function (Eqn. 7.1) used in the CPAR report, which may overestimate liner life time when the pressure ratio is low, the other models agree in that the resultant safety factor on time should be in the range of 10^2 when a safety factor of two is applied to the 50-year pressure. A safety factor that large may not be necessary.

Another way to apply an appropriate safety factor is to apply the safety factor directly to the desired service life of the liner to be installed. A factor of ten might seem reasonable. The maximum working pressure for a liner with a specific {*DR*, *G*, *OV*} characteristic can thus be determined as

$$P_D^* = \beta^* P_{cr} \qquad (9.8)$$

In the equation, the coefficient β^* (with a safety factor of ten being accounted for) is

$$\beta^* = b\left[\left(\frac{10T_D}{T_0}\right)^{1/n} + 1\right]^{-1} \tag{9.9}$$

For comparison, P_D^* and $P_D/2$ results are listed in Table 9.3 and plotted in Fig. 9.2. The results show that $P_D/2$ is significantly smaller than P_D^* in every case. These results will be reformatted in the next section to provide the design curves which can be used to determine a safe and economic liner thickness. For example, when the pipe is circular ($OV = 0\%$) and the gap ratio (G) is within the range 0.1% to 0.7%, liners with a DR of 50 can be used under 39.35 to 22.94 psi according to a safety factor of 10 on time, or 25.80 to 14.41 psi according to a safety factor of 2 on pressure.

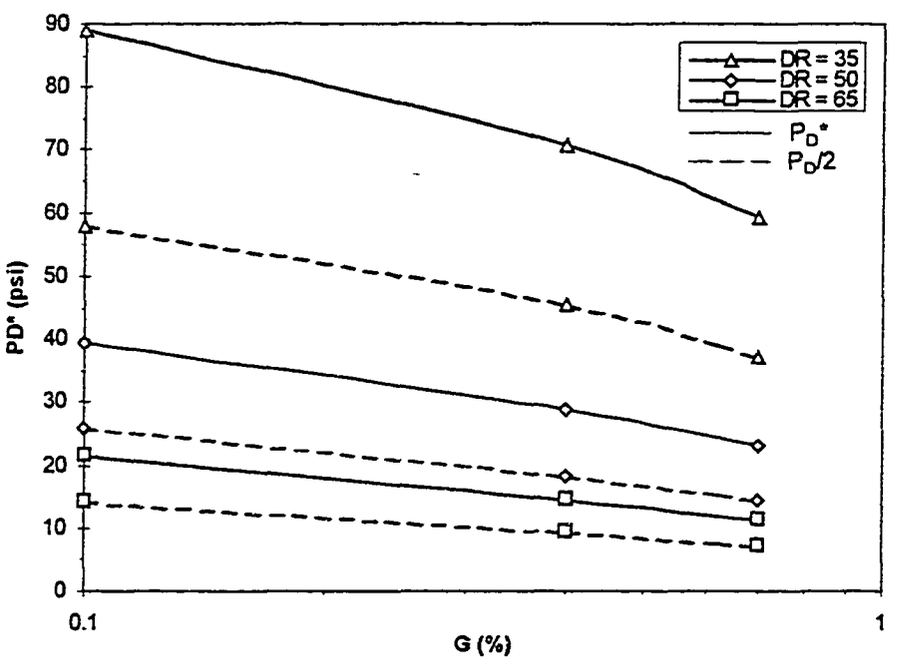

a. $OV = 0\%$

Fig. 9.2 Design pressure

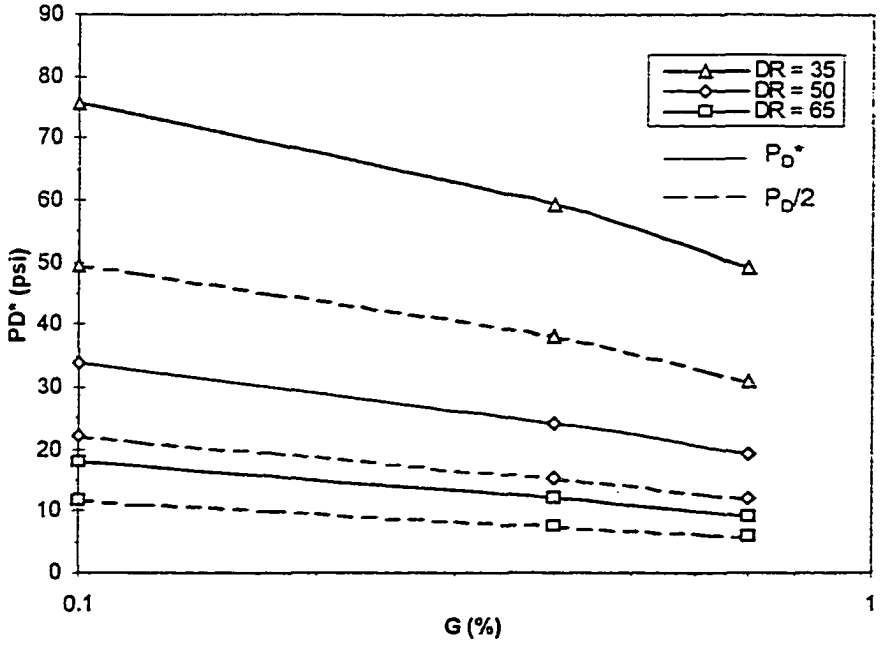

b. $OV = 3\%$

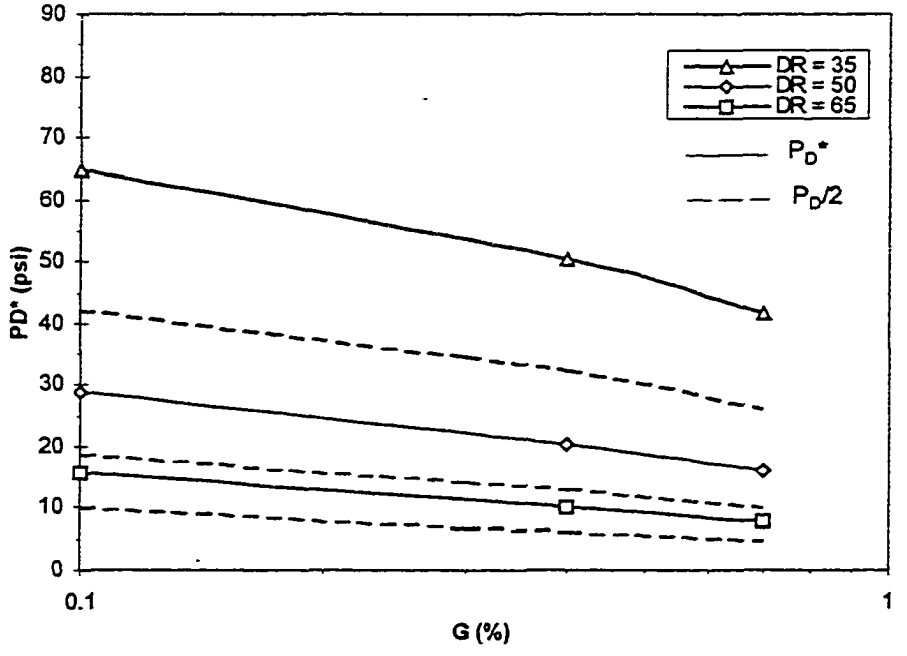

c. $OV = 6\%$

Fig. 9.2 Design pressure (cont'd)

Table 9.2 Safety factor on time due to a safety factor of two on fifty-year pressure

N_T	$OV = 0$			$OV = 3\%$			$OV = 6\%$		
DR	$G = 0.1\%$	$G = 0.4\%$	$G = 0.7\%$	$G = 0.1\%$	$G = 0.4\%$	$G = 0.7\%$	$G = 0.1\%$	$G = 0.4\%$	$G = 0.7\%$
35	200.05	254.01	349.71	166.21	252.09	319.97	190.92	243.37	331.85
50	183.60	287.18	404.61	201.22	283.85	388.39	198.84	331.62	361.90
65	207.21	358.38	449.04	177.21	341.77	453.30	254.93	338.19	450.34

Table 9.3 Determination of design pressure

a.

P_D^*	$OV = 0$			$OV = 3\%$			$OV = 6\%$		
DR	$G = 0.1\%$	$G = 0.4\%$	$G = 0.7\%$	$G = 0.1\%$	$G = 0.4\%$	$G = 0.7\%$	$G = 0.1\%$	$G = 0.4\%$	$G = 0.7\%$
35	89.03	70.85	59.24	75.57	59.45	49.30	64.92	50.35	41.58
50	39.35	28.83	22.94	33.75	24.04	19.19	28.73	20.44	16.01
65	21.41	14.41	11.13	18.08	11.99	9.28	15.66	10.01	7.77

b.

$P_D/2$	$OV = 0$			$OV = 3\%$			$OV = 6\%$		
DR	$G = 0.1\%$	$G = 0.4\%$	$G = 0.7\%$	$G = 0.1\%$	$G = 0.4\%$	$G = 0.7\%$	$G = 0.1\%$	$G = 0.4\%$	$G = 0.7\%$
35	57.87	45.33	37.29	49.60	38.09	31.13	42.38	32.27	26.16
50	25.80	18.40	14.41	22.06	15.36	12.06	18.78	12.98	10.09
65	13.96	9.13	6.98	11.89	7.62	5.82	10.12	6.36	4.87

9.3 Design Curves and Empirical Equations

As mentioned earlier, the basic design decision to make in CIPP liner application is to choose an appropriate thickness t which will guarantee that the liner survives the assumed service life (usually set at 50 years) under a certain underground water table. It is equally effective if the DR ratio of the liner can be determined because the diameter of the sewer and hence of the liner is also known in design. Therefore, the design curves will be given hereafter in the DR-P_D coordinate system.

Design curves for the cases of circular (OV = 0) and slightly oval (OV = 3% and 6%) host pipes are plotted in Figures 9.3 through 9.5. Each curve is associated with an individual gap ratio, G, which allows an engineer to pick an appropriate gap level in accordance with the specific installation and curing technique employed. The gap ratios observed under laboratory conditions (Hall, 1998a) were in the neighborhood of 0.2% to 0.4%. A CIPP system having a G value greater than 0.7% is very undesirable, and usually cannot be employed in rehabilitation. For instance, in the case of 12 inch pipe, a gap ratio (G) of 0.7% means a one-sided gap of over 0.16 inches (4 mm) or an evenly distributed gap of 0.08 inches (2mm).

As can be seen from Figures 9.3 to 9.5, the DR-P_D curves are approximately straight lines in the log-log scale. Simplified design equations can then be given in the form of

$$\lg P_D = a - b \lg DR \tag{9.10}$$

in which the slope $-b$ has a negative value, and a is the intercept at $DR = 1$. To determine the design DR ratio for a given pressure P_D, Eqn. (9.10) can be rewritten as

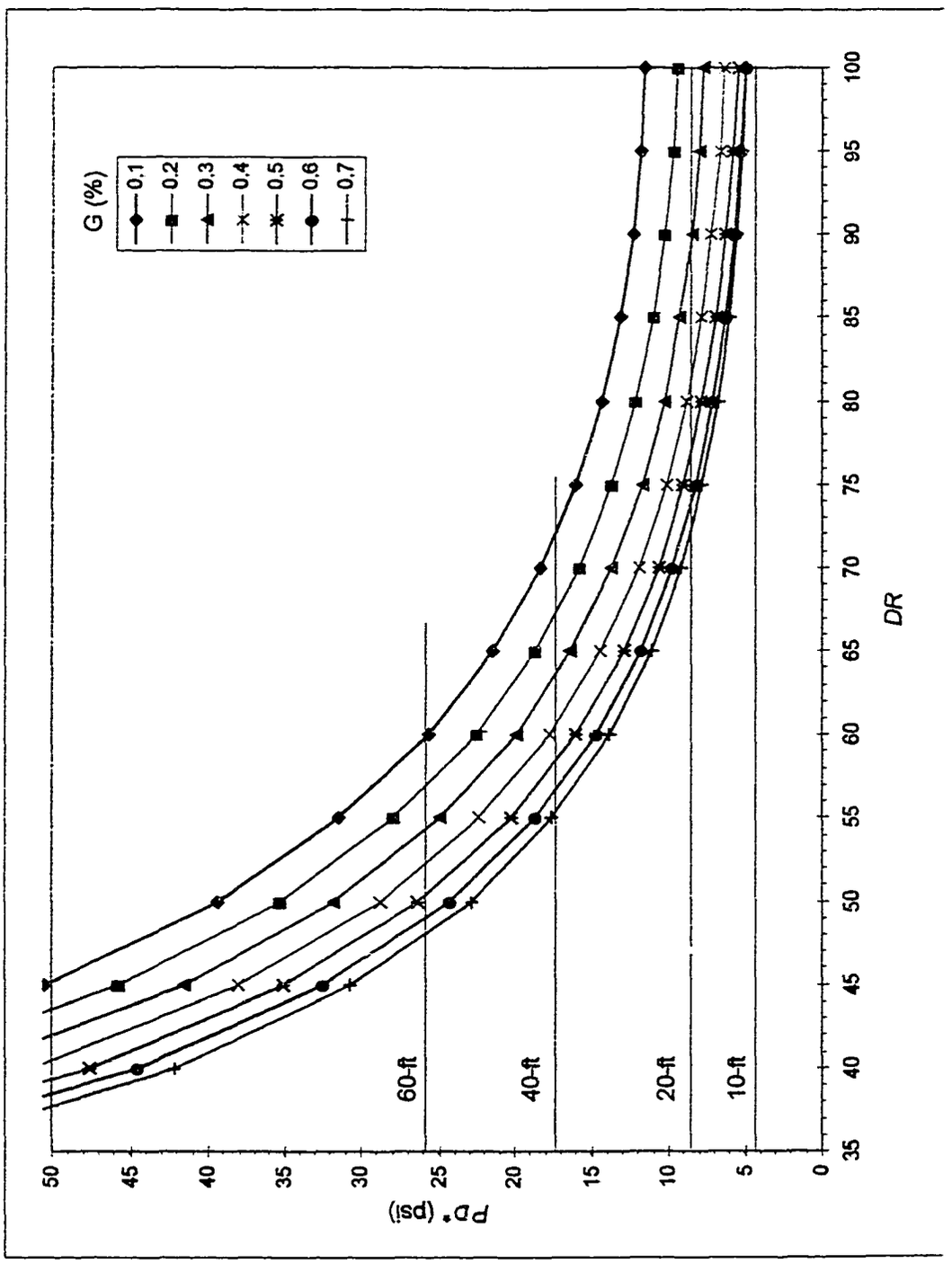

Fig. 9.3 Design curves for circular pipes (based on the material constant set LONG)

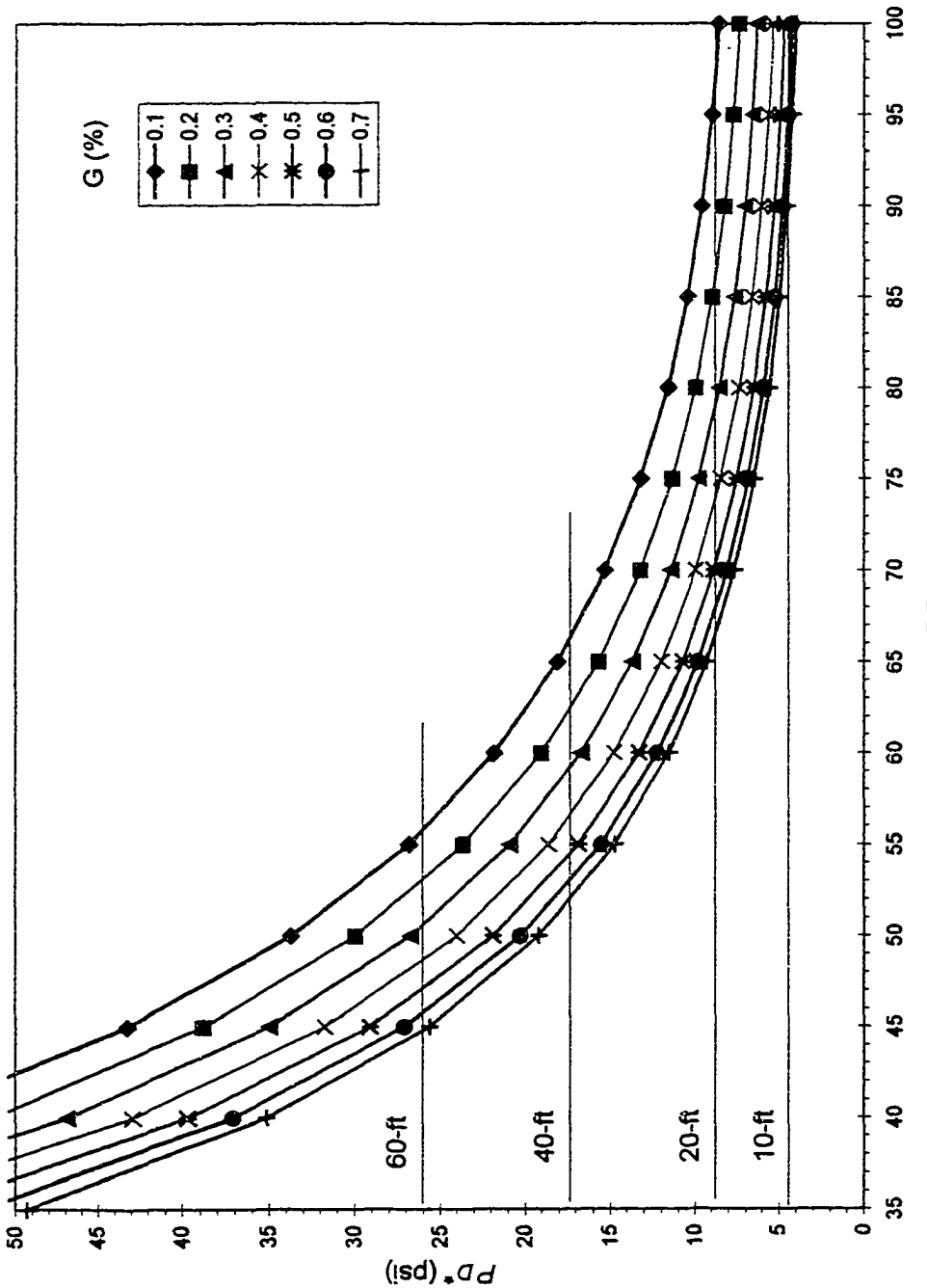

Fig. 9.4 Design curves for slightly oval pipes ($OV = 3\%$)

(based on the material constant set LONG)

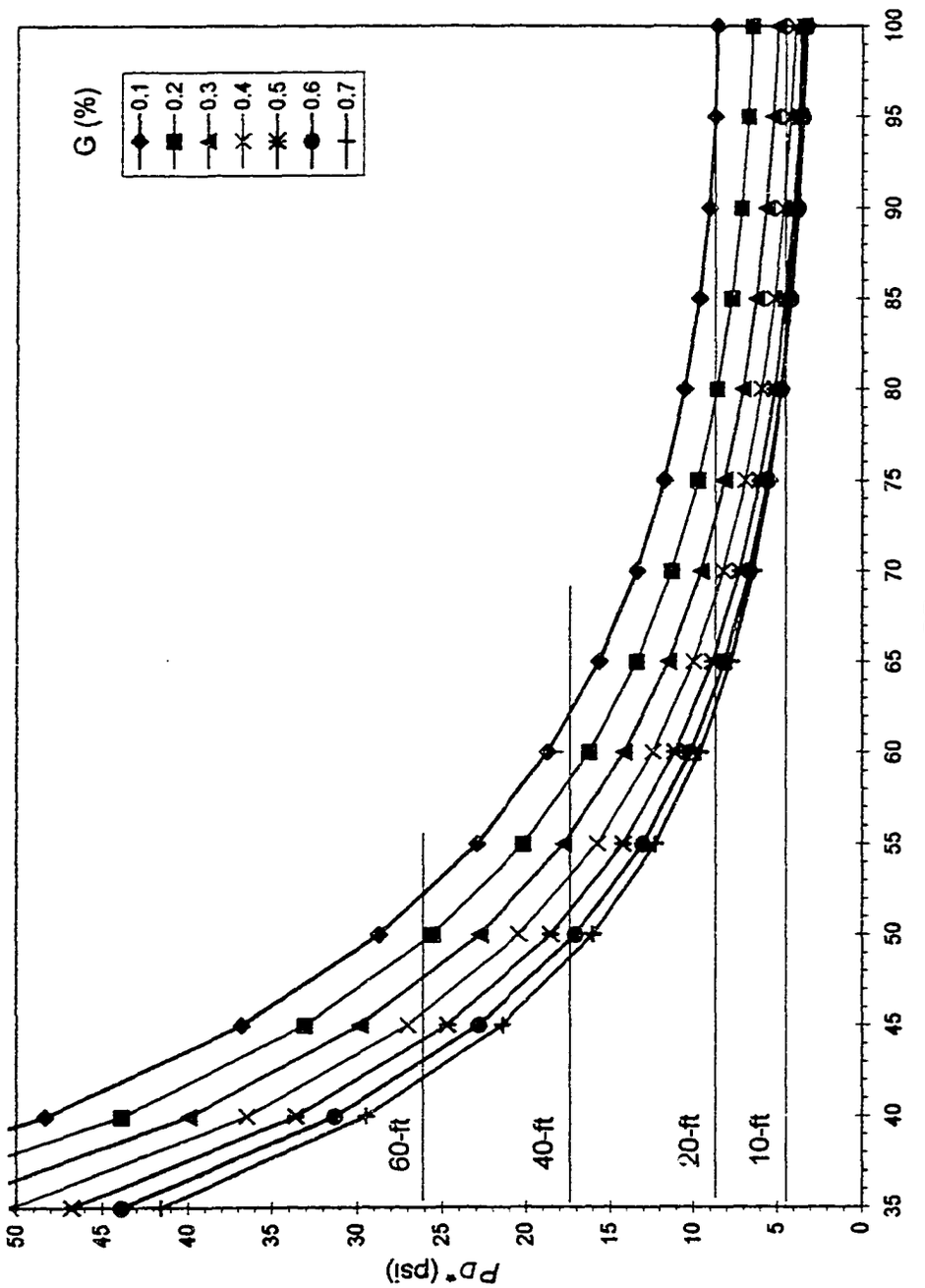

Fig. 9.5 Design curves for slightly oval pipes ($OV = 6\%$)

(based on the material constant set LONG)

$$\lg DR = c - d \lg P_D \tag{9.11}$$

or

$$DR = 10^c (P_D)^{-d} \tag{9.12}$$

The fitting parameters c and $-d$ are now functions of the gap ratio, G, and the host pipe ovality OV, as shown in Figures 9.6 and 9.7. These functions can be expressed empirically (using least squares) as follows:

$$c = (c_0 + c_1 G + c_2 G^2)(1 - 0.005 * OV) \tag{9.13}$$

$$d = d_0 + d_1 G + d_2 G^2 \tag{9.14}$$

The family of c curves can be generated from a master curve (corresponding to the circular pipe case) adjusted by the pipe ovality OV through the factor (1 - 0.005*OV), as shown in Fig. 9.6.

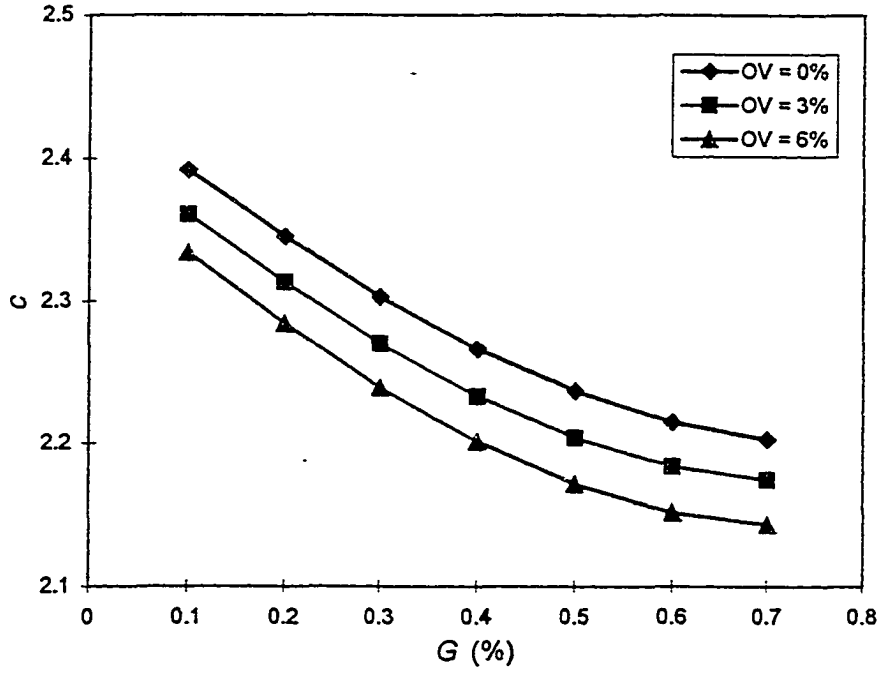

Fig. 9.6 Dependency of coefficient c on G and OV

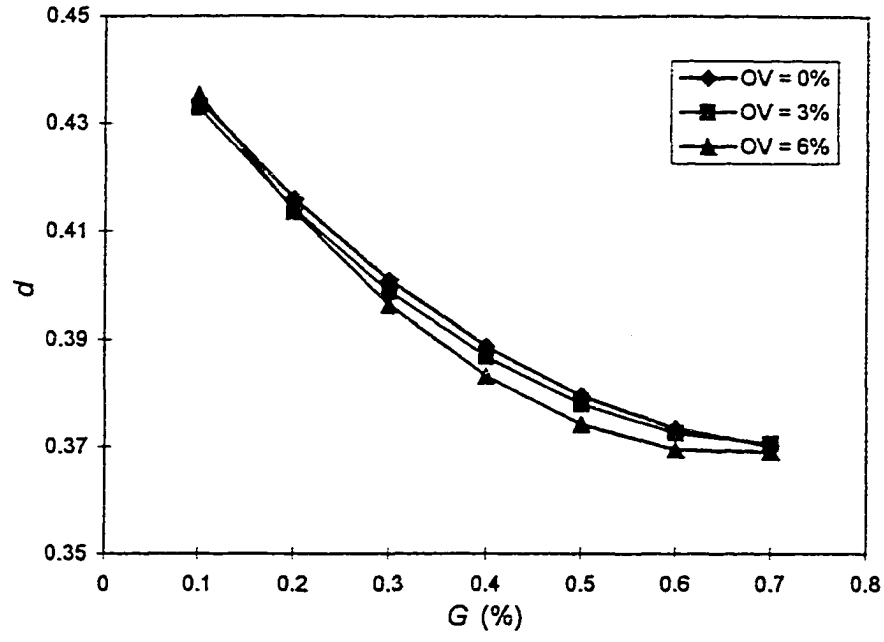

Fig. 9.7 Dependency of coefficient *d* on *G* and *OV*

The dependence of d on OV is not significant, but d depends on G. The lower bound envelope is thus given in Eqn. (9.14), which is on the conservative side. That is, a single d value can be used for all circular and slightly oval configurations.

The fitting constants c_i's and d_i's are listed in Table 9.4. Similar analyses have been conducted based on the safety factor 2 for pressure. The same trend is revealed and the corresponding coefficients c_i's and d_i's are also given in Table 9.4.

Once the DR ratio is determined, the minimum thickness t of the CIPP liner can be obtained by using the following equation.

$$t = \frac{D_P}{1+(1+2G)DR} \tag{9.15}$$

in which D_P is the inner diameter of the deteriorated sewer pipe.

9.4 Conclusions

In this chapter, design issues have been discussed, including the definition of a failure state, and an appropriate way to choose a safety factor. Methodology is presented by which finite element simulation results can be used in the CIPP liner design.

Design curves are given for designing CIPP liners made of the *Insituform Enhanced* resin as characterized by Lin (1994) and tested by Guice et al. (1993). An empirical design equation is presented which can determine a safe and cost-effective thickness for a given design pressure and a given pipe-liner system.

Table 9.4 Coefficients in empirical equations (9.13) and (9.14)

	c_0	c_1	c_2	d_0	d_1	d_2
$N_T = 10$	2.447158	-0.58885	0.342266	0.461271	-0.28008	0.211944
$N_P = 2$	2.370064	-0.60045	0.361546	0.457858	-0.27633	0.212063

CHAPTER 10

SUMMARY AND CONCLUSIONS

In the present study, the problem of long-term structural behavior of CIPP liners undergoing external hydrostatic pressure is characterized as a structural instability problem which is induced by time-dependent material property (i.e. creep). At the same time, it is a contact problem since the liner deflection is externally constrained by the host pipe.

This intrinsically nonlinear problem has been investigated by means of finite element simulation, with emphases on (a) the essential structural behaviors and mechanisms of buckling, and (b) the influences of inelastic material properties (i.e. plastic yield strengths and creep rates) and geometric parameters on liner's buckling resistance. Results from a series of finite element simulations verified against experimental observations on short- and long-term buckling, ware used to derive an appropriate CIPP liner design strategy. Specific contributions and conclusions drawn from this study are listed below.

10.1 Constraint/Loading Conditions

Based on an extensive survey of the literature, the following assumptions were adopted in this study:

1) The host pipe was assumed rigid, because its stiffness is typically much higher than that of a CIPP liner.
2) A liner was subjected only to the hydrostatic pressure built up by infiltration through cracks in the deteriorated host pipe. For simplicity, the pressure is assumed constant during the liner's service life.
3) The liner can be represented by a single cross-section with a width of unity to which the plain strain condition holds, and
4) The structural behavior of the 2-D configuration can be adequately modeled as a beam (or ring).

10.2 Material Behavior

The constitutive model for a specific liner product was assumed to be representative of the family of cured-in-place plastics, which are essentially amorphous substances with a randomly sidelinked network:

1) The total strain can be divided into three components: linearly elastic, perfectly plastic, and creep strain which follows a Norton-Bailey model.
2) The inelastic behaviors of CIPP materials depend not only on von Mises stresses, but on hydrostatic pressure as well.
3) Simplified constitutive relations reflecting dependency on stress state have been incorporated into the finite element models by means of the "composite" beam element, which is a combination of two normal beam elements. One of these two elements was assumed capable of resisting only tensile deformation and the other compressive deformation. Experimentally determined material properties (including

yield limits and creep strain rate) under uniaxial tension and compression tests were assigned to each of the two component beam elements.

4) The performance of the composite beam element was verified by comparing finite element simulation results and material characterization test data under both short- and long-term conditions.

10.3 Buckling Mechanism and Behavior

The interaction between a liner and its host pipe brings about a number of unique features to the deflection evolution of the constrained cylindrical shell subjected to short- and long-term external pressure:

1) Finite element results based on specific CIPP material properties showed that material failure (i.e. plastic yield) had a significant effect on the buckling resistance of the liner in both the instantaneous and long-term buckling cases.

2) Deformation until collapse of a constrained liner typically undergoes a two-step buckling process. The liner first buckles (as a free pipe) into a two-lobe pattern, mainly because of the existence of annual spacing between the liner and host pipe. With initial asymmetries in geometric and/or material properties being amplified by the increase in pressure or time duration, the two-lobe mode will transition to a one-lobe mode when one of the two competing lobes becomes dominant.

3) In the instantaneous buckling case, the two conventionally accepted buckling modes, one- and two-lobe modes, are found to give lower and upper bounds for all possible critical pressures. The finite element predictions and experimental data show excellent agreement, with most of the experimental data falling between the

predicted lower and upper bounds.

4) The load-deflection paths determined from finite element analysis are seen to fall between the paths corresponding to the conventional one-lobe and two-lobe buckling modes, depending on the specific conditions of the liner system (e.g. friction factor, initial gap, liner thickness variations, etc.)

5) Because the initial conditions are not controllable in many engineering applications, the design of such liner systems should be based on one-lobe buckling models corresponding to a conservative lower-bound buckling prediction.

10.4 Long-Term Buckling Model

The relationship between critical time and external pressure applied to the liner was derived from finite element simulation results. As shown in equation (7.6), critical time can be expressed as a monotonic function of the pressure ratio (P/P_{cr}), and reflects the intuition that the critical time at the two extreme pressure levels (zero and the critical pressure) are infinity and zero, respectively. The model gives excellent agreement with the finite element results, and is better than other models used in the literature for correlating experimentally observed buckling times to load levels.

10.5 Influence of Geometric Factors

The buckling resistance of CIPP liners depends to a great extent on some geometric parameters of the liner-host-pipe system. Finite element simulation was carried out to investigate the effects of three essential geometric parameters (i.e. the dimension ratio *DR* of the liner, gap *G* between the liner and its host pipe, and the ovality *OV* of host pipe) and two geometric imperfections (variation in liner thickness and initial local

imperfection in liner shape). The following conclusions can be summarized from the numerical results.

1) Generally, an increase in any of the geometric factors listed above tends to decrease the buckling resistance (critical pressure and critical time) of CIPP liners.
2) Critical pressure was empirically expressed as a power function of the liner's dimension ratio (Eqn. 6.1). The dependency of the two constants in the equation on gap ratio and pipe ovality was determined from a small number of finite element runs.
3) Similarly, critical time was expressed as a function of the pressure ratio (Eqn. 7.6). The dependency of the three constants in the equation on gap ratio and pipe ovality was determined from a small number of finite element runs.

10.6 Design Issues

Design issues were discussed, including the definition of a failure state and an appropriate way to choose a safety factor. Methodology was presented by which finite element simulation results could be used in CIPP liner design.

Design curves are given for designing CIPP liners made of the *Insituform Enhanced* resin as characterized by Lin (1994) and tested by Guice et al. (1993). An empirical design equation is derived which can determine a safe and cost-effective thickness for a given design pressure and a given pipe-liner system.

10.7 Recommendations for Further Studies

The fundamental buckling behavior of CIPP liners and the effects of geometric parameters were investigated in-depth in the present study. Finite element simulation

results and simplified empirical equations were presented in this dissertation.

Further studies in the following aspects are recommended.

1) More thorough material characterization tests, including the ones aiming at yield or failure mechanism, are highly recommended. The dependency of time-dependent and time-independent inelastic behaviors on the stress state should be investigated in detail. More sophisticated constitutive relations should be investigated.
2) Further studies should be undertaken that apply the present methodology to other CIPP materials or vary the creep rate coefficients. Such studies can reveal explicit relationships of critical time (or the constants in the empirical equation (7.6)) on creep properties of CIPP materials.
3) Previous and present studies are all based on the assumption that the external hydrostatic pressure is constant. Although it can be inferred from ArnoldÆs (1987) results that the effect of a varying load is not significant if the external pressure was always positive (i.e., no internal-external cyclic pressure), the behavior of CIPP liners subjected to seasonal fluctuation of underground water table is always worth studying. This might be accomplished by the following approaches: (a) employing a modified strain hardening law (which can reflect reversal in creep rate when stresses decrease) with the current simplified constitutive equation; and (b) following Arnold's (1987) visco-elastoplastic analysis.
4) The influence of various geometric factors were revealed in this study. At the same time, extensive measurements on geometry of actual liners used in buckling tests are underway at the TTC (1998c). Further numerical investigations can be conducted for comparisons with these experimental observations. Effects of coupled geometric

imperfections which are observed in test setup on critical time can thus be explored.

5) Three-dimensional finite element models can be used to investigate the effects of some factors that are not considered in the present study on the creep buckling behavior of CIPP liners. These factors include deflection patterns and the geometric imperfections along the longitudinal direction, as well as the boundary condition at the ends of a liner span. The effect of the length of a liner-span, which was discussed by several researchers (Bakeer and Berber, 1996; Moore, 1998) can also be determined. Furthermore, three-dimensional finite element analysis can help to explore the availability of the CIPP technique in rehabilitating pipelines with joints or other complex configurations.

6) The behavior of more advanced CIPP liner systems, such as those employing fiber reinforced plastics, may further improve liner's resistance to creep and thus enhance service life. Experiments coupled with finite element simulations are recommended.

APPENDIX A

MATERIAL PROPERTIES AND

TEST RESULTS USED

A.1. Material Characterization Tests

Table A.1 Material property set LONG
(Guice et al, 1993; Lin, 1994)

Short Term					
	E	E'	ν	σ_y	$\sigma_y^{'}$
Tensile	650000	740741	0.35	3500	3988
Compressive	650000	740741	0.35	8000	9117
Long Term					
	k	k'	m	n	
Tensile	3.50E-07	2.57E-07	1.150	0.11	
Compressive	4.20E-08	7.30E-08	1.146	0.24	

Note:

(1) $E' = E/(1-\nu^2)$

(2) $\sigma_y^{'} = \sigma_y/(1-\nu^2)$

(3) $k' = k(3/4)^{(n+1)/2}$

Table A.2 Material property set SHT1
(Boot and Javadi, 1998)

Test Type	**Statistical Property**	E (psi)	**Strain at Yield (%)**	**Stress at Yield (psi)**	**Ultimate Strain (%)**	**Ultimate Stress (psi)**
Tension	Mean (of 6)	556336	0.27	3142	3.00	3660
	Std. Error	20178	0.02	101	0.53	115
Flexure	Mean (of 7)	536595	0.67	3700	5.50	7350
	Std. Error	6774	0.03	187	0.40	101

Table A.3 Material property set SHT2
(Stokeld, 1998)

Test No.	E	σ_y	σ_{ult}	Note
atm02	562977.7	3683	3683	
btm02	781097.7	3686	3700	
dbm01	571863.9	3383	3400	
r1275	495348.8	3550	3850	
p1275	400189.0	3783	3500	
abm02	661142.9	2971	3700	*
ctm03	580829.5	2745	3900	*
cbm01	437578.6	4593	n/a	**
dmm02f	405907.7	2217	3650	**
Set of all 9 specimens				
Average	544104.0	3401.2	3672.9	
Deviation	150625.1	723.4	217.4	
Set of first 7 specimens				
Average	579064.2	3400.1	3676.143	
Deviation	111401.9	367.2	164.2319	
Set of first 5 specimens				
Average	562295.4	3616.9	3626.6	
Deviation	125480.5	138.5	158.7	

Note:

Material characterization tests conducted by Stokeld (1998) are summarized in the above table. Average and deviation values of elastic modulus and stress limits have been calculated for three subsets of the nine specimens:

1) All nine specimens;
2) The first seven specimens, deleted two outliers (with **) with respect to σ_y;
3) The first five specimens, deleted four outliers (with */**) with respect to σ_y.

The modulii are then determined as

E = 560000 psi
σ_y = 3600 psi

A.2. Short Term Buckling Test Results (TTC, 1998a)

Table A.4 Short-term buckling test results (circular pipes)

Test No.	t (in)	D_{mean} (in)	DR	P_{cr} (psi)
12"OD5.5mm1	0.200	11.64	58.22	64
12"OD5.5mm2	0.202	11.65	57.67	60
12"OD5.5mm3	0.197	11.66	59.11	54
12"OD5.5mm4	0.197	11.67	59.17	50
12"OD5.5mm5	0.205	11.68	57.04	36
Average	0.200	11.66	58.24	52.8
12"OD6.5mm1	0.244	11.67	47.90	80
12"OD6.5mm2	0.238	11.67	49.04	86
12"OD6.5mm3	0.232	11.66	50.32	92
12"OD6.5mm4	0.235	11.67	49.69	105
12"OD6.5mm5	0.241	11.65	48.38	98
Average	0.238	11.66	49.07	92.2
12"OD7.5mm1	0.259	11.68	45.12	138
12"OD7.5mm2	0.261	11.67	44.66	127
12"OD7.5mm3	0.263	11.62	44.14	103
12"OD7.5mm4	0.262	11.59	44.20	112
12"OD7.5mm5	0.267	11.59	43.47	139
Average	0.262	11.63	44.32	123.8
8"OD4.5mm1	0.148	7.83	52.99	80
8"OD4.5mm2	0.151	7.82	51.88	86
8"OD4.5mm3	0.150	7.85	52.41	80
8"OD4.5mm4	0.146	7.77	53.42	88
8"OD4.5mm5	0.154	7.86	51.16	78
Average	0.150	7.83	52.37	82.4
8"OD5.5mm1	0.160	7.79	48.65	92
8"OD5.5mm2	0.162	7.74	47.74	105
8"OD5.5mm3	0.165	7.81	47.29	110
8"OD5.5mm4	0.159	7.84	49.23	115
8"OD5.5mm5	0.159	7.81	49.19	112
Average	0.161	7.80	48.43	106.8
8"OD6.5mm1	0.182	7.79	42.78	113
8"OD6.5mm2	0.176	7.83	44.42	115
8"OD6.5mm3	0.176	7.79	44.39	133
8"OD6.5mm4	0.174	7.79	44.73	115
8"OD6.5mm5	0.177	7.77	43.92	113
Average	0.177	7.80	44.05	117.8

Table A.5 Short-term buckling test results (oval pipes)

Test No.	t (in)	D_{mean} (in)	DR	OV (%)	P_{cr} (psi)
12"OD0%OV1	0.308	11.65	37.85	n/a	134
12"OD0%OV2	0.293	11.64	39.80	n/a	117
12"OD0%OV3	0.294	11.77	40.06	n/a	125
12"OD0%OV4	0.295	11.66	39.54	n/a	131
12"OD0%OV5	0.302	11.69	38.76	n/a	109
Average	0.298	11.68	39.19	n/a	122.9
12"OD2%OV1	0.296	11.64	39.36	1.94	105
12"OD2%OV2	0.293	11.68	39.91	1.82	105
12"OD2%OV3	0.313	11.65	37.27	1.65	90
12"OD2%OV4	0.306	11.63	38.03	1.62	99
12"OD2%OV5	0.281	11.68	41.54	1.81	98
Average	0.298	11.66	39.17	1.77	99.3
12"OD5%OV1	0.304	11.68	38.46	3.56	75
12"OD5%OV2	0.293	11.66	39.75	4.59	81
12"OD5%OV3	0.291	11.71	40.28	5.35	67
12"OD5%OV4	0.293	11.66	39.77	4.72	74
12"OD5%OV5	0.302	11.62	38.523	4.19	78
Average	0.297	11.67	39.34	4.48	75.0

A.3. Long Term Buckling Test Results

Table A.6 Long-term buckling test summary
(Guice et al, 1993)

Test No.	*DR*	*G* (%)	*P* (psi)	T_{cr} (hr)
1	51.27	0.4174	75	0.5
2	51.09	0.2553	75	51
4	52.87	0.3408	75	68
5	52.44	0.3491	75	1.5
6	49.34	0.5986	70	33
7	52.96	0.2722	75	54
8	52.24	0.6806	69	0.2
9	53.82	0.6819	70	3
11	51.27	0.3322	70	2
12	52.39	0.4942	65	521
13	54.07	0.4261	70	136
14	52.30	0.5548	65	1056
15	53.27	0.5461	65	528
16	54.72	0.4590	60	2455
17	52.83	0.4604	60	200
18	52.44	0.2989	60	54
19	51.78	0.6722	60	2455
21	53.23	0.5979	60	494
22	52.30	0.5121	55	3272
23	54.02	0.5200	60	1536
24	53.43	0.6837	55	4349
25	55.10	0.4260	55	3384
26	53.82	0.4262	55	455
27	55.71	0.7692	55	144
28	55.90	0.4259	55	2236
29	54.02	0.5118	50	5379
31	53.57	0.4432	50	6013
32	53.86	0.3407	50	10000
33	54.02	0.5118	50	1272
34	53.32	0.4263	50	3302
35	52.83	0.4263	50	3338
36	52.98	0.5978	45	10000
37	53.77	0.5119	45	10000
38	53.18	0.7350	45	10000
39	54.58	0.5283	45	1616

APPENDIX B

TYPICAL ABAQUS INPUT FILES

Nine typical ABAQUS input files used in this study have been listed in this section for reference:

B.1. ABAQUS Input File `ALXYLD.inp`
`(Material Characterization Test -- Axial)`

B.2. ABAQUS Input File `FLXYLD.inp`
`(Material Characterization Test -- Flexural)`

B.3. ABAQUS Input File `ALXCRP.inp`
`(Creep Characterization Test -- Axial)`

B.4. ABAQUS Input File `FLXCRP.inp`
`(Creep Characterization Test -- Flexural)`

B.5. ABAQUS Input File `1LOBE.inp`
`(One-lobe Circular Pipe Model -- Short Term)`

B.6. ABAQUS Input File `2LOBE.inp`
`(Two-lobe Circular Pipe Model -- Short Term)`

B.7. ABAQUS Input File `FLOAT.inp`
`("Float" Circular Pipe Model -- Short Term)`

B.8. ABAQUS Input File `OVAL.inp`
`(One-lobe Oval Pipe Model -- Short Term)`

B.9. ABAQUS Input File `1LOBE.inp`
`(One-lobe Circular Pipe Model -- Creep Buckling)`

B.1 ABAQUS INPUT FILE ALXYLD.inp

```
*heading
 Material Characterization Test -- Axial
*wavefront minimization, suppress
*node
 1, 0., 0.
 2, 1., 0.
 3, 0., 1.
 4, 1., 1.
*element, type = b21, elset = TENS
 1, 1, 2
 2, 3, 4
*element, type = b21, elset = COMP
 11, 1, 2
 12, 3, 4
*beam sect, sect = rect, elset = TENS, material = SHT1_TENS
 0.21, 0.21
*material, name = SHT1_TENS
*no comp
*elastic
 550000.
*plastic
 3150.
 3650., .03
*beam sect, sect = rect, elset = COMP, material = SHT1_COMP
 0.21, 0.21
*material, name = SHT1_COMP
*no tens
*elastic
 550000.
*plastic
 8000.
*boundary
 1, encastre
 3, encastre
*restart, write
*step, nlgeom, inc = 100
*static
 0.1, 1.
*boundary
 2, 1, 0.05.
 4, 1, -0.1
*end step
```

B.2 ABAQUS INPUT FILE FLXYLD.inp

```
*heading
 Material Characterization Test -- Flexural
*wavefront minimization, suppress
**
*node
 1
 21, 1.68
*ngen, nset = beam
 1,21
*element, type = b21
 1, 1, 2
 21, 1, 2
*elgen, elset = TENS
 1, 20
*elgen, elset = COMP
 21, 20
**
** ...(beam section & material definitions, same as B.1)
**
*boundary
 1, 1
 1, 6
 21, 2
*restart, write, freq = 5
**
*step, nlgeom, inc = 100
*static
 0.1, 1.
*cload
 1, 2, -5.
*node print, freq = 50
 u
*el print, elset = TENS, freq = 50
 s11
*end step
```

B.3 ABAQUS INPUT FILE ALXCRP.inp

```
*heading
 Material Characterization Test -- Axial
*wavefront minimization, suppress
**
*node
 1, 0., 0.
 4, 3., 0.
 11, 0., 1.
 14, 3., 1.
*ngen, nset = fix
 1, 4
*ngen, nset = free
 11, 14
*element, type = b21
 1, 1, 11
 5, 1, 11
*elgen, elset = TENS
 1, 4
*elgen, elset = COMP
 5, 4
**
*beam sect, sect = rect, elset = TENS, material = LONG_TENS
 0.21, 0.21
*material, name = LONG_TENS
*no comp
*elastic
 650000.
*plastic
 3500.
*creep, law = strain
 0.2825866e-7, 1.15, -.89
**
*beam sect, sect = rect, elset = COMP, material = LONG_COMP
 0.21, 0.21
*material, name = LONG_COMP
*no tens
*elastic
 650000.
*plastic
 8500.
*creep, law = strain
 0.7296456481e-8, 1.14585, -.76
**
*boundary
```

```
 fix, encastre
*restart, write
**
*step, nlgeom, inc = 10
*static
 0.1, 1.
*cload
 11, 1, -22.05.
 12, 1, -44.1
 13, 1, -66.15.
 14, 1, -88.2
**
** the following data lines should be used in a separate run
** simulating the compressive creep tests
** 11, 1, 44.1
** 12, 1, 88.2
** 13, 1, 132.3
** 14, 1, 176.4
**
*end step
*step, nlgeom, inc = 500
*visco, cetol = 1.e-4
 1.e-8, 3000., 1.e-30, 24.
*node print, freq = 500
 u
*el print, elset = TENS, freq = 500
 s11
*end step
```

B.4 ABAQUS INPUT FILE FLXCRP.inp

```
*heading
 Creep Characterization Test -- Flexural
*wavefront minimization, suppress
**
** ...(node definition, same as B.2)
**
** ...(element definition, same as B.2)
**
** ...(beam section & material definitions, same as B.3)
**
*boundary
 1, 1
 1, 6
 21, 2
*restart, write, freq = 5
**
*step, nlgeom, inc = 100
*static
 1.e-5, 1.
*cload
 1, 2, -2.75625
**
** the concentrated load should be changed in each run to
** simulate one of the four stress levels in Lin's test
**      load:     -3.675    -2.75625  -1.8375   -0.91875
**      stress:   4000      3000      2000      1000
**
*node print, freq = 50
 u
*el print, elset = TENS, freq = 50
 s11
*end step
*step, nlgeom, inc = 500
*visco, cetol=1.e-4
 1.e-8, 3000., 1.e-30, 24.
*node print, freq = 500
 u
*el print, elset = TENS, freq = 500
 s11
*end step
```

B.5 ABAQUS INPUT FILE 1LOBE.inp

```
*heading
 one-lobe circular pipe model -- short term
*node
   1, 0., 6.
  73, 6.
 145, 0., -6.
*ngen, nset = RING, line = c
  1,  73, 1, 0, 0.0
 73, 145, 1, 0, 0.0
*element, type = b21
   1, 1, 2
 501, 1, 2
*elgen, elset = TENS
 1, 144
*elgen, elset = COMP
 501, 144
*beam sect, elset = TENS, material = SHT2_TENS, sect = rect
 1., .24
*material, name = SHT2_TENS
*no comp
*elastic
 638177., .35
*plastic
 4100.
**
*beam sect, elset = COMP, material = SHT2_COMP, sect = rect
1., .24
*material, name = SHT2_COMP
*no tens
*elastic
 638177., .35
*plastic
 9116.8
**
** mesh definition for host pipe
**
*node
 1001, 0., 6.096
 1073, 6.048, 0.048
 1145, 0., -6.
*ngen, nset = HOSTPIPE, line = c
 1001, 1073, 1, 0, 0. , 0.048
 1073, 1145, 1, 0, 0. , 0.048
*element, type = r2d2
```

```
 1001, 1001, 1002
*elgen, elset = HOSTPIPE
 1001, 144
*rigid body, elset = HOSTPIPE, ref node = 1001
**
** contact condition
**      (ASURF :: contact surface on liner)
*surface definition, name = ASURF
 TENS, spos
**
**      (BSURF :: rigid host pipe)
*surface def, name = BSURF
 HOSTPIPE, sneg
**
**      (contact pair)
*contact pair, interaction = SMOOTH
 ASURF, BSURF
*surface interaction, name = SMOOTH
**
*boundary
    1, 1
    1, 6
  145, encastre
 1001, encastre
**
*restart, write, freq = 5
**
** loading
**
*step, nlgeom, inc = 30
*static
 1.e-1, 1., 1.e-10
*cload
 73, 1, 1.e-1
*node print, freq = 50
 u
*el print, elset = TENS, freq = 50
 s
*end step
**
*step, nlgeom, inc = 1000
*static
1.e-3, 2., 1.e-10, 1.e-2
*dload
 TENS, p2, -200.
*node print, freq = 500
```

```
 u
*el print, elset = TENS, freq = 500
 s
*end step
```

B.6 ABAQUS INPUT FILE 2LOBE.inp

```
*heading
 two-lobe circular pipe model -- short term
*node
   1, 0., 6.
  73, 6.
*ngen, nset = RING, line = c
  1,  73, 1, 0, 0.0
*element, type = b21
   1, 1, 2
 501, 1, 2
*elgen, elset = TENS
 1, 72
*elgen, elset = COMP
 501, 72
**
** ...(beam section & material definitions, same as B.5)
**
**
** mesh definition for host pipe
**
*node
 1001, 0., 6.048
 1073, 6.048
*ngen, nset = HOSTPIPE, line = c
 1001, 1073, 1, 0, 0., 0.
*element, type = r2d2
 1001, 1001, 1002
*elgen, elset = HOSTPIPE
 1001, 72
*rigid body, elset = HOSTPIPE, ref node = 1001
**
** ...(contact condition, same as B.5)
**
*boundary
    1, 1
    1, 6
   73, 2
   73, 6
 1001, encastre
**
** ...(loading, same as B.5)
**
```

B.7 ABAQUS INPUT FILE FLOAT.inp

```
*heading
 "float" circular pipe model -- short term
**
** ...(liner node & element definitions, same as B.5)
**
** ...(beam section & material definitions, same as B.5)
**
** spring & dashpot elements
**
*element, type = spring1, elset = SPX
 1000, 145
*spring, elset = SPX
 2
 1.e-2
*element, type = dashpot1, elset = DPX
 2000, 1
 3000, 145
*dashpot, elset = DPX
 2
 1.e-3
**
** mesh definition for host pipe
**
*node
 1001, 0., 6.048
 1073, 6.048
 1145, 0., -6.048
*ngen, nset = HOSTPIPE, line = c
 1001, 1073, 1, 0, 0., 0.
 1073, 1145, 1, 0, 0., 0.
*element, type = r2d2
 1001, 1001, 1002
*elgen, elset = HOSTPIPE
 1001, 144
*rigid body, elset = HOSTPIPE, ref node = 1001
**
** ...(contact conditions, same as B.5)
**
*boundary
    1, 1
    1, 6
  145, 1
  145, 6
 1001, encastre
```

```
**
** ...(loading, same as B.5)
**
```

B.8 ABAQUS INPUT FILE OVAL.inp

```
*heading
 one-lobe oval pipe model -- short term
*node, input = d:\yyy\gap.dat
**
** ...(all other info, same as B.1; except for node
**      definition for host pipe, which is given in the
**      following file)
**
```

A separate file, `d:\yyy\gap.dat`, defining liner and host pipe nodes, will be input at runtime to provide nodal information.

```
1     0.000      6.000
2     0.131      5.999
3     0.262      5.994
4     0.392      5.987
5     0.523      5.977
6     0.653      5.964
7     0.783      5.949
8     0.913      5.930
9     1.042      5.909
10    1.171      5.885
(...  ...)
140   0.653      -5.964
141   0.523      -5.977
142   0.392      -5.987
143   0.262      -5.994
144   0.131      -5.999
145   -0.000     -6.000
**
1001 0.000       6.168
1002 0.133       6.167
1003 0.265       6.162
1004 0.398       6.155
1005 0.530       6.145
1006 0.662       6.132
1007 0.794       6.116
1008 0.926       6.097
1009 1.056       6.076
1010 1.187       6.051
(... ...)
1140 0.662       -5.964
1141 0.530       -5.977
1142 0.398       -5.987
```

```
1143 0.265      -5.994
1144 0.133      -5.999
1145 -0.000     -6.000
```

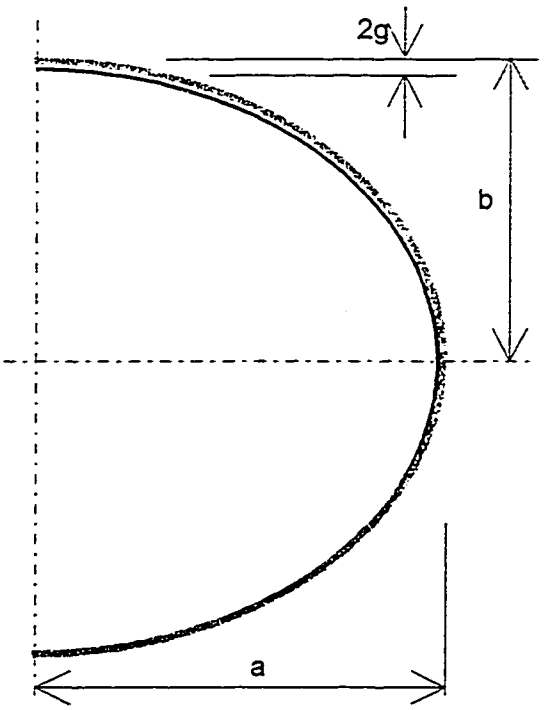

(The liner and its host pipe share the same ovality: $OV = (a-b) / (a+b)$)

Fig. B.1 Schematic of FEA model for oval pipes

B.9 ABAQUS INPUT FILE CRPBKL.inp

```
*heading
 one-lobe circular pipe model -- creep buckling
**
** ...(liner node & element definitions, same as B.5)
**
*beam sect, elset = TENS, material = LONG_TENS, sect = rect
 1., .24
*material, name = LONG_TENS
*no comp
*density
 0.0361
*elastic
 740741., .35
*plastic
 4100.
*creep, law = strain
 0.2825866e-7, 1.15, -.89
**
*beam sect, elset = COMP, material = LONG_COMP, sect = rect
1., .24
*material, name = LONG_COMP
*no tens
*elastic
 740741., .35
*plastic
 9116.8
*creep, law = strain
 1.00788e-8, 1.14585, -.76
**
** ...(mesh definition for host pipe, same as B.5)
**
** ...(contact conditions, same as B.5)
**
** ...(boundary conditions, same as B.5)
**
** loading
**
*step, nlgeom, inc = 30
*static
 1.e-1, 1., 1.e-10
*cload
 73, 1, 1.e-1
*node print, freq = 50
 u
```

```
*el print, elset = TENS, freq = 50
 s
*end step
**
*step, nlgeom, inc = 1000
*static
1.e-6, 0.05, 1.e-10, 1.e-2
*dload
 TENS, p2, -50.
**
** external pressure should be changed in each
**
*node print, freq = 500
 u
*el print, elset = TENS, freq = 500
 s
*end step
*step, nlgeom, inc = 500
*visco, cetol=1.e-4
 1.e-8, 1.e8, 1.e-30
*node print, freq = 500
 u
*el print, elset = TENS, freq = 500
 s11
*end step
```

APPENDIX C

FINITE ELEMENT ANALYSIS RESULTS

C.1 Long-Term Buckling Analysis

Table C.1 Predicted critical time (hr) for *OV* = 0%

OV = 0%				
G	***PR***	***DR* = 35**	***DR* = 50**	***DR* = 65**
0.1%	0.80	1312.27	385.09	216.04
	0.75	5117.95	1710.75	1010.67
	0.70	16466.93	6046.56	3784.23
	0.60	127917.90	53328.06	36841.02
	0.50	842452.50	387529.00	286476.40
0.4%	0.80	894.72	231.87	106.15
	0.75	4330.37	1370.38	619.09
	0.70	14925.18	5492.81	2780.15
	0.60	141535.50	62974.71	34507.52
	0.50	1026898.00	530857.10	332989.50
0.7%	0.80	589.63	190.51	72.01
	0.75	3340.16	1183.06	489.95
	0.70	13219.02	5347.22	2412.02
	0.60	141164.20	67000.59	34678.23
	0.50	1153603.00	636467.80	363311.90

Table C.2 Predicted critical time (hr) for $OV = 3\%$

$OV = 3\%$				
G	*PR*	*DR* = 35	*DR* = 50	*DR* = 65
0.1%	0.80	1310.10	345.80	183.45
	0.75	5190.30	1455.97	941.43
	0.70	16915.00	5172.14	3531.65
	0.60	126751.00	45835.32	36283.23
	0.50	807905.80	338127.90	272725.50
0.4%	0.80	918.88	233.28	102.46
	0.75	4197.36	1293.91	602.88
	0.70	14764.71	5468.03	2657.95
	0.60	133959.70	59489.02	34453.61
	0.50	964555.00	508261.90	315772.50
0.7%	0.80	1135.10	221.74	82.26
	0.75	5188.14	1405.48	534.43
	0.70	20154.41	5979.26	2475.20
	0.60	193634.40	73971.81	36367.96
	0.50	1432658.00	680662.20	370467.60

Table C.3 Predicted critical time (hr) for $OV = 6\%$

$OV = 6\%$				
G	*PR*	*DR* = 35	*DR* = 50	*DR* = 65
0.1%	0.80	1150.94	325.59	143.35
	0.75	4301.66	1397.92	681.26
	0.70	13863.23	5004.20	2622.10
	0.60	107887.20	46244.24	28120.72
	0.50	703582.10	331255.00	231777.50
0.4%	0.80	900.59	281.38	70.76
	0.75	4410.87	1383.63	446.12
	0.70	15767.19	5935.69	2028.87
	0.60	139603.30	62039.01	28500.49
	0.50	1033571.00	528886.40	262040.40
0.7%	0.80	1193.41	345.64	80.99
	0.75	6041.72	1835.17	543.95
	0.70	23219.09	7934.70	2541.46
	0.60	223674.20	92041.01	35482.11
	0.50	1699721.00	770561.90	372676.80

C.2. Results of Mesh Refinement Study

Table C.4 Predicted critical time for different mesh densities

Number of elements	Case 1	Case 2	Case 3	Case 4
36	2942	5555	267	17493
72	2668	5292	230	16102
144	2462	5187	221	15354
288	2429	5117	216	14925

Table C.5 Relative critical time for different mesh densities

Number of elements	Case 1	Case 2	Case 3	Case 4
36	100.0	100.0	100.0	100.0
72	90.7	95.3	86.1	92.1
144	83.7	93.4	82.6	87.8
288	82.6	92.1	80.8	85.2

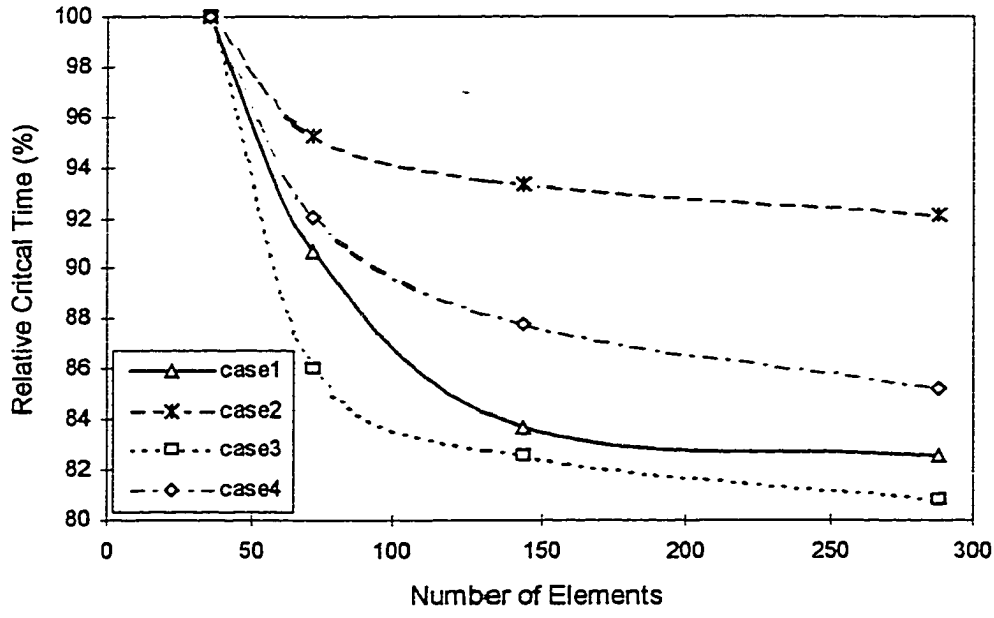

Fig. C.1 Relative critical time versus number of elements

APPENDIX D

SOURCE CODES

D.1 The Critical Time Fitting Program

```
      program fit
c
c This program is designed to fit critical time predicted by
c FEA to the proposed empirical model, Eqn. (7.6).
c
c A standard least-square fitting algorithm is employed to
c determine the exponent (n) and the time coefficient (T0)
c in Eqn. (7.6) for a given adjustment factor (b). The main
c program loops by utilizing a bisection algorithm until the
c best fit is achieved at a optimum value of b.
c
      implicit real*8 (a-h, o-z)
      dimension pin(20), tin(20), pu(20), pb(20), tfit(20)
      open (5, file='fit.inn')
      open (6, file='fit.out')
c
c Input number of p-tcr pairs, critical pressure, and upper
c and bottom bounds for b, followed by the p-tcr.
c The pressure (p) values will be normalized to pressure
c ratio (PR) by dividing pcr.
c
      read(5, *) n, pcr, bottom, upper
      if (upper.le.5.d-1) upper = 1.d0
      if (bottom.le.5.d-1) bottom = .90d0
      do i=1, n
        read(5, *) pin(i), tin(i)
      end do
      do i = 1, n
        if (pin(i).gt.1.d0) then
          pu(i) = pcr/pin(i)
          pb(i) = pu(i)*bottom
        else
          pu(i) = upper/pin(i)
```

```
            pb(i) = bottom/pin(i)
          end if
        end do
        call lstsq(n, upper, pu, tin, uerr, expou, t0u)
        call lstsq(n, bottom, pb, tin, berr, expob, t0b)
     10 continue
c
c Fitting errors w.r.t. upper and lower bounds of b are
c calculated and compared. Either upper or lower bound of b
c will be updated by the bisection point accordingly. The
c calculation will be repeated until the upper and lower
c bounds coincide.
c
      if (uerr.lt.berr.or.(upper-bottom).lt.(2.d-4)) then
        bottom = (bottom + upper)/2.d0
        do i = 1, n
          pb(i) = (pb(i) + pu(i))/2.d0
        end do
        call lstsq(n, bottom, pb, tin, berr, expob, t0b)
      else
        upper = (bottom + upper)/2.d0
        do i = 1, n
          pu(i) = (pb(i) + pu(i))/2.d0
        end do
        call lstsq(n, upper, pu, tin, uerr, expou, t0u)
      end if
      if ((upper-bottom).ge.(1.d-4)) then
        goto 10
      end if
      write (6, *) expob, t0b, bottom, berr
      do i = 1, n
        tfit(i) = t0b * (pb(i) - 1.d0)**expob
        write (6,20) pin(i), tin(i), tfit(i)
      end do
   20 format (f7.2, 1x, e14.7, 1x, e14.7)
      close (5)
      close (6)
      stop
      end
cc
cc
      subroutine lstsq(n, p0, x, y, err, expo, t0)
      implicit real*8 (a-h, o-z)
      dimension x(20), y(20), fx(20), fy(20)
c
c Initialize loop variables.
```

```
c
      err = 0.d0
      sumx = 0.d0
      sumy = 0.d0
      sumxy = 0.d0
      sumxx = 0.d0
      write (6, *) p0
c
c Map variables to the logarithm scale.
c
      do i = 1, n
        fx(i) = x(i) - 1.d0
        fx(i) = dlog10(fx(i))
        fy(i) = dlog10(y(i))
      end do
      do i = 1, n
        sumx = sumx + fx(i)
        sumy = sumy + fy(i)
        sumxy = sumxy + fx(i)*fy(i)
        sumxx = sumxx + fx(i)**2
      end do
      rr = (n*sumxx - sumx*sumx)
      expo = (n*sumxy - sumx*sumy)/rr
      t0 = (sumxx*sumy - sumxy*sumx)/rr
c
c Relative errors are used and accumulated.
c
      do i = 1, n
        yi = t0 + expo * fx(i)
        write (6, *) fx(i), fy(i), yi
        err = dabs((10.d0**fy(i)-10.d0**yi)/10.d0**fy(i))
     1        + err
      end do
      t0 = 10.d0**t0
      write (6, *) expo, t0, err
      return
      end
```

REFERENCES

Aggarwal, S.C. and Cooper, M.J. (1984). "External Pressure Testing of Insituform Lining," Internal Report.

Allen, H.G. and Bulson, P.S. (1980) *Background to Buckling*, McGraw-Hill, London, UK.

Amstutz, E. (1950) "Das Einbeulen von Schacht- und Stollenpanzerungen," *Schweizerische Bauzeitung*, 68(9), 102-105.

Amstutz, E. (1953) "Das Einbeulen von vorgestpannten Schacht- und Stollenpanzerungen," *Schweizerische Bauzeitung*, 71(16), 229-231.

Amstutz, E. (1969) "Das Einbeulen von Schacht- und Stollenpanzerungen," *Schweizerische Bauzeitung*, 87(28), 541-549.

ASTM F1216-93 (1993) *Standard Practice for Rehabilitation of Existing Pipelines and Conduits by the Inversion and Curing of a Resin-Impregnated Tube*, ASTM, Philadelphia, PA..

Bailey, B. (1929) "*Creep of Steel under Simple and Compound Stresses and the use of High Initial Temperature in Steam Power Plant*", Trans. Tokyo Section Meeting of the World Power Conf., p1089.

Bakeer, R. M. and Berber, M. E. (1997) "Evaluation of U-Liner Technology for Trenchless Sewer Rehabilitation", Final Report submitted to LEQSF (Contract # 1993-96-RD-B-12), Civil and Environmental Engineering Department

Bargmann, (1972) "Effect of Time-Varying External Pressure on Creep Collapse of a Cylindrical Shell," *AIAA Journal*, 10, 327-329.

Boot, J.C. and Welch, A.J. (1989) "Establishing and Implementing the Long Term Constitutive Behavior of Structural Plastic Pipe Linings," *The Life of Structures*, Armer, G.S.T., Clarke, J.L. and Garas, F.K. (Ed.), Butterworths, London, UK.

Boot, J.C. and Welch, A.J. (1996) "Creep Buckling of Thin-walled Polymeric Pipe Linings Subject to External Groundwater Pressure," *Thin-Walled Structures* 24(2), 191-210. Elsevire Science Ltd., UK.

Boot, J.C. and Javadi, A.A. (1998) "The Structural Behavior of Cured-In-Place Pipe," *Proc. Plastics Pipes X*, Gothenburg, Sweden..

Borot, H. (1957) "Flambage d'um cylindre a paroi mince, place dans une enveloppe rigide et soumis a une pression exterieure," *La Houille Blanche*, No. 6, 881-887.

Bresse, M. (1866) *Cours de Mechanique Appliquee*, 2nd Ed., Paris, France.

Bryan, G.H. (1888) "Application of the Energy Test to the Collapse of a Long Pipe under External Pressure," *Poc. Cambridge Philosophical Soc.*, Vol. 6, Cambridge, UK.

Cheney, J. A. (1971) "Buckling of Soil-Surrounded Tubes," *ASCE Journal of the Engineering Mechanics Division*, 97, EM4, 1121-1132.

Chicurel, R. (1968) "Shrink Buckling of Thin Circular Rings," *J. Appl. Mech.*, 35(3), 608-610.

Chern, J. M. (1978) "A Simplified Approach to the Prediction of Creep Buckling Time in Structures," Barsoum, R.S.(Ed.), *Simplified Methods in Pressure Vessel Analysis*, Montreal, Quebec, Canada

Cohen, A. and Arends, C.B. (1988a) "Creep Induced Buckling of Plastic Materials," *Polym. Eng. Sci.* 28(8) 506-509. Stamford, CONN.

Cohen, A. and Arends, C.B. (1988b) "Application of a Concept of Distributed Damage to Creep Induced Buckling of High Density Polyethylene Specimens," *Polym. Eng. Sci.* 28(16) 1066-1070. Stamford, CONN.

Conway, J.B. (1967) *Numerical Methods for Creep and Rupture Analyses*, Gordon and Breach, Science Publishers, New York, NY.

Courtney, T.H. (1990) *Mechanical Behavior of Materials*, McGraw-Hill, New York, NY.

Ellington, (1960) *Creep Collapse of Tubes under External Pressure*, DEG-Report 162(R), UK Atomic Energy Authority, Risley, Warrington, Lancashire, UK.

El-Sawy, K. & Moore, I. D. (1997) "Parametric Study for Buckling of Liners: Effect of Liner Geometry and Imperfections," *Proceedings of 1997 ASCE Conference on Trenchless Pipeline Projects*, 416-423, Boston, MA.

Eslami, M.R.& Shariyat, M. (1997) "Elastic, Plastic, and Creep Buckling of Imperfect Cylinders Under Mechanical and Thermal Loading," *Journal of Pressure Vessel Technology*, 119(1), 27-36.

Fairbairn, W. (1858) "On the Resistance of Tubes to Collapse," *Phil. Trans. Royal Soc.*, 148, London, UK.

Falter, B. (1996) "Structural Analysis of Sewer Linings," *Trenchless Technol. Res.*, 11(2), 27-41.

Findley, W. N. (1950) "Comments on Creep and Damping Properties of Polystyre," *J. Appl. Physics*, 21, 258-261.

Findley, W. N. and Khosla, G. (1955) "Application of the Superposition Principle and Theories of Mechanical Equation of State, Strain, and Time Hardening to Creep of Plastics under Changing Loads," *J. Appl. Physics*, 26(7), 821-831.

Findley, W. N. (1960) "Mechanism and Mechanics of Creep of Plastics," *SPE J.*, 12(1), 57-65.

Findley, W. N. (1971) "Combined Stress Creep of Non-Linear Viscoelastic Material," *Advances in Creep Design*, 263-286, John Wiley & Sons, Inc., New York.

Findley, W. N. (1987) "26-Year Creep and Recovery of Poly(Vinyl Chloride) and Polyethylene," *Polymer Engineering and Science*, 27(8), 582-585.

Finnie, I. and Heller, W.R. (1959) *Creep of Engineering Materials*, McGraw-Hill, New York, NY.

Gerard, G. (1952) "Note on Creep Buckling of Columns," *Journal of Aero/Space Science*, 19, 714-716.

Gerard, G. (1956) "A Creep Buckling Hypothesis," *Journal of Aero/Space Science*, 23, 879-882.

Gerdeen, J.G. & V.K. Sazawal, V.K. (1974) "A Review of Creep Instability in High-Temperature Piping and Pressure Vessels," *WRC Bulletin* 159, 33-56, the Pressure Vessel Research Committee of the Welding Research Council.

Glock, D. (1977) "Behavior of Liners for Rigid Pipeline Under External Water Pressure and Thermal Expansion"(English Translation), *Der Stahlbau*, 7, 212-217.

Guice, L.K., Sraughan, T., Norris, C.R., and Bennett, R.D. (1994) *Long-Term Structural Behavior of Pipeline Rehabilitation Systems*, Trenchless Technology Center, Louisiana Tech University, Ruston, LA.

Gumble, J.E. (1997) "Structural Design of Pipe Linings Review of Principles, Practice and Current Developments Worldwide." *Proc. International No-Dig '97, Taipei.*

Hall, C. (1981) *Polymer Materials*, Wiley, New York, NY.

Hall, D.E., Jordan, W., and Nassar, R.(1997) "Modeling and Accelerated Testing of Cured-In-Place Plastic Sewer Rehabilitation Liners", funded proposal to the National Science Foundation.

Heller, P. and Anderson, R.G. (1984) "Creep Buckling: an Experiment, an 'Exact' Solution and some Simple Thoughts," *Applied Solid Mechanics*, 2(1), 95-112.

HKS, Inc. (1995) *ABAQUS/Standard Manuals*, Version 5.5, Hibbitt, Karlsson & Sorensen Inc., Pawtucket, RI.

Hoff, N.J. (1958) "A Survey of the Theory of Creep Buckling," *Proc. 3rd US National Congress of Applied Mechanics*, Brown University, RI.

Hoff, N.J. Jashman, W.E. and Nachbar, W. (1959) "A Study of Creep Collapse of a Long Circular Cylindrical Shell Under Uniform External Pressure," *J. Aero/Space Sciences*, 663-669.

Kaji, Y., Ioka, I., Nishiguchi, I. and Miyamoto, Y. (1996) "Estimation of Creep Buckling Deformation Under External Pressure at Elevated Temperature," *Trans. ASME Journal of Pressure Vessel Technology*, 118(6), 460-463.

Koundy, V., Forgeron, T. And Hivroz, J. (1996) "Creep Buckling of Ovalized Tubes under External Pressure," *Trans. ASME Journal of Pressure Vessel Technology*, 118(3), 194-198.

Kraus, H. (1980) *Creep Analysis*, John Wiley & Sons, Inc., New York, NY.

Lin, H. (1995) *Creep Characterization of CIPP Material Under Tension, Compression and Bending*, MS Thesis, Louisiana Tech University, Ruston, LA.

Lo, K.H., Chang, B.T.A., Zhang, Q. and Wright, W.J. (1993) "Collapse Resistance of Cured-In-Place Pipes," *Proc. North American No-Dig '93*, NASTT, San Jose, CA.

Lo, K.H. and Zhang, J. Q. (1994) "Collapse Resistance Modeling of Encased Pipes," Dave Eckstein (Ed.) *Buried Plastic Pipe Technology: 2nd Volume*, ASTM STP 1222, ASTM, Philadelphia, PA.

Mahalingam, R. (1996) *A Viscoelastic Model to Determine the Long-Term Buckling Pressure of CIPP Liners*, MS thesis, Louisiana Tech University, Ruston, LA.

McCaig, I.W. and Folberth, J. (1962) "The Buckling Resistance of Steel Liners for Circular Pressure Tunnels," *Water Power*, 14(7), 272-278.

Menges, G. And Gaube, E. (1969) "Failure by Buckling," *Modern Plastics*, 9(7), 96-110.

Moore, I. D. (1998) "Tests for Pipe Liner Stability: What We Can and Cannot Learn," *Proceedings of North American No-Dig '98*, NASTT, Albuquerque, NM, 443-457.

Nishiguchi, I, Kaji, Y., Ioka, I., Yamamura, T. and Yamada, Y. (1990) "A Simplified Method for Predicting Creep Collapse of a Tube Under External Pressure," *Journal of Pressure Vessel Technology*, 112(8), 233-239.

Norton, F.H. (1929) *Creep of Steel at High Temperature*, McGraw-Hill, New York, NY.

Omara, A. M. (1996) *Analysis of Cured-In-Place Pipes (CIPP) Installed in Circular and Oval Deteriorated Host Pipes*, D.E. Dissertation, Louisiana Tech University, Ruston, LA.

Omara, A.M., Guice, L.K., Straughan, W.T., and Akl, F.A. (1997) "Buckling Models of Thin Circular Pipes Encased in Rigid Cavity," *J. Engr. Mech.* 123(12), 1294-1301.

Rabotnov, G.N. & Sherikov, S.A. (1957) "Creep Stability of Columns and Plates," *Journal of the Mechanics and Physics of Solids*, 6(1), 27-34.

Sammari, A. and Jullien, J.F. (1995) "Creep Buckling of Cylindrical Shells Under External Lateral Pressure," *Thin-Walled Structures*, 23(2), 255-269, Elsevire Science Ltd., UK.

Shanley, F.R. (1952) *Weight-Strength Analysis of Aircraft Structures, 1st Ed.*, Mcgraw-Hill, New York, NY.

Shatton, R.K. and Boot, J.C. (1995) "Details of Proposed Laboratory and Numerical Testing of CIPP Linings" Research Report No. 49, Dept Civil and Environmental Engr., University of Bradford, UK.

Skrzykep, J.J. (1993) *Plasticity and Creep: Theory, Examples, and Problems*, CRC Press, Boca Raton, FL.

Song, Y., Sheinman, I. and Simitses, G.J. (1995), "Thermoelastoviscoplastic Buckling Behavior of Cylinder Shells," *Journal of Engineering Mechanics*, 121(1), 62-70.

Stokeld, M. (1998) Internal Test Data, The Trenchless Technology Center, Louisiana Tech University, Ruston, LA.

Sundstrom, E. (1958) "Creep Buckling of Cylinder Shells," *Trans. Royal Inst. Tech.*, No. 115, Stockolm, Sweden.

Timoshenko, S.P. and Gere, J.M. (1961) *Theory of Elastic Stability*. McGraw-Hill, New York, NY.

TTC (1998a) *Preliminary Short-Term Buckling Results*, The Trenchless Technology Center, Louisiana Tech University, Ruston, LA.

TTC (1998b) Internal test data on long-term buckling tests, The Trenchless Technology Center, Louisiana Tech University, Ruston, LA.

TTC (1998c) Video tapes. The Trenchless Technology Center, Louisiana Tech University, Ruston, LA.

Ullman, F. (1964) External water pressure designs for steel-lined pressure shafts. Water Power, 16(7), 298-305.

Vaughan, E.W. (1956) "Steel Linings for Pressure Shafts in Solid Rocks," *Proc. ASCE, Vol. 82*, No. PO2.

Wagner, V. (1992) "Beulnachweis bei der Sanierung von nichtbegehbaren, undichten Abwasserkanalen mit dem Schlauchverfahren.," *Diss. TU*, Berlin, Germany.

Welch, A.J. (1989) *Creep Buckling of Infinitely Long Constrained Cylinders Under Hydrostatic Loading*, Ph.D. Thesis, University of Bradford, Bradford, UK.

WRc (1993) *Manual of Sewer Condition Classification, 3rd Ed.* UK Water Industry Engineering and Operations Committee, WRc plc., UK.

Yamamoto, Y. & Matsubara, N. (1981) "Buckling Strength of Steel Cylindrical Liners for Waterway Tunnels," *Theoretical and Applied Mechanics*, 30, 225-235, University of Tokyo Press, Japan.

VITA

Qiang Zhao, the son of Zhonggan Zhao and Li Wang, was born in Beijing, China on June 19, 1965. After completing his schooling in 1982, he entered the University of Science and Technology of China, Hefei, China, receiving a B. S. in Solid Mechanics in May, 1987. Beginning in August, 1987, he attended the Beijing Institute of Information and Control, pursuing his graduate study under the guidance of Prof. Qian Chen. He graduated with an M. S. in Computer Applications (with specialization in Computer Aided Structural Design) in April, 1990, after completing two research projects concerning the state-of-the-art FEA techniques and the structural dynamics for damped aerospace structures. From May, 1990 through July, 1995, he worked for the Institute of Mechanics, Beijing, a research institution subordinated to the Chinese Academy of Sciences. He was a Research Engineer at the Lab for Structural Dynamics, and also affiliated to the Joint Lab for Ocean Engineering of CAS. He married Ruiyuan Yang in June, 1990, and their son Guanyun Zhao was born on November 3, 1994. In August, 1995, Qiang attended the Applied and Computational Analysis and Modeling Program at Louisiana Tech University to pursue his Ph.D. under the guidance of Dr. Raja Nassar and Dr. David E. Hall.

IMAGE EVALUATION TEST TARGET (QA-3)

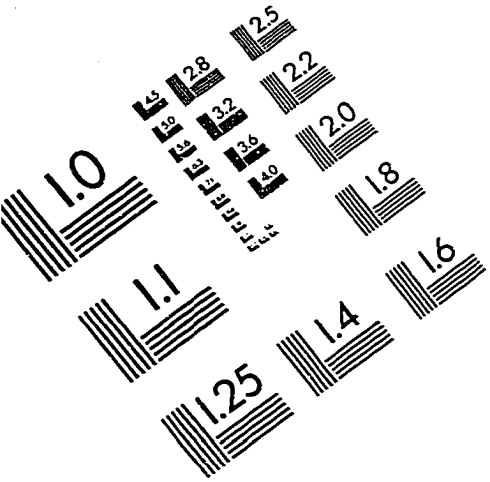

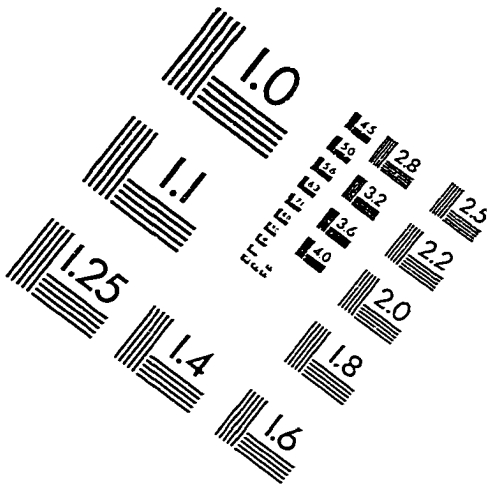

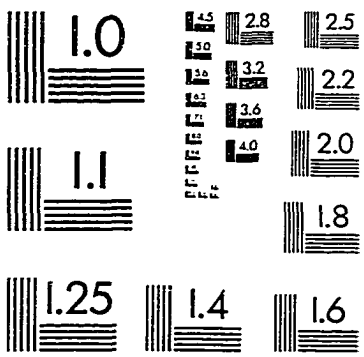

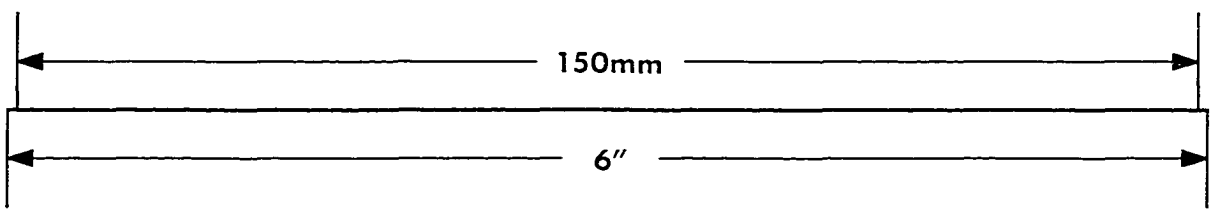

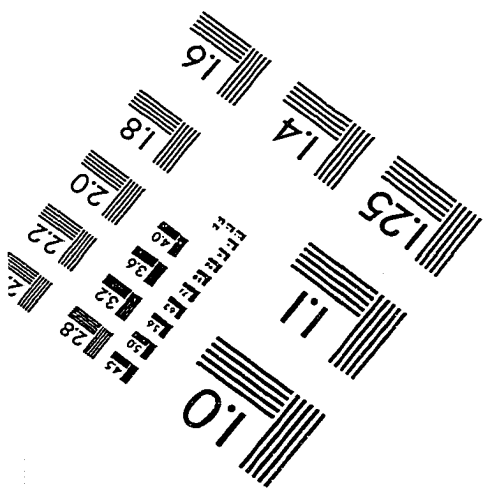

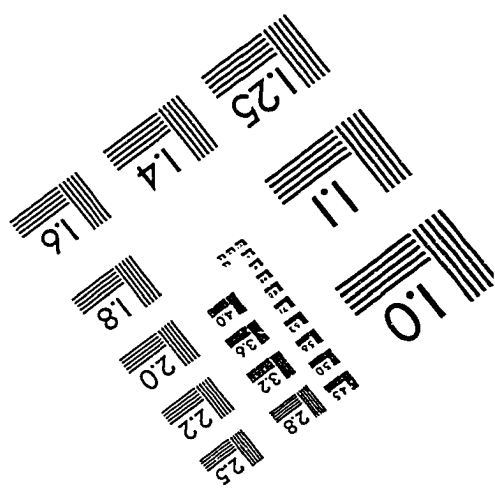

APPLIED IMAGE, Inc
1653 East Main Street
Rochester, NY 14609 USA
Phone: 716/482-0300
Fax: 716/288-5989